

Are Dawn Storms Jupiter's auroral substorms?

B. Bonfond^{1*}, Z. H. Yao^{2,1**}, G. R. Gladstone³, D. Grodent¹, J.-C. Gérard¹, J. Matar¹, B. Palmaerts¹, T. K. Greathouse³, V. Hue³, M. H. Versteeg³, J. A. Kammer³, R. S. Giles³, C. Tao⁴, M. F. Vogt⁵, A. Mura⁶, A. Adriani⁶, B. H. Mauk⁷, W. S. Kurth⁸, S. J. Bolton³

¹ Space Science, Technologies and Astrophysical Research Institute, Laboratory for Planetary and Atmospheric Physics, University of Liège, Liège, Belgium.

² Key Laboratory of Earth and Planetary Physics, Institute of Geology and Geophysics, Chinese Academy of Sciences, Beijing, China.

³ Southwest Research Institute, San Antonio, TX, USA.

⁴ National Institute of Information and Communications Technology, Tokyo, Japan.

⁵ Center for Space Physics, Boston University, MA, USA.

⁶ Institute for Space Astrophysics and Planetology, National Institute for Astrophysics, Rome, Italy.

⁷ Applied Physics Laboratory, Johns Hopkins University, Laurel, MD, USA.

⁸ Department of Physics and Astronomy, University of Iowa, Iowa City, IA, USA.

Are Dawn Storms Jupiter's auroral substorms?

B. Bonfond^{1*†}, Z. H. Yao^{2,1*†}, G. R. Gladstone³, D. Grodent¹, J.-C. Gérard¹, J. Matar¹, B. Palmaerts¹, T. K. Greathouse³, V. Hue³, M. H. Versteeg³, J. A. Kammer³, R. S. Giles³, C. Tao⁴, M. F. Vogt⁵, A. Mura⁶, A. Adriani⁶, B. H. Mauk⁷, W. S. Kurth⁸, S. J. Bolton³

¹ Space Science, Technologies and Astrophysical Research Institute, Laboratory for Planetary and Atmospheric Physics, University of Liège, Liège, Belgium.

² Key laboratory of Earth and Planetary Physics, Institute of Geology and Geophysics, Chinese Academy of Sciences, Beijing, China.

³ Southwest Research Institute, San Antonio, TX, USA.

⁴ National Institute of Information and Communications Technology, Tokyo, Japan.

⁵ Center for Space Physics, Boston University, MA, USA.

⁶ Institute for Space Astrophysics and Planetology, National Institute for Astrophysics, Rome, Italy.

⁷ Applied Physics Laboratory, Johns Hopkins University, Laurel, MD, USA.

⁸ Department of Physics and Astronomy, University of Iowa, Iowa City, IA, USA.

*Correspondence to: b.bonfond@uliege.be, zhonghua.yao@uliege.be.

†These authors contributed equally to this work.

Key points:

- Juno's observations provide the first global description of dawn storms in Jupiter's aurorae, from their initiation to their end.
- Examples of non-isolated dawn storms and smaller events named pseudo-dawn storms have been identified.
- Jovian dawn storms and terrestrial auroral substorms share many morphological and temporal characteristics.

Abstract

Dawn storms are among the brightest events in the Jovian aurorae. Up to now, they had only been observed from Earth-based observatories, only showing the Sun-facing side of the planet. Here we show for the first time global views of the phenomenon, from its initiation to its end and from the nightside of the aurora onto the dayside. Based on Juno's first 20 orbits, some patterns now emerge. Small short-lived spots are often seen for a couple of hours before the main emission starts to brighten and evolve from a straight arc to a more irregular one in the midnight sector. As the whole feature rotates dawn-ward, the arc then separates into two arcs with a central initially void region that is progressively filled with emissions. A gap in longitude then often forms before the whole feature dims. Finally, it transforms into an equatorward-moving patch of auroral emissions associated with plasma injection signatures. Some dawn storms remain weak and never fully develop. We also found cases of successive dawn storms within a few hours. Dawn storms thus share many fundamental features with the auroral signatures of the substorms at Earth, despite the substantial differences between the dynamics of the magnetosphere at the two planets.

Plain language summary

Polar aurorae are a direct consequence of the dynamics of the plasma in the magnetosphere. The sources of mass and energy differ between the Earth's and Jupiter's magnetospheres, leading to fundamentally distinct auroral morphologies and very different responses to solar wind variations. Here we report on the imaging of all development stages of spectacular auroral events at Jupiter, called dawn storms, including, for the first time, their initiation on the nightside. Our results reveal surprising similarities with auroral substorms at Earth, which are auroral events stemming from explosive magnetospheric reconfigurations. These findings demonstrate that,

51 whatever their sources, mass and energy do not always circulate smoothly in planetary
52 magnetospheres. Instead they often accumulate until the magnetospheres reconfigure and
53 generate substorm-like responses in the planetary aurorae, although the temporal and spatial
54 scales are different for different planets.

55 1. Introduction

56 The specificity of the dawn storms among the various auroral morphologies at Jupiter was
57 recognized as soon as the first high resolution ultraviolet (UV) images of the aurorae on Jupiter
58 became available (Gérard et al., 1994). As observed from the Hubble Space Telescope (HST),
59 having only access to the Earth-facing side of the aurora, they consist of a thickening and a major
60 enhancement of the brightness of the dawn arc of the main auroral emission (main oval). They
61 seem to last for at least 1-2 hours (Ballester et al., 1996), but given the typical length of HST
62 sequences is ~45 minutes, HST could not provide a complete and uninterrupted view of the
63 process. Dawn storms are also characterized by clear signatures of methane absorption,
64 indicating that the charged particles causing them can precipitate deep below the methane
65 homopause, with energies up to 460 keV (Gustin et al., 2006) in the case of electrons. Based on
66 the large HST observation campaign carried out in 2007, dawn storms appeared rare (3 cases out
67 of 54 observations) and occurred independently from the state of the solar wind (Nichols et al.,
68 2009). However, the dawn storm observed during the HST campaign supporting the Juno
69 mission as it approached Jupiter in 2016 occurred just as a coronal mass ejection hit Jupiter's
70 magnetosphere, re-igniting the debate on the relationship between dawn storms and solar wind
71 fluctuations (Kimura et al., 2017).

72 Simultaneous in-situ measurements in the dawn-side magnetosphere with Juno and auroral
73 images from the Hubble Space Telescope showed that dawn storms are associated with

74 reconnection and dipolarization signatures (Yao, Bonfond, Clark, et al., 2020). Observations
75 from Galileo also showed signatures of dipolarization, plasmoid release and plasma energization
76 in the magnetotail, which were associated with substorm-like events (Ge et al., 2007; Kronberg
77 et al., 2005, 2008; Krupp et al., 1998), because of the analogy with similar processes taking place
78 during terrestrial substorms. Magnetospheric substorms are defined as “a transient process
79 initiated on the night side of the Earth in which a significant amount of energy derived from the
80 solar wind-magnetosphere interaction is deposited in the auroral ionosphere and magnetosphere”
81 (Rostoker et al., 1980). It is however unlikely that the solar wind, and especially dayside
82 magnetopause reconnection, would play a similar role in the internally driven Jovian
83 magnetosphere (Delamere & Bagenal, 2010).

84 So far, our understanding of auroral dawn storms has been incomplete mainly because we have
85 been unable to observe the whole extent of the event, both temporally and spatially. New data
86 from the Juno mission reveal for the first time where and how the dawn storms start and their
87 consequences.

88 2. Image processing

89 Juno is a NASA New Frontiers spacecraft orbiting Jupiter since 4 July 2016. Its 53-day eccentric
90 polar orbit brings its perijove (PJ) to ~4000 km above the surface (1 bar level) at low latitudes.
91 This orbit allows its ultraviolet spectrograph (UVS) to acquire spectrally resolved images of the
92 polar aurorae from approximately 4 hours before the PJ (in the northern hemisphere) to
93 approximately 4 hours after PJ (in the southern hemisphere) with a ~1-hour interruption in
94 between during the closest approach at low latitude.

95 Juno-UVS is an imaging spectrograph operating in the 68 to 210 nm range (Gladstone et al.,
96 2017; Greathouse et al., 2013). Its dog-bone shaped slit is 7.2° long, 0.025° wide in the center

97 and 0.2° wide in the two extremities. The slit is generally oriented perpendicularly to the Juno
98 spin plane. However, a scan mirror located at the entrance of the instrument allows to shift the
99 field of view by up to $\pm 30^\circ$ from the spin plane. In the present work, only the data from the wide
100 parts of the slit are used, in order to optimize the signal to noise ratio. Moreover, the wavelength
101 range from 155 to 162 nm is selected in order to avoid regions affected by absorption of the UV
102 light by hydrocarbon molecules in the Jovian atmosphere (mostly methane) below 155 nm and
103 by reflected sunlight beyond 162 nm.

104 The calibrated data from Juno-UVS are available through the Planetary Data System in the
105 form of FITS files, which contain information about each event collected by the detector, such as
106 the time of the event, its position in X and Y on the detector, the corresponding wavelength, etc.
107 This first step of the processing consists of removing the noise due to particle (typically
108 relativistic electrons) penetrating into the instrument and impacting the detector from the signal
109 caused by UV photons. Contrary to photons, which are diffracted by the grating, penetrating
110 particles illuminate the detector in an almost homogenous fashion, as confirmed by observations
111 carried out in the radiation belts. We use a region between pixels 345 to 550 in the X direction
112 (corresponding to ~ 59.7 to 80.9 nm) and pixels 20 to 255 in the Y direction, which has a very
113 low effective area for extreme-UV photons (Hue et al., 2019), in order to estimate the count rate
114 per pixel due to radiation. This background noise is then removed from the photon illuminated
115 part of the detector.

116 The second step consists, for each detection event, of projecting the four corners of each
117 field of view element along the slit onto a Jupiter-shaped ellipsoid located 400 km above the 1-
118 bar level, using the SPICE kernels listed in the FITS file header. The brightness, derived from
119 the weighted counts and the exposure time, is then attributed to a quadrilateral formed by these 4

120 points. A map of the aurora is then progressively built by adding all the detected events for a
121 given Juno spin. Simultaneously, an exposure map, identifying the regions of the planet covered
122 by the instrument's field of view, is also constructed. Images of the whole aurorae are then
123 assembled by performing a weighted sum of the consecutive spins, with a higher weight being
124 attributed to the latest spin. Going back in time, each weighting coefficient is $1/10^{\text{th}}$ of the
125 previous one. We then divide the weighted sum of the counts with a weighted sum of the
126 exposure maps to derive our final brightness map. This method offers the best compromise
127 between the completeness of the auroral map and the dynamics of the auroral features. However,
128 since UVS cannot observe the whole aurora during a given spin during the perijove sequence, the
129 exact timing and duration of some transient events is uncertain, with temporal knowledge gaps of
130 30 seconds at best due to the spinning spacecraft.

131 Three main sources of uncertainty affect estimates of the total emitted power by the H_2
132 molecules in the UV: 1) systematic calibration uncertainties estimated on the order of 16% (J.-C.
133 Gérard et al., 2020), 2) shot noise uncertainty, which depends on the number of counts in the
134 region of interest and is typically below 5% for the small spots and below 1% for the larger dawn
135 storm features and 3) the selection uncertainty, which depends on the way the region of interest
136 is defined and which may reach up to 15%. The quadratic sum of all these uncertainties can be
137 rounded to a reasonable value of 25% for power estimates.

138 3. Observations of dawn storms

139 3.1. Development sequence of typical dawn storms

140 For the first time, Juno-UVS granted us a complete and global picture of the auroral dawn
141 storms, from their initiation to their vanishing. Indeed, Juno captured views of dawn storms at
142 different stages of development in approximately half of the first 20 perijoves (Table 1).

143 For example, on 7 February 2018 (PJ11), Juno-UVS captured the initiation of a dawn storm from
144 low altitude (~ 43000 km) above the north pole, thus allowing unprecedented high spatial
145 resolution observations (Figure 1). Around 13:06 UT, the event started with a relatively bright
146 midnight arc (~ 2000 kR). Then a few spots began to appear poleward of this arc, creating a
147 string of approximately a dozen spots within 14 minutes, each one forming ~ 1000 km dusk-ward
148 of the previous (Figure 2). These spots are approximately ~ 1000 km long (in the north-south
149 direction) and ~ 150 km wide, which corresponds to the projection of the instrumental point
150 spread function (PSF) on the planet. Hence, the apparent North-South extension probably result
151 from the asymmetry of the PSF. They each typically emit ~ 1 GW of total power and appear with
152 a peak brightness of ~ 800 kR. Using the flux mapping method of (Vogt et al., 2015), but with
153 JRM09 (Connerney et al., 2018) as an internal field model, these spots map to a distance of 65-
154 110 Jovian radii (R_J) and a local time range between 22:40 UT and 23:45 UT, which broadly
155 corresponds to the X-line, where magnetotail reconnections take place (Vogt et al., 2010). When
156 mapped in the magnetosphere, the inter-spot distance corresponds to $1-2^\circ$ of longitude, or to a
157 mapped distance of 6-7 R_J . The distance between the mapped locations of the first (and dawn-
158 most) and last (and dusk-most) spots is about 42 R_J ($\sim 3 \cdot 10^6$ km), and the associated propagation
159 speed would be on the order of 3600 km/s in the azimuthal direction. If we focus on the brightest
160 central spots, this apparent mapped azimuthal velocity reaches 10 000 km/s. If these spots indeed
161 correspond to magnetic reconnection on the X-line, it is however quite likely that these high
162 values do not correspond to any physical velocity in the magnetosheet, and that the time interval
163 rather corresponds to a phase delay. Furthermore, these numbers should be considered as rough
164 estimates only, since 1) the mapping uncertainty strongly increases with radial distance, and 2)
165 any static mapping model is inaccurate, whatever the planet, during magnetospheric

166 reconfiguration events. Even though the spin modulated sampling rate of UVS does not allow
167 for easy monitoring, individual spots appear to vanish after a few minutes. These short-lived
168 spots may be similar to the midnight spots occasionally observed from the Hubble Space
169 Telescope at the limb of the planet (D. Grodent et al., 2004; Radioti et al., 2011). Another
170 example of transient bright spots was found during PJ16 (see Figure S1 in the supplemental
171 material).

172 Two hours later, Juno was located over the southern hemisphere when the main emission began
173 to brighten and broaden irregularly, forming a bead-like pattern in the same midnight sector
174 (Figure S2). Fly-bys carried out at lower altitude during this phase of the dawn storm, such as
175 during PJ3 at 15:37 UT, render this pattern, with beads with ~ 1500 km ($\sim 2^\circ$) spacing, even more
176 obvious. Once mapped into the magnetodisk, these beads appear to originate from a region ~ 50
177 R_J from Jupiter and are azimuthally separated by $\sim 8 R_J$ (3° of longitude) in the magnetospheric
178 local time range between $\sim 1:45$ and $\sim 3:00$ LT. Hence, the enhancement of the main emission,
179 leading to the full-fledged dawn storm, actually started around magnetospheric midnight. This
180 feature then slowly migrated to the dawn sector at a pace corresponding to $\sim 25\%$ of corotation
181 with the planet. Around 16:22 UT, the main arc split into two parts, with one moving ~ 2500 km
182 towards the pole while the other remain relatively still. Because it is likely that these auroral
183 features arise from a reconfiguration of the magnetic field, static magnetic field mapping models
184 would most probably provide misleading results. The whole feature continued to rotate,
185 progressively accelerating towards co-rotation with the magnetic field as the dawn storm
186 developed. Around 17:15 UT, the feature appeared to split, but longitudinally this time. The gap
187 extends over $\sim 10^\circ$ of longitude in the upper atmosphere. At its peak, the total power reached

188 850 GW, which is among the brightest events observed during Juno's first 20 orbits (see Table
189 1). The UVS perijove observations ended at 18:50 UT, even though the event was still ongoing.
190 On 19 May 2017 (PJ6), the Juno-UVS observations missed the beginning of an event, but
191 allowed us to examine the next phases. After the broadening and the latitudinal splitting of the
192 main emission, the outer-most arc transformed into large patches. On the same day, subsequent
193 HST images acquired with the Space Telescope Imaging Spectrograph (STIS) confirmed that the
194 patches continued their evolution, forming latitudinally extended fingers slowly expanding
195 equatorward. Such features have been associated with large and fresh plasma injection signatures
196 (Dumont et al., 2018). While such a connection between dawn storms and large injection
197 signatures has been proposed previously, based on the simultaneous presence of a dawn storm
198 and large injection signatures on the same image (Gray et al., 2016; Denis Grodent et al., 2018),
199 this long and continuous set of observations from Juno and Hubble is the first to clearly
200 demonstrate the transition from one into the other. It should also be noted that some (less
201 intense) injection signatures can also appear independently from dawn storms, as was observed
202 during PJ1 for example (B. Bonfond et al., 2017).

3.2. Non-isolated dawn storms

3.3. Juno-UVS observations of dawn storms show that they sometimes occur as a series, rather than isolated events. For example, on 27 March 2017 (PJ5), a first dawn storm was ongoing when the observations started at 03:57 UT and was finished by approximately 06:51 UT, after which a second one was observed peaking around 08:08 UT. Figure 3 (top) show the aurora at 04:06, during the first brightening, at 07:25, after it finished and at 08:08, during the second brightening.. In other cases, there appears to be no gap between consecutive events. For example, during PJ3 (11 December 2016), the dawn storm expansion phase seemed to never really stop, continuously going on at the same local time. The dawn storm was first observed with the apparition of beads around 15:21 UT, as Juno was flying over the northern hemisphere, and continued until auroral observations were interrupted by Juno's low latitude fly-by. When observations of the southern hemisphere started over, a dawn storm was still ongoing and this continued until the end of the sequence at 22:01 UT, with the emitted power increasing around the end. **Pseudo-dawn storms**

During PJ16 (29 October 2018), Juno-UVS observed the development of a particularly limited dawn storm-like event (Figure 4). Around 20:19 UT, the instrument captured the appearance of three transient (~6 minutes) spots poleward of the midnight arc of the main emission. Moreover, the midnight arc itself was fainter than during PJ11 and the number of spots was also smaller. The brightness of the enhanced the dawn arc of the main emission observed at 23:39 UT was fairly dim (~500 kR), and the area concerned with the enhancement was limited (~10° in longitude). While the sequence of events is similar to the one observed on PJ11, which is why we identify it here as a dawn storm, it would probably not have qualified as a dawn storm in previous studies, due to its limited extent and brightness. This reason, together with the fact that Juno observes the whole auroral region, including the nightside where dawn storms arise, almost continuously for ~8 hours explains the discrepancy between our detection rate and the one deduced from HST, which only focused on the dawn storm expansion phase. The second dawn storm on PJ5 is another example of such a limited dawn storm (Figure 3, top right panel).

4. Discussion

Put together, the Juno-UVS observations paint a brand new picture of dawn storms. They consist of a 5-10 hour long chain of events, starting with the transient spots (Figure S1), followed 2-3 hours later by the formation of bead-like features on the midnight part of the main emissions (Figure S2). This time delay between events taking place at 90 and 50 R_J , respectively, suggests a propagation speed of 250-400 km/s, which is consistent with estimates of the fast mode velocity in the plasma sheet (Kivelson, 2015; Manners et al., 2018). This is followed by a longitudinal and latitudinal (mostly poleward) expansion phase, during which the main emission brightens, expands, thickens and forks into two branches (Figure S3 in the supplemental material). This chain of events is very similar to the one observed during terrestrial auroral substorms (Figure 5). Substorms are global reconfigurations of the magnetosphere during which the magnetic energy stored in the magnetotail is converted into particle energy, which lead to spectacular auroral brightening in nightside polar regions which generally follow a well-established sequence of features (Akasofu, 2013). The transient spots observed in Jupiter's aurora share several morphological and temporal characteristics with transient meso-scale features on Earth, sometimes associated with poleward boundary intensifications (PBIs) and sometimes with streamers (Forsyth et al., 2020). Both are often observed before the substorm onset (Nishimura et al., 2011), even if the exact relationship between streamers and substorms is disputed (Miyashita & Ieda, 2018). Both phenomena are associated with reconnection in the magnetotail and the subsequent inward flow of plasma and dipolarizing field lines (Angelopoulos et al., 2008). At Jupiter, the tentative connection between magnetotail reconnection and dawn storm has been evocated by several authors (Ballester et al., 1996; Ge et al., 2010). Recently, the most compelling examples of such a connection come from

258 contemporaneous in situ particle and fields measurements by Juno and HST images of the aurora
259 (Yao, Bonfond, Clark, et al., 2020). These observations show large reconnection signatures on
260 magnetic field lines mapping poleward of a dawn storm and then dipolarization signatures
261 preceding auroral injection signatures. The pre-expansion beads observed in the context of
262 terrestrial substorms (Henderson, 2009) are associated with plasma instabilities in the near
263 magnetotail, such as the ballooning instability (Yao et al., 2017). The expansion phases of
264 Jupiter's dawn storms and the Earth's substorms also share fundamental similarities, and the
265 latter is known to be associated with a dipolarization/current disruption in the magnetosphere. In
266 particular, the apparition of a bifurcated oval at Jupiter resembles terrestrial bulge-type aurora
267 observed during substorms (Gjerloev et al., 2007, 2008). Finally, the auroral patches in the
268 equatorward emissions manifest massive plasma injections (Figure S6). Plasma injections in the
269 inner terrestrial magnetosphere are indeed observed by in situ instruments during substorm
270 events (Gabrielse et al., 2019) and they can also give rise to equatorward moving auroral
271 enhancements (Sergeev et al., 2010). One notable difference is that auroral substorms do not
272 rotate with the Earth, but evolve in fixed local time, i.e., around midnight (with a slight
273 preference at pre-midnight (Gjerloev et al., 2004)).

274 At Earth, substorms do not always occur as isolated events. Instead, multiple substorm
275 expansions can happen consecutively (Liou et al., 2013). A similar behavior is observed for
276 dawn storms at Jupiter. The occurrence of successive dawn storms separated by a delay of a few
277 hours could explain why images of dawn storms from HST often display large injection
278 signatures in the post-noon sector (Gray et al., 2016; Denis Grodent et al., 2018). Furthermore, (
279 Yao, Bonfond, Clark, et al., 2020) suggest that successive dawn storms are responsible for the
280 multiple injection auroral structures.

281 Terrestrial substorms vary considerably in intensity and those which could not fully develop are
282 called pseudo-breakups (Pulkkinen et al., 1998). The event observed during PJ16 (29 October
283 2018) was limited to a small intensification, which might be analogous to terrestrial pseudo-
284 breakups (Figure 4).

285 The orientation of the interplanetary magnetic field (and, to a lesser extent, the dynamic pressure
286 of the solar wind) controls the occurrence and intensity of Earth substorms (Kullen & Karlsson,
287 2004). Unfortunately, these solar wind parameters are difficult to obtain at Jupiter while Juno
288 carries out its perijove observations. Therefore, we used the propagation model from Tao et al.,
289 (2005), which relies on measurements acquired at one astronomical unit from the Sun (from
290 either the OMNI data or the Stereo A spacecraft) to estimate the solar wind velocity and dynamic
291 pressure at Jupiter when Jupiter and the observatory are sufficiently well aligned ($<40^\circ$) (Figures
292 S6-S8). Most dawn storms for which such an estimate was possible (i.e. PJ5, PJ9, PJ14 and
293 PJ20) happened more than 2 days away from any solar wind enhancement, which confirms that
294 dawn storm may occur during relaxed solar wind conditions. However, they can also occur at
295 times closer to a solar wind enhancement (e.g. PJ1, PJ6 and PJ16), suggesting that solar wind
296 shocks do not necessarily prevent their occurrence. The comparison of the location of the
297 magnetopause measured by Juno and the aurora observed by HST also suggests that dawn storms
298 happen independently of the state of compression of the magnetosphere and are most probably
299 internally driven, contrary to the global main emission brightenings, which only occur in the
300 compressed state (Yao, Bonfond, Grodent, et al., 2020).

301 Regardless of the similarities between terrestrial substorms and Jovian dawn storms, it is also
302 important to stress the major differences between the Earth's and Jupiter's magnetospheres
303 (Mauk & Bagenal, 2013). The first is dominated by its interaction with the solar wind, and

304 magnetic reconnections on the dayside magnetopause drive the plasma convection in the
305 magnetosphere through the so-called Dungey cycle (Dungey, 1961). On the other hand, the
306 Jovian magnetosphere is inflated with plasma originating from the volcanic moon Io and the
307 rotation of the planet controls the motion and the energization of the magnetospheric plasma.
308 The mechanism through which the mass injected at Io is ultimately released via reconnection on
309 closed field lines is called the Vasyliunas cycle (Kronberg et al., 2007; Vasyliunas, 1983).
310 Reconnection on the dayside magnetopause, while it does exist at Jupiter (Ebert et al., 2017),
311 cannot open a significant amount of flux (Desroche et al., 2012; Masters, 2017), leading to a very
312 different type of magnetospheric topology where the amount of flux open to the solar wind is
313 very limited and intertwined with flux closed tubes connected to the distant magnetotail (Zhang
314 et al., 2020). By comparing the occurrence of magnetotail reconnection and plasmoid release to
315 predictions of the solar wind input, (Vogt et al., 2019) showed that these large scale
316 reconfigurations of the magnetotail were mostly independent from solar wind compression.

317 However, regardless of the different reasons for the loading, in both cases plasma and energy
318 regularly accumulates within the system, which grows increasingly unstable, especially in the
319 midnight magnetotail where the field lines are the most elongated. While the long term
320 (~months) global evolution of the position of the main auroral emissions has been attributed to
321 the variations of the mass output from Io (B. Bonfond et al., 2012), the shorter term variations of
322 its position at different local times are poorly understood. Hence, since its typical location at
323 midnight for the various System III longitudes is unknown, we were unable to identify any
324 equatorward departure from it, as typically observed for the terrestrial growth phase auroral arcs.

325 Such a stretching of the field lines provides favorable conditions for reconnection to occur. At
326 Earth, such reconnection closes the magnetic field lines open to the solar wind in the

327 magnetotail, while at Jupiter, reconnection is internally driven (Ge et al., 2010; Kronberg et al.,
328 2005; Vogt et al., 2019; Woch et al., 2002) and is expected to take place on closed field lines. In
329 the middle magnetosphere, various plasma instabilities may occur, such as ballooning instability
330 (Hameiri et al., 1991; Kalmoni et al., 2018; Oberhagemann & Mann, 2020), cross-field current
331 instability (Lui et al., 1991), shear flow ballooning (Viñas & Madden, 1986) or shear flow-
332 interchange instability (Derr et al., 2020). Since the magnetic field lines in Jupiter’s outer
333 magnetosphere are also highly stretched, and the magnetosphere consists of more energetic ions
334 than the Earth’s magnetotail, many plasma instabilities identified in Earth’s magnetotail would
335 likely take place in Jupiter’s outer magnetosphere. Such instabilities can then lead to a disruption
336 of the azimuthal currents in the middle magnetosphere and a dipolarization of the field lines.
337 While the dipolarizing field lines would remain in the night sector at Earth, they would be
338 progressively swept away in azimuthal direction by the planetary rotation at Jupiter as they
339 progress inward. This makes studies of east-ward or west-ward expansion of the dawn storm
340 almost impossible at Jupiter, because the exact longitudinal expansion would be very difficult to
341 disentangle from partial corotation. These processes would also bring hot and sparse plasma
342 from the outer magnetosphere further into the system and energize it, forming plasma injections (
343 Yao, Bonfond, Clark, et al., 2020). Their study also shows that dipolarization at Jupiter may
344 corotate with the planet, as a counterpart of corotating auroral injection.

345 The above explanation probably gives the impression that the dawn storm auroral sequence
346 implies that the magnetotail reconfigurations at Jupiter are systematically “outside-in” in nature, ,
347 rather than “inside-out”, . Here the “outside-in” means starting with reconnection at $\sim 90R_J$
348 before propagating inward and disrupt the plasma sheet closer to Jupiter ($\sim 60-40R_J$, where the
349 main emissions map) and finally trigger plasma injections in the middle magnetosphere (30-10

350 R_J) and “inside-out” means starting in the middle magnetosphere with plasma injections, before
351 disrupting the region where the main emissions maps (40-60 R_J) and finally triggering
352 reconnection and the release of plasmoids in the distant magnetotail (~90R_J). . For the terrestrial
353 case, this debate around models such as the near-Earth neutral line model (outside-in) (Baker et
354 al., 1996) and near Earth current disruption model (inside-out) (Lui, 2015) has been raging for
355 years despite the flotilla of dedicated spacecraft cruising in the magnetosphere and we certainly
356 would not want to suggest that with the few cases presented here, Juno has single handedly
357 solved the problem at Jupiter. As a possible counter-example, the auroral observations during
358 PJ1 with Juno-UVS have shown the progressive development of injection signature all around
359 the pole before a poleward protrusion (the shape of which may be reminiscent of omega bands at
360 Earth) appeared on the midnight arcs of the main emissions (Bonfond et al., 2017). It then took 2
361 hours for bead-like features and then a dawn storm expansion phase to appear on infrared images
362 (see supplemental material S9). Contrary to the other sequences discussed here, this particular
363 one thus suggests that magnetospheric instabilities appeared closer to Jupiter before they
364 developed further out. Some studies also suggested that both situations might appear at Earth
365 (Murphy et al., 2014; Panov et al., 2020). Rather than a unique causal process leading to
366 systematic chain of events, a possible interpretation is that the accumulation of mass and energy
367 makes the different regions of the magnetosphere progressively susceptible to different types of
368 plasma instabilities (including, at places, reconnection). Once one of these regions reaches the
369 instability threshold and collapses, the generated disturbance propagates to the other regions,
370 making their own collapse more likely.

371 While they have some unique characteristics as well, the magnetosphere and aurorae at Saturn
372 are generally understood as representing an intermediate case between the Earth and Jupiter.

373 Indeed several lines of evidence (Bader et al., 2019) show that Saturn supports a combination of
374 Vasyliunas and rotating Dungey cycles (Cowley et al., 2005). It is thus less of a surprise to find
375 similar auroral features, such as transpolar arcs (Radioti et al., 2013) or auroral beads (Radioti et
376 al., 2019) in both the terrestrial and the Kronian aurorae. On the other hand, both observational
377 and theoretical arguments indicate that the overall dynamics of the plasma in the two
378 magnetospheres are fundamentally different (Delamere et al., 2015; Delamere & Bagenal, 2010;
379 Louarn et al., 2000), one being mostly externally driven and the other being mostly internally
380 driven. It is thus remarkable that universal processes releasing the accumulated matter and
381 energy from the systems generate strikingly similar auroral signatures.

382 Finally, we note that, if our interpretation is correct, the evolution of the dawn storms is another
383 demonstration that many, if not most, auroral processes and Jupiter cannot be explained by the
384 corotation enforcement currents paradigm (Bonfond et al., 2020). Indeed, on both planets,
385 currents and auroral intensities appear directly correlated only in specific places (Korth et al.,
386 2014).

387 Summary and conclusions

388 Freed from all the biases related to Earth-based observations, we detected dawn storms in
389 approximately half of the Juno perijove sequences (10 dawn storm observations over 19
390 orbits – no observations were carried out during PJ2). This is due to three factors: 1) longer
391 observations, providing additional chances to catch dawn storm at any stage of their
392 development, 2) a view of the nightside, where the dawn storms actually form and 3) a
393 looser definition of the dawn storm, which is no longer restricted to the brighter examples.
394 Moreover, the occurrence of dawn storms appears independent of the arrival of a solar
395 wind compression region at Jupiter.

396 While every feature has not been observed in each case, the dawn storms appear to follow
397 a systematic sequence of events (Figure 5), some of which are being reported here for the
398 first time. A dawn storm precursor appears to be the appearance of a series of transient
399 spots separated by ~ 1000 km, mapping to the pre-midnight sector. Approximately 2 to 3
400 hours later, the midnight section of the main emission starts to brighten, often forming
401 regularly spaced (~ 1500 km apart) beads. The arc further brightens and expands in
402 longitude as it progressively starts to co-rotate with the planet and to move towards the
403 dawn side. Then it bifurcates, with a branch moving poleward. The void between the arcs
404 then fills progressively as the arcs broaden in latitude. A longitudinal gap also generally
405 forms within the feature. Finally, the whole feature dims and the equatorward part of the
406 dawn storms evolves as an equatorward patch of emission associated with plasma
407 injection signatures, providing a direct link between dawn storms and some plasma
408 injection signatures.

409 Many of these auroral forms at Jupiter resemble meso-scale (Forsyth et al., 2020) and large
410 scale auroral forms observed during substorms at Earth. Furthermore, we found cases of
411 consecutive dawn storms occurring within a few hours, similar to the non-isolated
412 substorms at Earth. We also found cases of particularly weak dawn storm, reminiscent of
413 pseudo-breakups at Earth.

414 The magnetospheric processes associated with substorm magnetotail reconfigurations,
415 such as tail reconnection, dipolarization or hot plasma injection have also been observed at
416 Jupiter (Kronberg et al., 2005; Louarn et al., 2014; B. H. Mauk et al., 1997; Vogt et al., 2010;
417 Woch et al., 2002). The connection between these processes and dawn storms, was

418 proposed based on measurements from either in situ magnetic field or auroral images (Ge
419 et al., 2010; Kimura et al., 2017), and was later confirmed by contemporaneous
420 measurements from Juno and HST (Yao, Bonfond, Clark, et al., 2020), associated with dawn
421 storms. Despite the fact that the mass and energy loading in the magnetotail at Earth and
422 Jupiter are very different, the evidence presented here show that the auroral signatures of
423 the processes releasing them at Jupiter are remarkably similar to terrestrial auroral
424 substorm.

425

426
427
428
429
430
431
432
433
434
435
436
437
438
439
440
441
442
443
444
445
446
447
448
449
450
451
452
453

References

Adriani, A., Filacchione, G., Di Iorio, T., Turrini, D., Noschese, R., Cicchetti, A., et al. (2017). JIRAM, the Jovian Infrared Auroral Mapper. *Space Science Reviews*, 213(1), 393–446. <https://doi.org/10.1007/s11214-014-0094-y>

Akasofu, S.-I. (2013). Auroral Morphology: A Historical Account and Major Auroral Features During Auroral Substorms. In *Auroral Phenomenology and Magnetospheric Processes: Earth And Other Planets* (pp. 29–38). American Geophysical Union (AGU). <https://doi.org/10.1029/2011GM001156>

Angelopoulos, V., McFadden, J. P., Larson, D., Carlson, C. W., Mende, S. B., Frey, H., et al. (2008). Tail Reconnection Triggering Substorm Onset. *Science*, 321(5891), 931–935. <https://doi.org/10.1126/science.1160495>

Bader, A., Badman, S. V., Cowley, S. W. H., Yao, Z. H., Ray, L. C., Kinrade, J., et al. (2019). The Dynamics of Saturn’s Main Aurorae. *Geophysical Research Letters*, 46(17–18), 10283–10294. <https://doi.org/10.1029/2019GL084620>

Baker, D. N., Pulkkinen, T. I., Angelopoulos, V., Baumjohann, W., & McPherron, R. L. (1996). Neutral line model of substorms: Past results and present view. *Journal of Geophysical Research: Space Physics*, 101(A6), 12975–13010. <https://doi.org/10.1029/95JA03753>

Ballester, G. E., Clarke, J. T., Trauger, J. T., Harris, W. M., Stapelfeldt, K. R., Crisp, D., et al. (1996). Time-Resolved Observations of Jupiter’s Far-Ultraviolet Aurora. *Science*, 274, 409–413. <https://doi.org/10.1126/science.274.5286.409>

Bonfond, B., Grodent, D., Gérard, J.-C., Stallard, T., Clarke, J. T., Yoneda, M., et al. (2012). Auroral evidence of Io’s control over the magnetosphere of Jupiter. *Geophysical Research Letters*, 39(1). <https://doi.org/10.1029/2011GL050253>

Bonfond, B., Gladstone, G. R., Grodent, D., Greathouse, T. K., Versteeg, M. H., Hue, V., et al. (2017). Morphology of the UV aurorae Jupiter during Juno’s first perijove observations. *Geophysical Research Letters*, 44(10), 4463–4471. <https://doi.org/10.1002/2017GL073114>

Bonfond, Bertrand, Yao, Z., & Grodent, D. (2020). Six Pieces of Evidence Against the Corotation Enforcement Theory to Explain the Main Aurora at Jupiter. *Journal of Geophysical Research: Space Physics*, 125(11), e2020JA028152. <https://doi.org/10.1029/2020JA028152>

454 Connerney, J. E. P., Kotsiaros, S., Oliverson, R. J., Espley, J. R., Joergensen, J. L., Joergensen, P. S., et al. (2018). A
455 New Model of Jupiter's Magnetic Field From Juno's First Nine Orbits. *Geophysical Research Letters*,
456 45(6), 2590–2596. <https://doi.org/10.1002/2018GL077312>

457 Cowley, S. W. H., Badman, S. V., Bunce, E. J., Clarke, J. T., Gérard, J.-C., Grodent, D., et al. (2005). Reconnection
458 in a rotation-dominated magnetosphere and its relation to Saturn's auroral dynamics. *Journal of*
459 *Geophysical Research: Space Physics*, 110(A2). <https://doi.org/10.1029/2004JA010796>

460 Delamere, P. A., & Bagenal, F. (2010). Solar wind interaction with Jupiter's magnetosphere. *Journal of Geophysical*
461 *Research: Space Physics*, 115(A10). <https://doi.org/10.1029/2010JA015347>

462 Delamere, P. A., Bagenal, F., Paranicas, C., Masters, A., Radioti, A., Bonfond, B., et al. (2015). Solar Wind and
463 Internally Driven Dynamics: Influences on Magnetodiscs and Auroral Responses. *Space Science Reviews*,
464 187(1), 51–97. <https://doi.org/10.1007/s11214-014-0075-1>

465 Derr, J., Horton, W., & Wolf, R. (2020). Shear Flow-Interchange Instability in Nightside Magnetotail as Proposed
466 Cause of Auroral Beads as a Signature of Substorm Onset. *Journal of Geophysical Research: Space*
467 *Physics*, 125(1), e2019JA026885. <https://doi.org/10.1029/2019JA026885>

468 Desroche, M., Bagenal, F., Delamere, P. A., & Erkaev, N. (2012). Conditions at the expanded Jovian magnetopause
469 and implications for the solar wind interaction. *Journal of Geophysical Research: Space Physics*, 117(A7).
470 <https://doi.org/10.1029/2012JA017621>

471 Dumont, M., Grodent, D., Radioti, A., Bonfond, B., Roussos, E., & Paranicas, C. (2018). Evolution of the Auroral
472 Signatures of Jupiter's Magnetospheric Injections. *Journal of Geophysical Research: Space Physics*, 0(0).
473 <https://doi.org/10.1029/2018JA025708>

474 Dungey, J. W. (1961). Interplanetary Magnetic Field and the Auroral Zones. *Physical Review Letters*, 6(2), 47–48.
475 <https://doi.org/10.1103/PhysRevLett.6.47>

476 Ebert, R. W., Allegrini, F., Bagenal, F., Bolton, S. J., Connerney, J. E. P., Clark, G., et al. (2017). Accelerated flows
477 at Jupiter's magnetopause: Evidence for magnetic reconnection along the dawn flank. *Geophysical*
478 *Research Letters*, 44(10), 4401–4409. <https://doi.org/10.1002/2016GL072187>

479 Forsyth, C., Sergeev, V. A., Henderson, M. G., Nishimura, Y., & Gallardo-Lacourt, B. (2020). Physical Processes of
480 Meso-Scale, Dynamic Auroral Forms. *Space Science Reviews*, 216(4), 46. [https://doi.org/10.1007/s11214-](https://doi.org/10.1007/s11214-020-00665-y)
481 [020-00665-y](https://doi.org/10.1007/s11214-020-00665-y)

482 Gabrielse, C., Spanswick, E., Artemyev, A., Nishimura, Y., Runov, A., Lyons, L., et al. (2019). Utilizing the
483 Heliophysics/Geospace System Observatory to Understand Particle Injections: Their Scale Sizes and
484 Propagation Directions. *Journal of Geophysical Research: Space Physics*, *124*(7), 5584–5609.
485 <https://doi.org/10.1029/2018JA025588>

486 Ge, Y. S., Jian, L. K., & Russell, C. T. (2007). Growth phase of Jovian substorms. *Geophysical Research Letters*,
487 *34*(23). <https://doi.org/10.1029/2007GL031987>

488 Ge, Y. S., Russell, C. T., & Khurana, K. K. (2010). Reconnection sites in Jupiter’s magnetotail and relation to
489 Jovian auroras. *Planetary and Space Science*, *58*(11), 1455–1469. <https://doi.org/10.1016/j.pss.2010.06.013>

490 Gérard, J. C., Grodent, D., Dols, V., Prangé, R., Waite, J. H., Gladstone, G. R., et al. (1994). A Remarkable Auroral
491 Event on Jupiter Observed in the Ultraviolet with the Hubble Space Telescope. *Science*, *266*(5191), 1675–
492 1678. <https://doi.org/10.1126/science.266.5191.1675>

493 Gérard, J.-C., Gkouvelis, L., Bonfond, B., Grodent, D., Gladstone, G. R., Hue, V., et al. (2020). Spatial distribution
494 of the Pedersen conductance in the Jovian aurora from Juno-UVS spectral images. *Journal of Geophysical*
495 *Research: Space Physics*, *n/a*(n/a), e2020JA028142. <https://doi.org/10.1029/2020JA028142>

496 Gjerloev, J. W., Hoffman, R. A., Friel, M. M., Frank, L. A., & Sigwarth, J. B. (2004). Substorm behavior of the
497 auroral electrojet indices. *Annales Geophysicae*, *22*(6), 2135–2149. [https://doi.org/10.5194/angeo-22-2135-](https://doi.org/10.5194/angeo-22-2135-2004)
498 2004

499 Gjerloev, J. W., Hoffman, R. A., Sigwarth, J. B., & Frank, L. A. (2007). Statistical description of the bulge-type
500 auroral substorm in the far ultraviolet. *Journal of Geophysical Research: Space Physics*, *112*(A7).
501 <https://doi.org/10.1029/2006JA012189>

502 Gjerloev, J. W., Hoffman, R. A., Sigwarth, J. B., Frank, L. A., & Baker, J. B. H. (2008). Typical auroral substorm:
503 A bifurcated oval. *Journal of Geophysical Research: Space Physics*, *113*(A3).
504 <https://doi.org/10.1029/2007JA012431>

505 Gladstone, G. R., Persyn, S. C., Eterno, J. S., Walther, B. C., Slater, D. C., Davis, M. W., et al. (2017). The
506 Ultraviolet Spectrograph on NASA’s Juno Mission. *Space Science Reviews*, *213*(1), 447–473.
507 <https://doi.org/10.1007/s11214-014-0040-z>

508 Gray, R. L., Badman, S. V., Bonfond, B., Kimura, T., Misawa, H., Nichols, J. D., et al. (2016). Auroral evidence of
509 radial transport at Jupiter during January 2014. *Journal of Geophysical Research: Space Physics*, *121*(10),
510 9972–9984. <https://doi.org/10.1002/2016JA023007>

511 Greathouse, T. K., Gladstone, G. R., Davis, M. W., Slater, D. C., Versteeg, M. H., Persson, K. B., et al. (2013).
512 Performance results from in-flight commissioning of the Juno Ultraviolet Spectrograph (Juno-UVS). In
513 *UV, X-Ray, and Gamma-Ray Space Instrumentation for Astronomy XVIII* (Vol. 8859, p. 88590T).
514 International Society for Optics and Photonics. <https://doi.org/10.1117/12.2024537>

515 Grodent, D., Gérard, J.-C., Clarke, J. T., Gladstone, G. R., & Waite, J. H. (2004). A possible auroral signature of a
516 magnetotail reconnection process on Jupiter. *Journal of Geophysical Research: Space Physics*, *109*(A5).
517 <https://doi.org/10.1029/2003JA010341>

518 Grodent, Denis, Bonfond, B., Yao, Z., Gérard, J.-C., Radioti, A., Dumont, M., et al. (2018). Jupiter’s Aurora
519 Observed With HST During Juno Orbits 3 to 7. *Journal of Geophysical Research: Space Physics*, *123*(5),
520 3299–3319. <https://doi.org/10.1002/2017JA025046>

521 Gustin, J., Cowley, S. W. H., Gérard, J.-C., Gladstone, G. R., Grodent, D., & Clarke, J. T. (2006). Characteristics of
522 Jovian morning bright FUV aurora from Hubble Space Telescope/Space Telescope Imaging Spectrograph
523 imaging and spectral observations. *Journal of Geophysical Research: Space Physics*, *111*(A9).
524 <https://doi.org/10.1029/2006JA011730>

525 Hameiri, E., Laurence, P., & Mond, M. (1991). The ballooning instability in space plasmas. *Journal of Geophysical*
526 *Research: Space Physics*, *96*(A2), 1513–1526. <https://doi.org/10.1029/90JA02100>

527 Henderson, M. G. (2009). Observational evidence for an inside-out substorm onset scenario. *Annales Geophysicae*,
528 *27*(5), 2129–2140. <https://doi.org/10.5194/angeo-27-2129-2009>

529 Hue, V., Gladstone, G. R., Greathouse, T. K., Kammer, J. A., Davis, M. W., Bonfond, B., et al. (2019). In-flight
530 Characterization and Calibration of the Juno-ultraviolet Spectrograph (Juno-UVS). *The Astronomical*
531 *Journal*, *157*(2), 90. <https://doi.org/10.3847/1538-3881/aafb36>

532 Kalmoni, N. M. E., Rae, I. J., Watt, C. E. J., Murphy, K. R., Samara, M., Michell, R. G., et al. (2018). A diagnosis of
533 the plasma waves responsible for the explosive energy release of substorm onset. *Nature Communications*,
534 *9*(1), 4806. <https://doi.org/10.1038/s41467-018-07086-0>

535 Kimura, T., Nichols, J. D., Gray, R. L., Tao, C., Murakami, G., Yamazaki, A., et al. (2017). Transient brightening of
536 Jupiter's aurora observed by the Hisaki satellite and Hubble Space Telescope during approach phase of the
537 Juno spacecraft. *Geophysical Research Letters*, *44*(10), 4523–4531. <https://doi.org/10.1002/2017GL072912>

538 Kivelson, M. G. (2015). Planetary Magnetodiscs: Some Unanswered Questions. *Space Science Reviews*, *187*(1), 5–
539 21. <https://doi.org/10.1007/s11214-014-0046-6>

540 Korth, H., Zhang, Y., Anderson, B. J., Sotirelis, T., & Waters, C. L. (2014). Statistical relationship between large-
541 scale upward field-aligned currents and electron precipitation. *Journal of Geophysical Research: Space*
542 *Physics*, *119*(8), 6715–6731. <https://doi.org/10.1002/2014JA019961>

543 Kronberg, E. A., Woch, J., Krupp, N., Lagg, A., Khurana, K. K., & Glassmeier, K.-H. (2005). Mass release at
544 Jupiter: Substorm-like processes in the Jovian magnetotail. *Journal of Geophysical Research: Space*
545 *Physics*, *110*(A3). <https://doi.org/10.1029/2004JA010777>

546 Kronberg, E. A., Glassmeier, K.-H., Woch, J., Krupp, N., Lagg, A., & Dougherty, M. K. (2007). A possible intrinsic
547 mechanism for the quasi-periodic dynamics of the Jovian magnetosphere. *Journal of Geophysical*
548 *Research: Space Physics*, *112*(A5). <https://doi.org/10.1029/2006JA011994>

549 Kronberg, E. A., Woch, J., Krupp, N., Lagg, A., Daly, P. W., & Korth, A. (2008). Comparison of periodic substorms
550 at Jupiter and Earth: PERIODIC SUBSTORMS AT JUPITER AND EARTH. *Journal of Geophysical*
551 *Research: Space Physics*, *113*(A4), n/a-n/a. <https://doi.org/10.1029/2007JA012880>

552 Krupp, N., Woch, J., Lagg, A., Wilken, B., Livi, S., & Williams, D. J. (1998). Energetic particle bursts in the
553 predawn Jovian magnetotail. *Geophysical Research Letters*, *25*(8), 1249–1252.
554 <https://doi.org/10.1029/98GL00863>

555 Kullen, A., & Karlsson, T. (2004). On the relation between solar wind, pseudobreakups, and substorms. *Journal of*
556 *Geophysical Research: Space Physics*, *109*(A12). <https://doi.org/10.1029/2004JA010488>

557 Liou, K., Newell, P. T., Zhang, Y.-L., & Paxton, L. J. (2013). Statistical comparison of isolated and non-isolated
558 auroral substorms. *Journal of Geophysical Research: Space Physics*, *118*(5), 2466–2477.
559 <https://doi.org/10.1002/jgra.50218>

560 Louarn, P., Roux, A., Perraut, S., Kurth, W. S., & Gurnett, D. A. (2000). A study of the Jovian “energetic
561 magnetospheric events” observed by Galileo: role in the radial plasma transport. *Journal of Geophysical*
562 *Research: Space Physics*, *105*(A6), 13073–13088. <https://doi.org/10.1029/1999JA900478>

563 Louarn, P., Paranicas, C. P., & Kurth, W. S. (2014). Global magnetodisk disturbances and energetic particle
564 injections at Jupiter. *Journal of Geophysical Research: Space Physics*, *119*(6), 4495–4511.
565 <https://doi.org/10.1002/2014JA019846>

566 Lui, A. T. Y., Chang, C.-L., Mankofsky, A., Wong, H.-K., & Winske, D. (1991). A cross-field current instability for
567 substorm expansions. *Journal of Geophysical Research: Space Physics*, *96*(A7), 11389–11401.
568 <https://doi.org/10.1029/91JA00892>

569 Lui, Anthony T. Y. (2015). Magnetospheric Substorm Onset by Current Disruption Processes. In *Auroral Dynamics*
570 *and Space Weather* (pp. 163–176). American Geophysical Union (AGU).
571 <https://doi.org/10.1002/9781118978719.ch12>

572 Manners, H., Masters, A., & Yates, J. N. (2018). Standing Alfvén Waves in Jupiter’s Magnetosphere as a Source of
573 ~10- to 60-Min Quasiperiodic Pulsations. *Geophysical Research Letters*, *45*(17), 8746–8754.
574 <https://doi.org/10.1029/2018GL078891>

575 Masters, A. (2017). Model-Based Assessments of Magnetic Reconnection and Kelvin-Helmholtz Instability at
576 Jupiter’s Magnetopause. *Journal of Geophysical Research: Space Physics*, *122*(11), 11,154–11,174.
577 <https://doi.org/10.1002/2017JA024736>

578 Mauk, B., & Bagenal, F. (2013). Comparative Auroral Physics: Earth and Other Planets. In *Auroral Phenomenology*
579 *and Magnetospheric Processes: Earth And Other Planets* (pp. 3–26). American Geophysical Union
580 (AGU). <https://doi.org/10.1029/2011GM001192>

581 Mauk, B. H., Williams, D. J., & McEntire, R. W. (1997). Energy-time dispersed charged particle signatures of
582 dynamic injections in Jupiter’s inner magnetosphere. *Geophysical Research Letters*, *24*(23), 2949–2952.
583 <https://doi.org/10.1029/97GL03026>

584 Miyashita, Y., & Ieda, A. (2018). Revisiting substorm events with preonset aurora. *Annales Geophysicae*, *36*(5),
585 1419–1438. <https://doi.org/10.5194/angeo-36-1419-2018>

586 Mura, A., Adriani, A., Altieri, F., Connerney, J. E. P., Bolton, S. J., Moriconi, M. L., et al. (2017). Infrared
587 observations of Jovian aurora from Juno’s first orbits: Main oval and satellite footprints. *Geophysical*
588 *Research Letters*, *44*, 5308–5316. <https://doi.org/10.1002/2017GL072954>

589 Murphy, K. R., Mann, I. R., Rae, I. J., Walsh, A. P., & Frey, H. U. (2014). Inner magnetospheric onset preceding
590 reconnection and tail dynamics during substorms: Can substorms initiate in two different regions? *Journal*
591 *of Geophysical Research: Space Physics*, *119*(12), 9684–9701. <https://doi.org/10.1002/2014JA019795>

592 Nichols, J. D., Clarke, J. T., Gérard, J. C., Grodent, D., & Hansen, K. C. (2009). Variation of different components
593 of Jupiter’s auroral emission. *Journal of Geophysical Research (Space Physics)*, *114*(A13), A06210.
594 <https://doi.org/10.1029/2009JA014051>

595 Nishimura, Y., Lyons, L., Zou, S., Angelopoulos, V., & Mende, S. (2010). Substorm triggering by new plasma
596 intrusion: THEMIS all-sky imager observations. *Journal of Geophysical Research: Space Physics*,
597 *115*(A7). <https://doi.org/10.1029/2009JA015166>

598 Nishimura, Y., Lyons, L. R., Angelopoulos, V., Kikuchi, T., Zou, S., & Mende, S. B. (2011). Relations between
599 multiple auroral streamers, pre-onset thin arc formation, and substorm auroral onset. *Journal of*
600 *Geophysical Research: Space Physics*, *116*(A9). <https://doi.org/10.1029/2011JA016768>

601 Oberhagemann, L. R., & Mann, I. R. (2020). A New Substorm Onset Mechanism: Increasingly Parallel Pressure
602 Anisotropic Ballooning. *Geophysical Research Letters*, *47*(2), e2019GL085271.
603 <https://doi.org/10.1029/2019GL085271>

604 Panov, E. V., Lu, S., & Pritchett, P. L. (2020). Understanding Spacecraft Trajectories Through Detached
605 Magnetotail Interchange Heads. *Journal of Geophysical Research: Space Physics*, *125*(5), e2020JA027930.
606 <https://doi.org/10.1029/2020JA027930>

607 Pulkkinen, T. I., Baker, D. N., Wiltberger, M., Goodrich, C., Lopez, R. E., & Lyon, J. G. (1998). Pseudobreakup and
608 substorm onset: Observations and MHD simulations compared. *Journal of Geophysical Research: Space*
609 *Physics*, *103*(A7), 14847–14854. <https://doi.org/10.1029/97JA03244>

610 Radioti, A., Grodent, D., Gérard, J.-C., Vogt, M. F., Lystrup, M., & Bonfond, B. (2011). Nightside reconnection at
611 Jupiter: Auroral and magnetic field observations from 26 July 1998. *Journal of Geophysical Research:*
612 *Space Physics*, *116*(A3). <https://doi.org/10.1029/2010JA016200>

613 Radioti, A., Grodent, D., Gérard, J.-C., Bonfond, B., Gustin, J., Pryor, W., et al. (2013). Auroral signatures of
614 multiple magnetopause reconnection at Saturn. *Geophysical Research Letters*, *40*(17), 4498–4502.
615 <https://doi.org/10.1002/grl.50889>

616 Radioti, A., Yao, Z., Grodent, D., Palmaerts, B., Roussos, E., Dialynas, K., et al. (2019). Auroral Beads at Saturn
617 and the Driving Mechanism: Cassini Proximal Orbits. *The Astrophysical Journal*, 885(1), L16.
618 <https://doi.org/10.3847/2041-8213/ab4e20>

619 Rostoker, G., Akasofu, S.-I., Foster, J., Greenwald, R. A., Kamide, Y., Kawasaki, K., et al. (1980). Magnetospheric
620 substorms—definition and signatures. *Journal of Geophysical Research: Space Physics*, 85(A4), 1663–
621 1668. <https://doi.org/10.1029/JA085iA04p01663>

622 Sergeev, V. A., Kornilova, T. A., Kornilov, I. A., Angelopoulos, V., Kubyshkina, M. V., Fillingim, M., et al. (2010).
623 Auroral signatures of the plasma injection and dipolarization in the inner magnetosphere. *Journal of*
624 *Geophysical Research: Space Physics*, 115(A2). <https://doi.org/10.1029/2009JA014522>

625 Tao, C., Kataoka, R., Fukunishi, H., Takahashi, Y., & Yokoyama, T. (2005). Magnetic field variations in the Jovian
626 magnetotail induced by solar wind dynamic pressure enhancements. *Journal of Geophysical Research:*
627 *Space Physics*, 110(A11). <https://doi.org/10.1029/2004JA010959>

628 Vasyliunas, V. M. (1983). Physics of the Jovian magnetosphere. In A. J. Dessler (Ed.), *Physics of the Jovian*
629 *Magnetosphere* (pp. 395–453). Cambridge University Press.

630 Viñas, A. F., & Madden, T. R. (1986). Shear flow-ballooning instability as a possible mechanism for hydromagnetic
631 fluctuations. *Journal of Geophysical Research: Space Physics*, 91(A2), 1519–1528.
632 <https://doi.org/10.1029/JA091iA02p01519>

633 Vogt, M. F., Kivelson, M. G., Khurana, K. K., Joy, S. P., & Walker, R. J. (2010). Reconnection and flows in the
634 Jovian magnetotail as inferred from magnetometer observations. *Journal of Geophysical Research: Space*
635 *Physics*, 115(A6). <https://doi.org/10.1029/2009JA015098>

636 Vogt, M. F., Bunce, E. J., Kivelson, M. G., Khurana, K. K., Walker, R. J., Radioti, A., et al. (2015). Magnetosphere-
637 ionosphere mapping at Jupiter: Quantifying the effects of using different internal field models. *Journal of*
638 *Geophysical Research: Space Physics*, 120(4), 2584–2599. <https://doi.org/10.1002/2014JA020729>

639 Vogt, M. F., Gyalay, S., Kronberg, E. A., Bunce, E. J., Kurth, W. S., Zieger, B., & Tao, C. (2019). Solar Wind
640 Interaction With Jupiter’s Magnetosphere: A Statistical Study of Galileo In Situ Data and Modeled
641 Upstream Solar Wind Conditions. *Journal of Geophysical Research: Space Physics*, 124(12), 10170–
642 10199. <https://doi.org/10.1029/2019JA026950>

643 Woch, J., Krupp, N., & Lagg, A. (2002). Particle bursts in the Jovian magnetosphere: Evidence for a near-Jupiter
644 neutral line. *Geophysical Research Letters*, 29(7), 42-1-42-4. <https://doi.org/10.1029/2001GL014080>
645 Yao, Z., Pu, Z. Y., Rae, I. J., Radioti, A., & Kubyshkina, M. V. (2017). Auroral streamer and its role in driving
646 wave-like pre-onset aurora. *Geoscience Letters*, 4(1), 8. <https://doi.org/10.1186/s40562-017-0075-6>
647 Yao, Z. H., Bonfond, B., Grodent, D., Chané, E., Dunn, W. R., Kurth, W. S., et al. (2020). Auroral diagnosis of solar
648 wind interaction with Jupiter's magnetosphere. *ArXiv:2004.10140 [Physics]*. Retrieved from
649 <http://arxiv.org/abs/2004.10140>
650 Yao, Z. H., Bonfond, B., Clark, G., Grodent, D., Dunn, W. R., Vogt, M. F., et al. (2020). Reconnection- and
651 Dipolarization-Driven Auroral Dawn Storms and Injections. *Journal of Geophysical Research: Space*
652 *Physics*, 125(8), e2019JA027663. <https://doi.org/10.1029/2019JA027663>
653 Zhang, B., Delamere, P. A., Yao, Z., Bonfond, B., Lin, D., Sorathia, K. A., et al. (2020). How Jupiter's Unusual
654 Magnetospheric Topology Structures Its Aurora. *ArXiv E-Prints*, 2006, arXiv:2006.14834.

655

656 Data

657 The data included herein are either archived in NASA's Planetary Data System ([http://pds-](http://pds-atmospheres.nmsu.edu/data_and_services/atmospheres_data/JUNO/juno.html)
658 [atmospheres.nmsu.edu/data_and_services/atmospheres_data/JUNO/juno.html](http://pds-atmospheres.nmsu.edu/data_and_services/atmospheres_data/JUNO/juno.html)). This research is
659 also based on publicly available observations acquired with the NASA/ESA Hubble Space
660 Telescope and obtained at the Space Telescope Science Institute, which is operated by AURA
661 for NASA (<https://archive.stsci.edu/hst/search.php>). Data analysis was performed with the
662 AMDA science analysis system provided by the Centre de Données de la Physique des Plasmas
663 (CDPP) supported by CNRS, CNES, Observatoire de Paris and Université Paul Sabatier,
664 Toulouse. The THEMIS data are available from <http://themis.ssl.berkeley.edu/data/themis/>. The
665 IMAGE-WIC images can be accessed at <https://spdf.gsfc.nasa.gov/pub/data/image/fuv/> and were
666 processed using the FUVIEW3 software (<http://sprg.ssl.berkeley.edu/image/>).

667

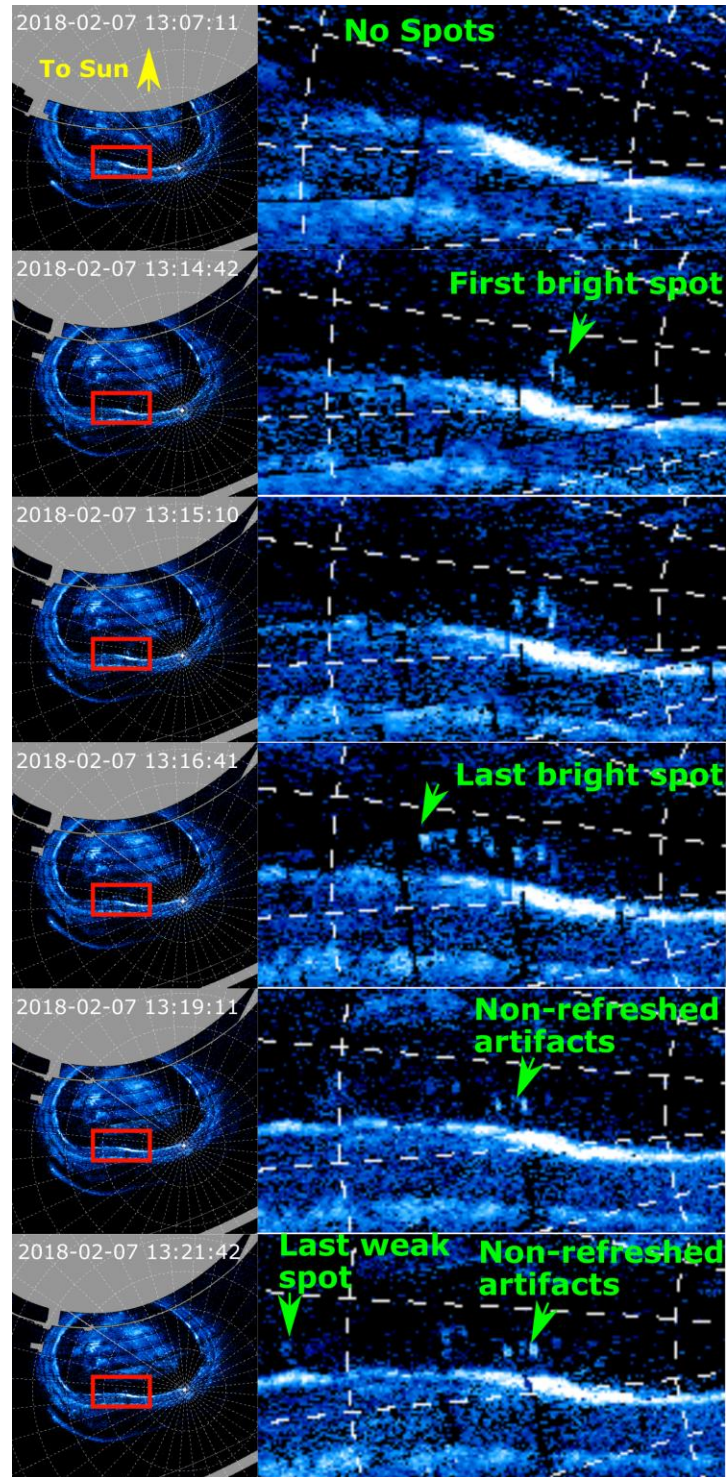
668 Acknowledgments

669 The authors are grateful to J.E.P. Connerney for helpful discussions concerning the manuscript.
670 B.B. is a Research Associate of the Fonds de la Recherche Scientifique - FNRS. We are grateful
671 to NASA and contributing institutions which have made the Juno mission possible. This work
672 was funded by NASA's New Frontiers Program for Juno via contract with the Southwest
673 Research Institute. B.B., D.G., J.-C.G., B.P. and J.M. acknowledge financial support from the
674 Belgian Federal Science Policy Office (BELSPO) via the PRODEX Programme of ESA. The
675 research at the University of Iowa was supported by NASA through Contract 699041X with

676 Southwest Research Institute. The authors wish to thank the International Space Science Institute
677 in Beijing (ISSI-BJ) for supporting and hosting the meetings of the International Team on 'The
678 morphology of auroras at Earth and giant planets: characteristics and their magnetospheric
679 implications', during which the discussions leading/contributing to this publication were held.;
680 **Author contributions:** Preparation of the manuscript, figures, calculations, data analysis was
681 performed by B.B and Z.Y.; additional help for the production of several figures by J.M. and
682 A.M.; data interpretation was performed by B.B., Z.Y., D.G., C.T. and A.M.; revisions of the
683 manuscript were made by B.B., Z.Y., G.G., D.G., J.-C.G., J.M., T.G., V.H., R.G., B.P. C.T.,
684 M.Vo. and W.K.; S.B. is the Juno principal investigator; G.G. is responsible for the UVS
685 instrument; A.A. is responsible for the JIRAM instrument; D.G. is the principal investigator of
686 the GO14634 HST campaign; modeling of the solar wind propagation by C.T.; modeling of the
687 Jovian magnetic field mapping by M.Vo.; preparation for measurements and data acquisition was
688 performed by G.G., V.H., T.G., M.Ve., J.K. and B.B.; calibration was done by G.G., V.H., T.G.,
689 J.K. and R.G.

690 **Supplementary Materials:**

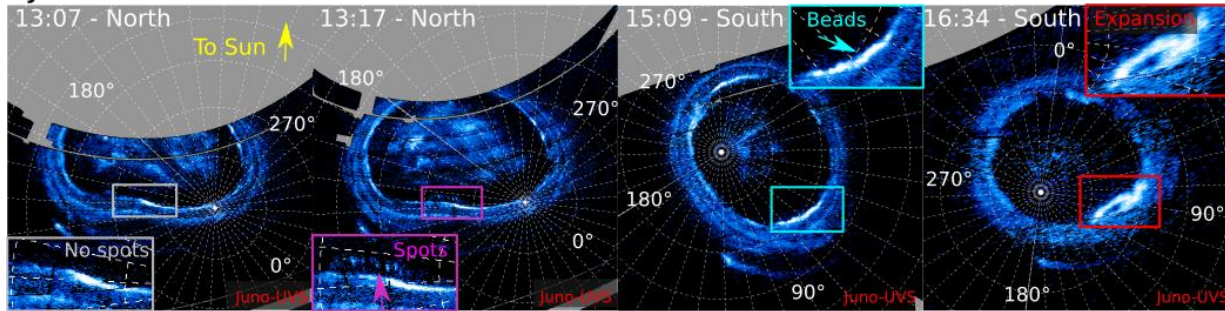
691 Figures S1-S9



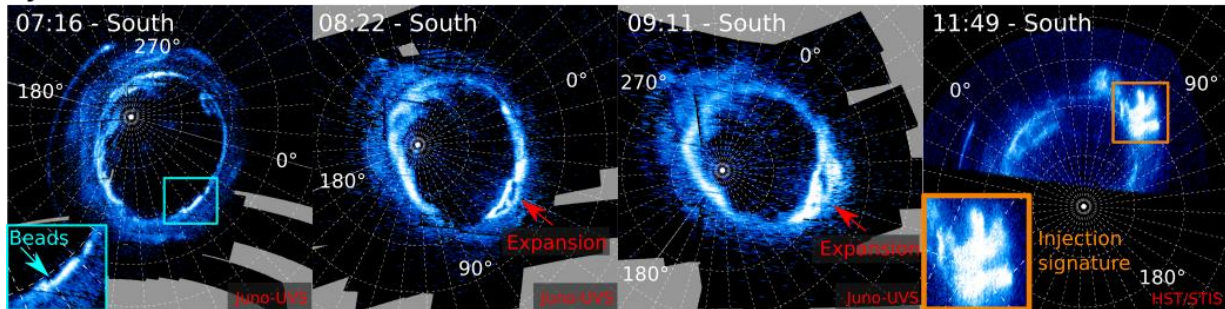
693
694
695
696
697
698
699
700

Figure 1. Details of the development of the transient spots during the PJ11 dawn storm. A polar projection of the whole northern aurora is shown on the left and a zoom on the region boxed in red is shown on the right. The Sun direction is towards the top and dashed lines show System III meridians and planetocentric parallel spaced every 10° . Bright spots of the size of the instrument al PSF successively appeared from dawn to dusk, approximately 1000 km apart. The two bright spots remaining on the center of the last two frames are due to the non-refreshment of this part of the image.

PJ11



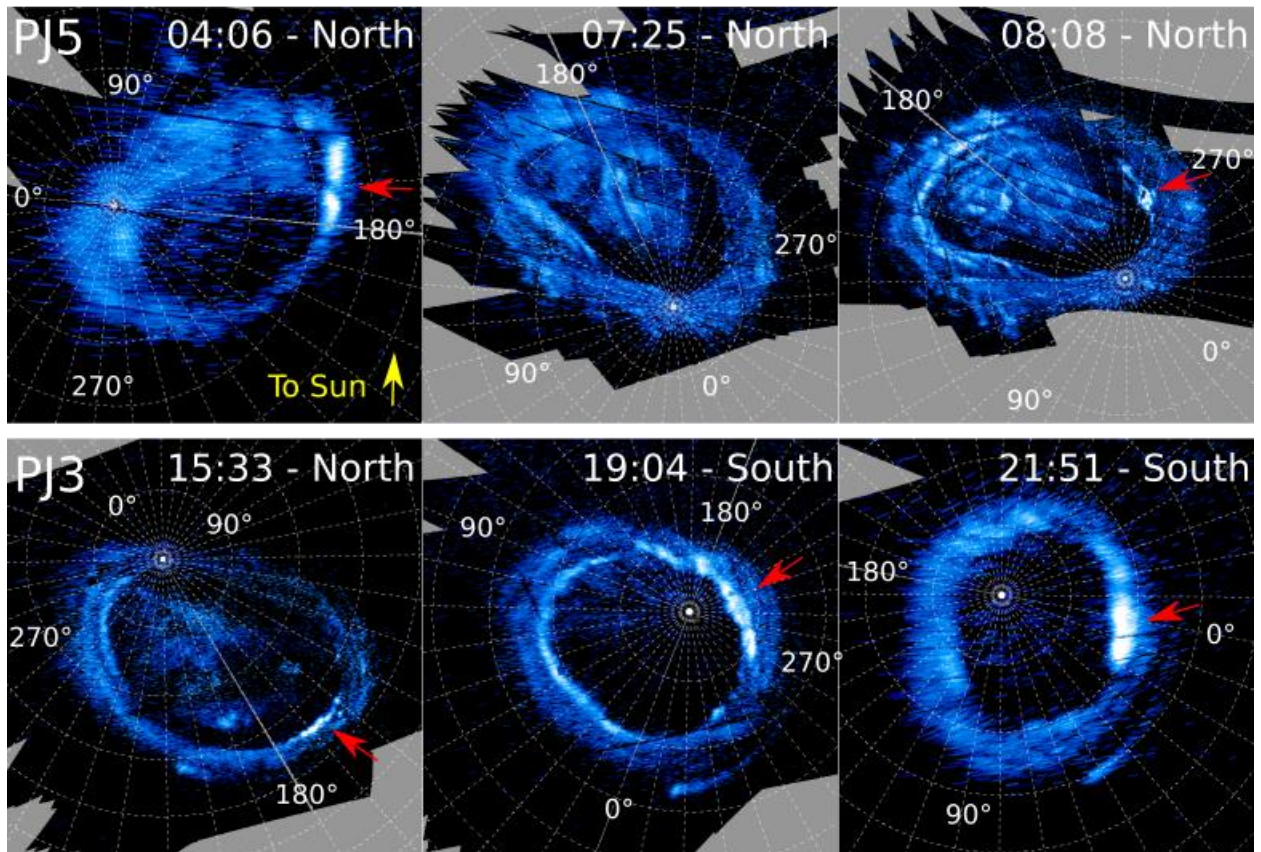
PJ6



701
702
703
704
705
706
707
708
709

Figure 2. Polar projection of the development of a dawn storm, based on observations acquired by Juno-UVS and HST/STIS during the 11th and the 6th perijove sequences. On PJ11, the event was preceded by the progressive appearance of a set of transient spots poleward of the main emission. Two hours later, the dawn storm itself started as an enhancement of the main emission in the form of beads before the arc began to fork and expand, both latitudinally and longitudinally. On the PJ6 sequence, the same sequence of emergence of beads, followed by the expansion phase is observed, but subsequent observations by both Juno-UVS and HST-STIS show that the equatorward arc transforms into a large injection signature.

Non-Isolated Dawn Storms



711

712

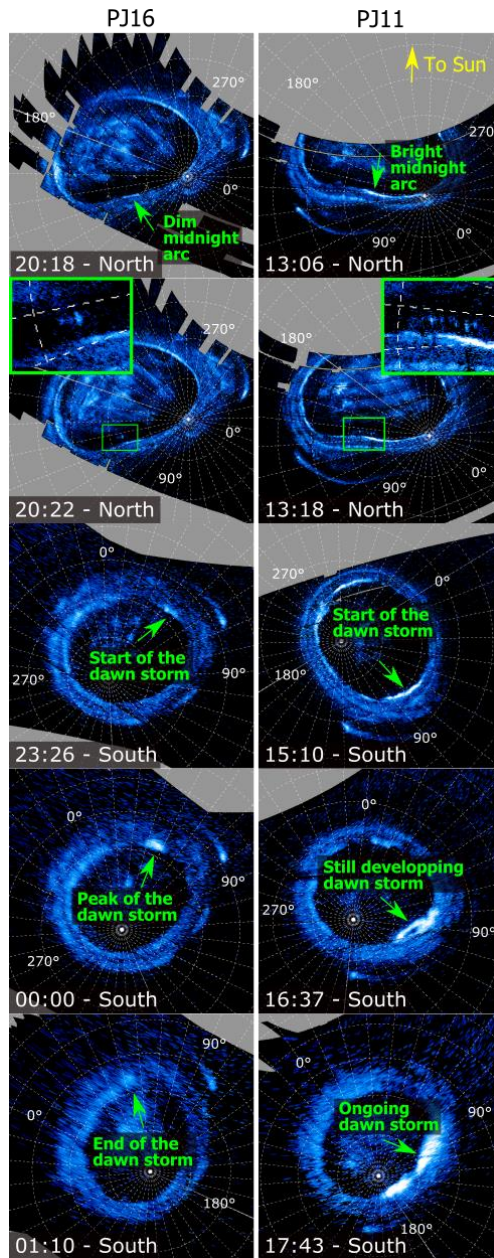
713

714

Figure 3. Polar projections of the development of non-isolated dawn storms during PJ3 and PJ5. The red arrow highlights the dawn storms. During PJ5, a second dawn storm took place ~3 hours after the first one. On PJ3, new dawn storms seem to appear during all the southern branch of the perijove sequence.

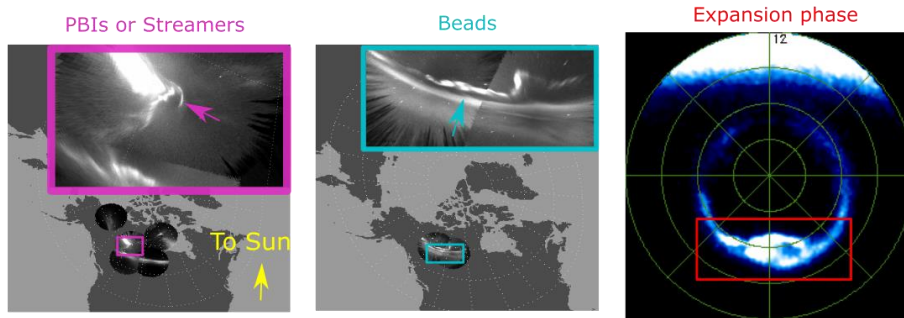
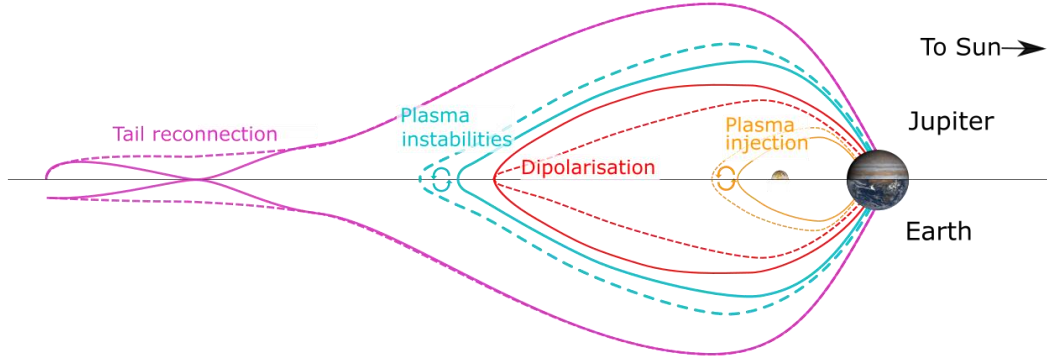
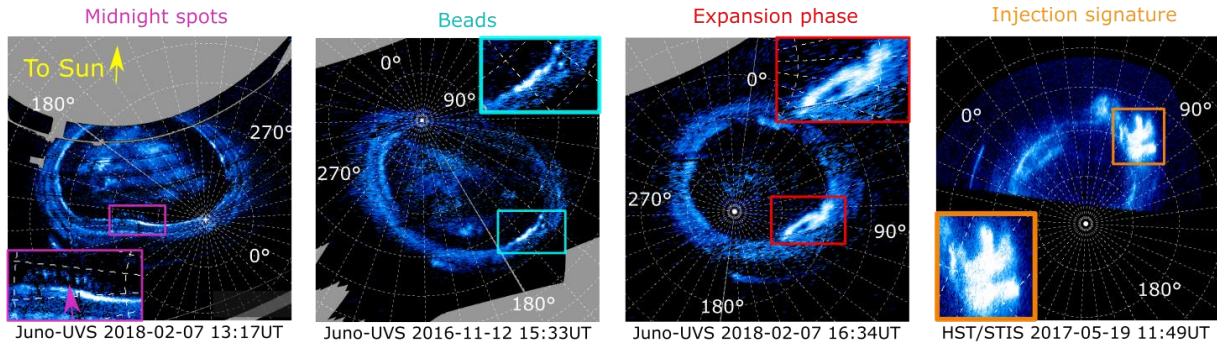
715

716



717
718
719
720
721

Figure 4. The left column shows polar projections of the aurorae during the 16th perijove, and the right column shows a similar sequence for the 11th perijove. While the sequence on PJ11 compares with a terrestrial substorm (Figure 1), the one on PJ16 is much more limited in size, emitted power and duration and would be more similar to a terrestrial pseudo-breakup.



722
 723 *Figure 5. Polar projections of the UV aurora showing four different phases of a Jovian dawn storm: 1) the short*
 724 *lived polar midnight spots, 2) the formation of irregularities on the main emission pre-dawn part 3) the expansion*
 725 *phase, with the two arcs splitting and 4) the injection signatures in the outer emission. The first three images are*
 726 *based on data from the Juno-UVS instrument and the fourth one comes from Hubble Space Telescope observations*
 727 *carried out to support Juno. These four phases appear to correspond to nightside tail reconnection, plasma*
 728 *instabilities, current disruption/dipolarization in the middle magnetosphere and to flux tube interchange,*
 729 *respectively, as illustrated in the general scheme shown in the central scheme (not to scale). These auroral features*
 730 *corresponding to these phases in the terrestrial aurora are show on the bottom raw. In the bottom, the first two*
 731 *images come from the THEMIS network of all-sky cameras (Nishimura et al., 2010; Z. Yao et al., 2017). The first two*
 732 *image corresponds to Earth's aurora as seen from IMAGE-WIC.*

733
 734

735
736

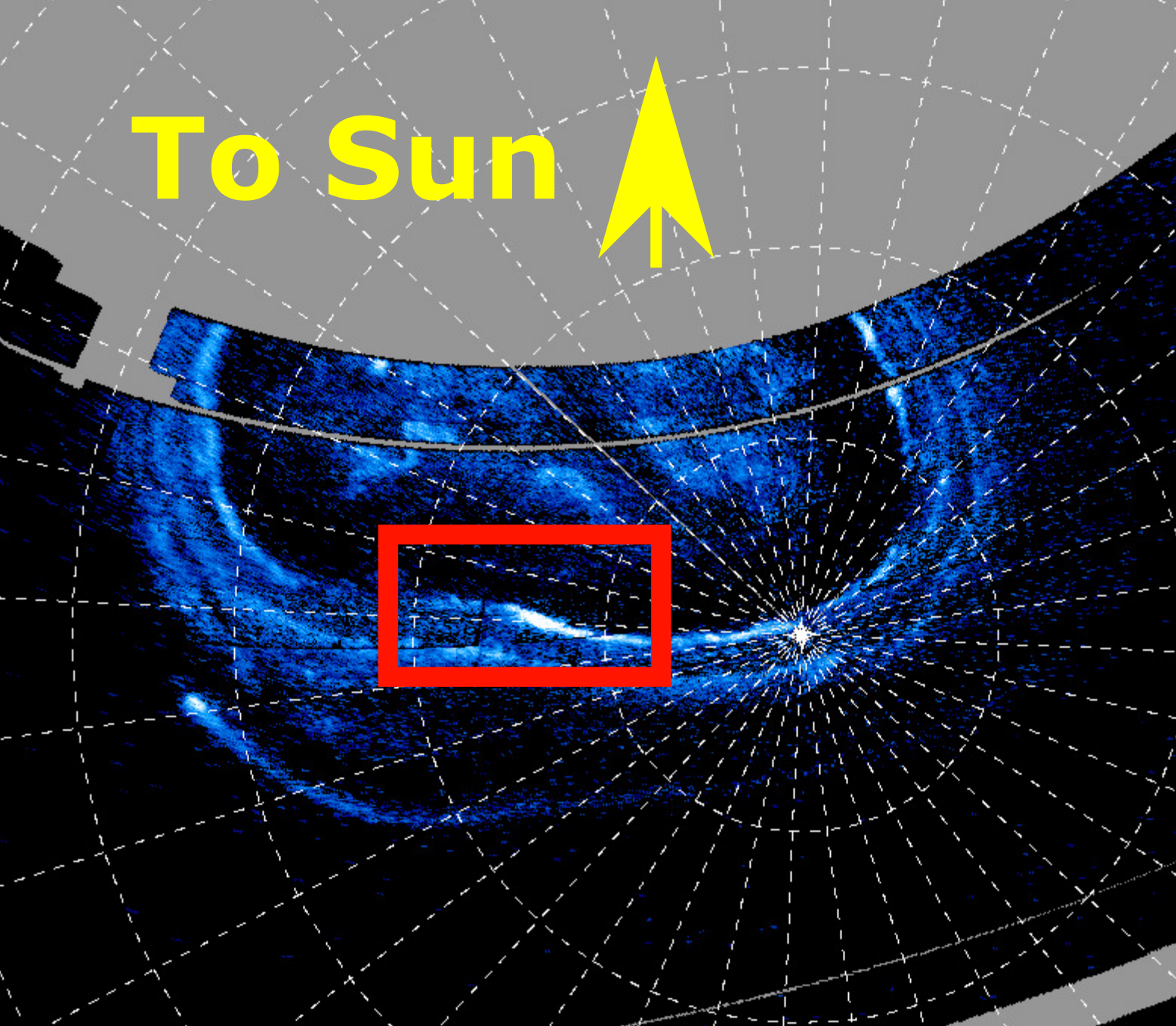
	date	Peak power (W)	Identified features
PJ1	27 Aug 2016 18:00 => 20:00		b?, e
PJ3	11 Dec 2016 15:10 = > 22:02	8.1 10 ¹¹	b, e, g, nids
PJ5	27 Mar 2017 3:56 => 06:00 7 :33=> 11 :09	1.5 10 ¹¹ 1.1 10 ¹¹	e, g, i, nids
PJ6	19 May 2017 07:14 => 10:54	1.6 10 ¹²	b?, e, i
PJ7	10 Jul 2017 22:43 => 00:00	2.7 10 ¹¹	e, i
PJ9	24 Oct 2017 12:19 => 13:50	6.0 10 ¹¹	e
PJ11	07 Feb 2018 12:58 => 18:49	8.5 10 ¹¹	s, b, e, g
PJ14	16 Jul 2018 08:42=> 10:15	6.5 10 ¹¹	e
PJ16	29 Oct 2018 23:20=> 01:00	1.4 10 ¹¹	s, e, i?
PJ20	29 May 2019 09 :30 => 12 :54	9.2 10 ¹¹	e, g, i

737
738
739
740
741
742
743
744
745
746

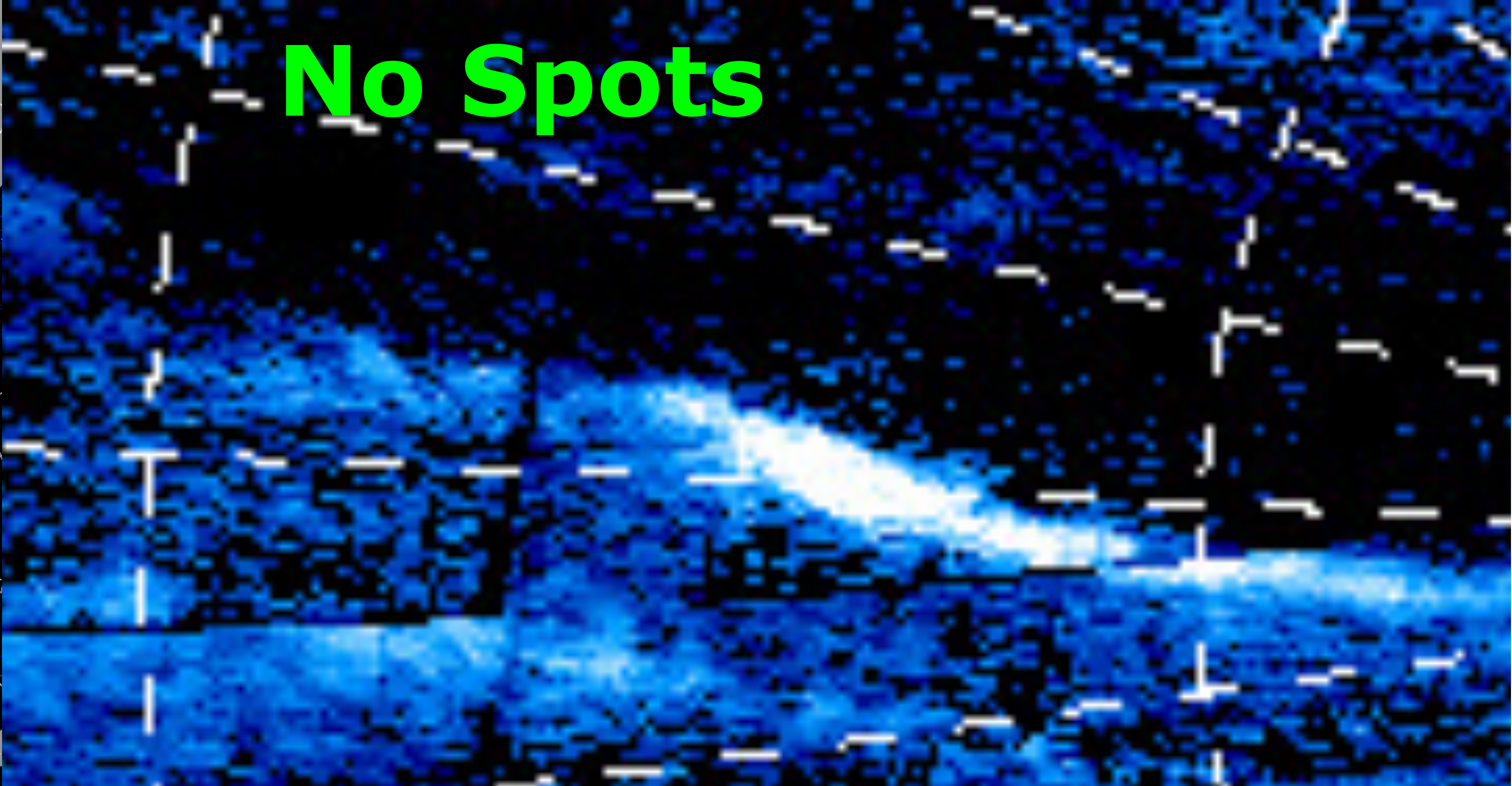
Table 1. List of the dawn storms identified during Juno's perijove observations sequences. The second column collects the approximate times of the expansion phases of the dawn storm. The end time in particular are approximate, as there is no clear criterion for when the phenomenon is finished. Start and end times in bold indicate that the observations started or ended at the indicated time, but the dawn storm probably lasted longer. The third column indicates the peak power reached by the dawn storm and the fourth column indicates the observed feature during this sequence, (s) meaning the spots, (b) the beads, (e) the expansion, (g) the gap, (i) the injections and (nids) the occurrence of non-isolated dawn storms. The PJ1 dawn storm started after the end of the UVS observations, but the beginning of the expansion phase was observed with the JIRAM (Jovian InfraRed Auroral Mapper) instrument (Adriani et al., 2017; Mura et al., 2017) (Figure S9).

2018-02-07 13:07:11

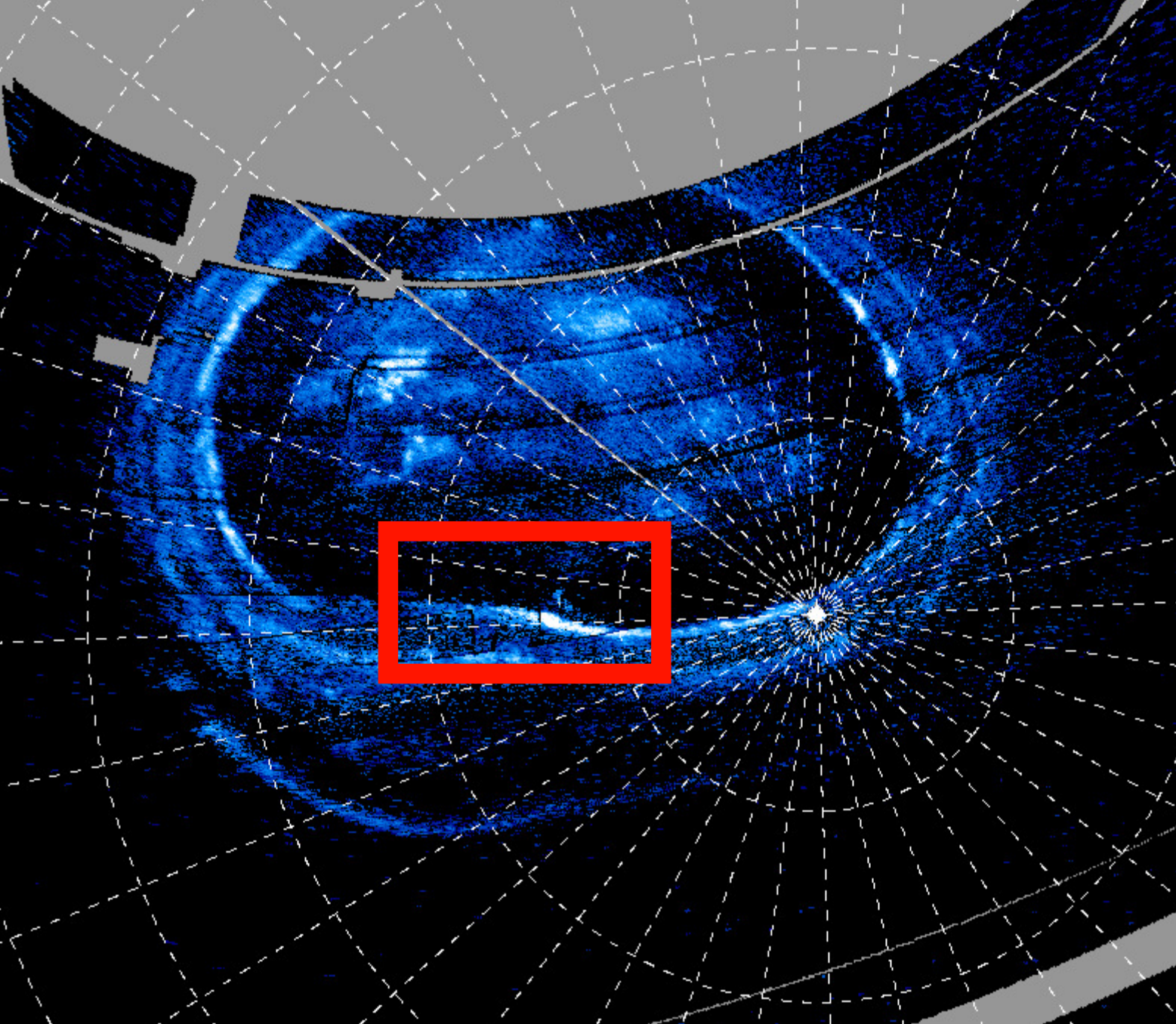
To Sun 



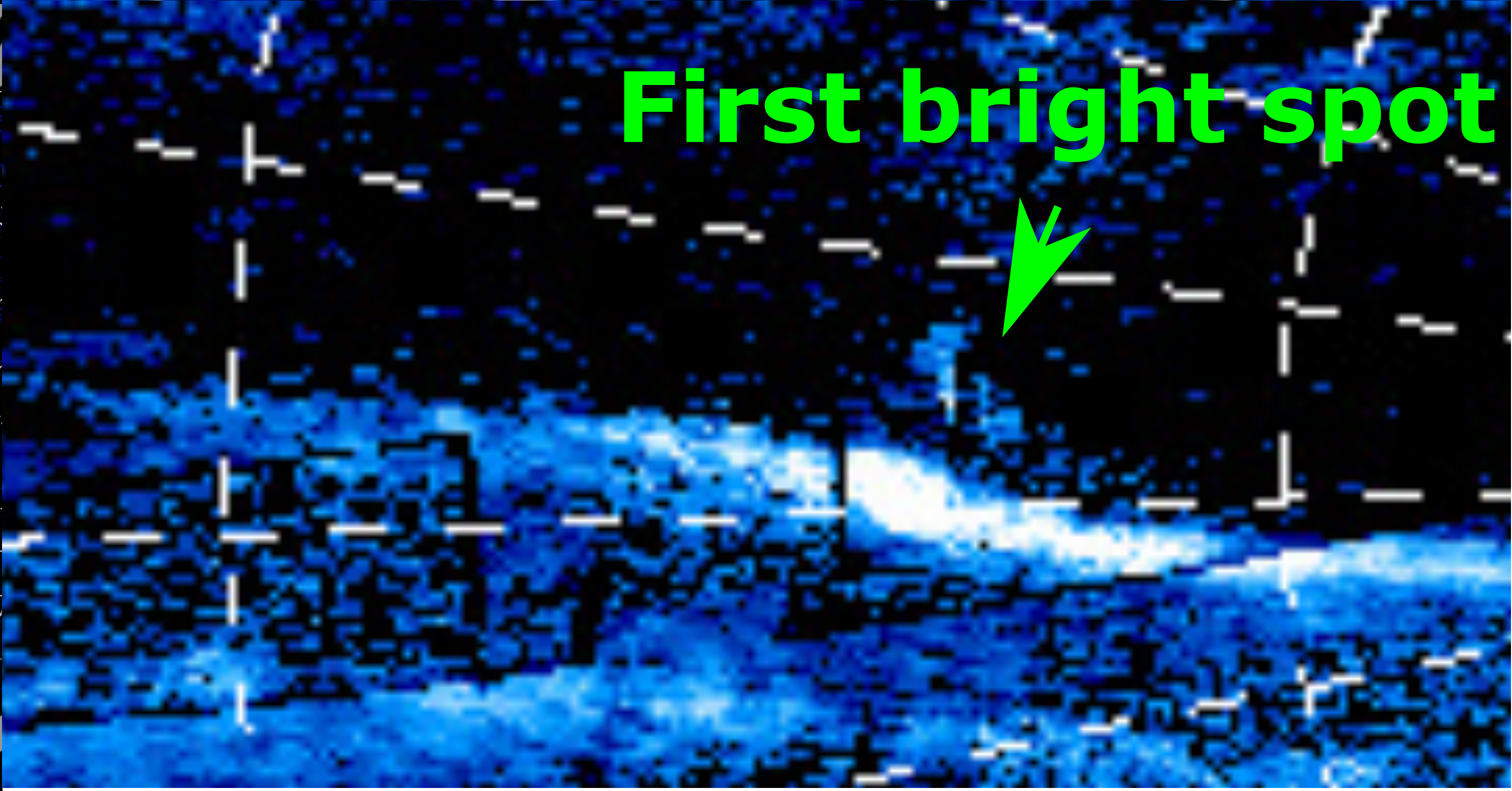
No Spots



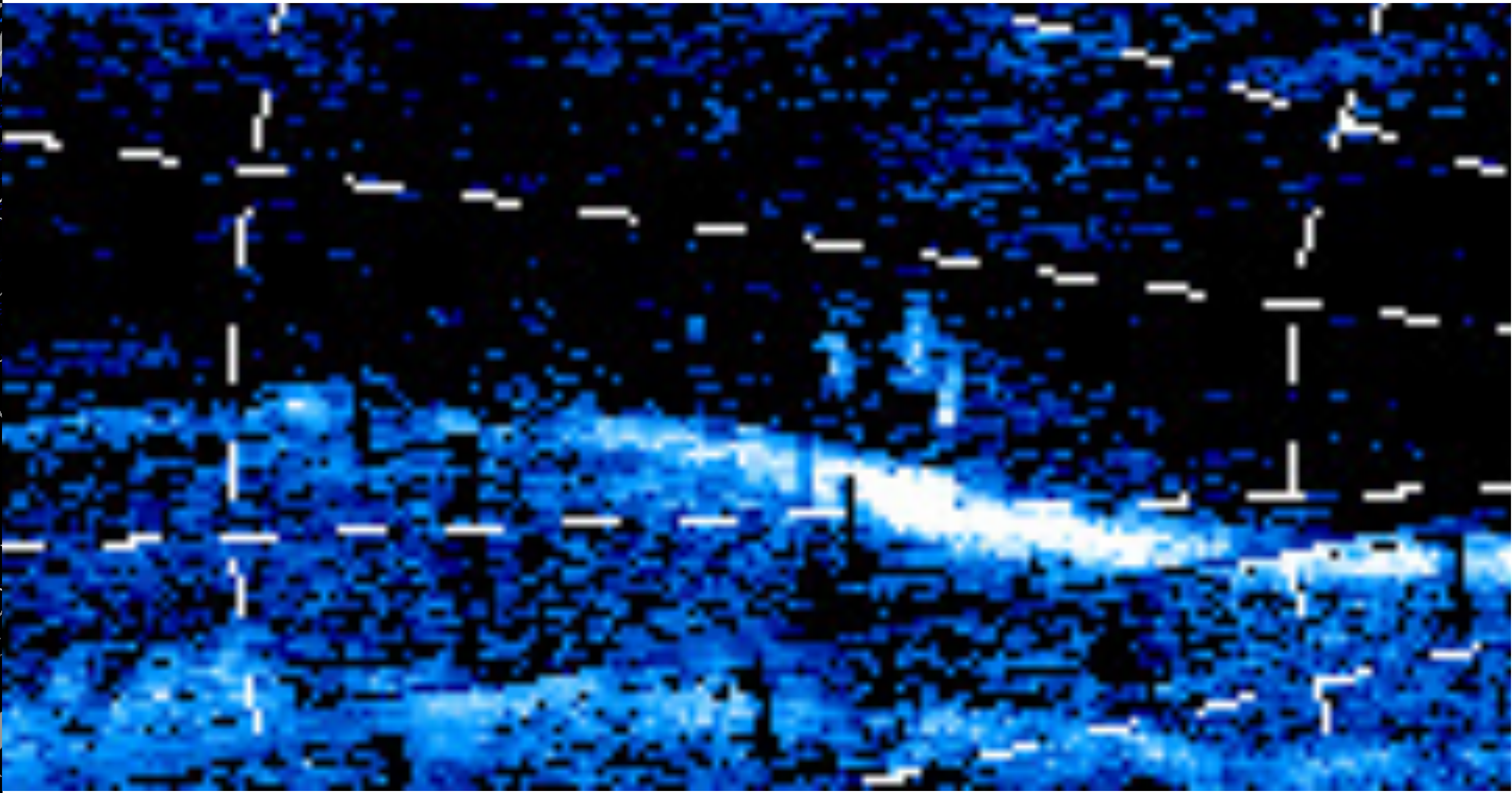
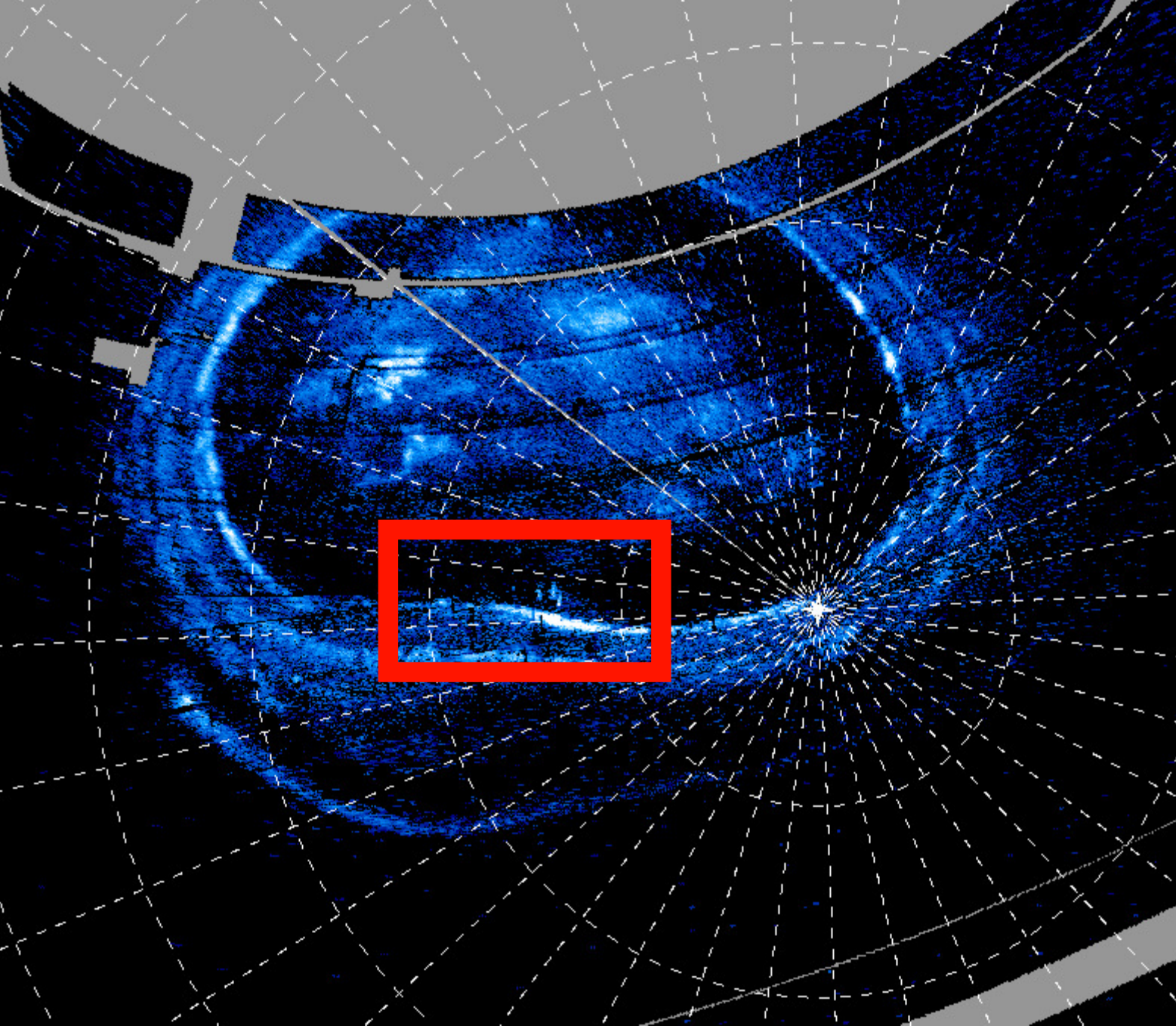
2018-02-07 13:14:42



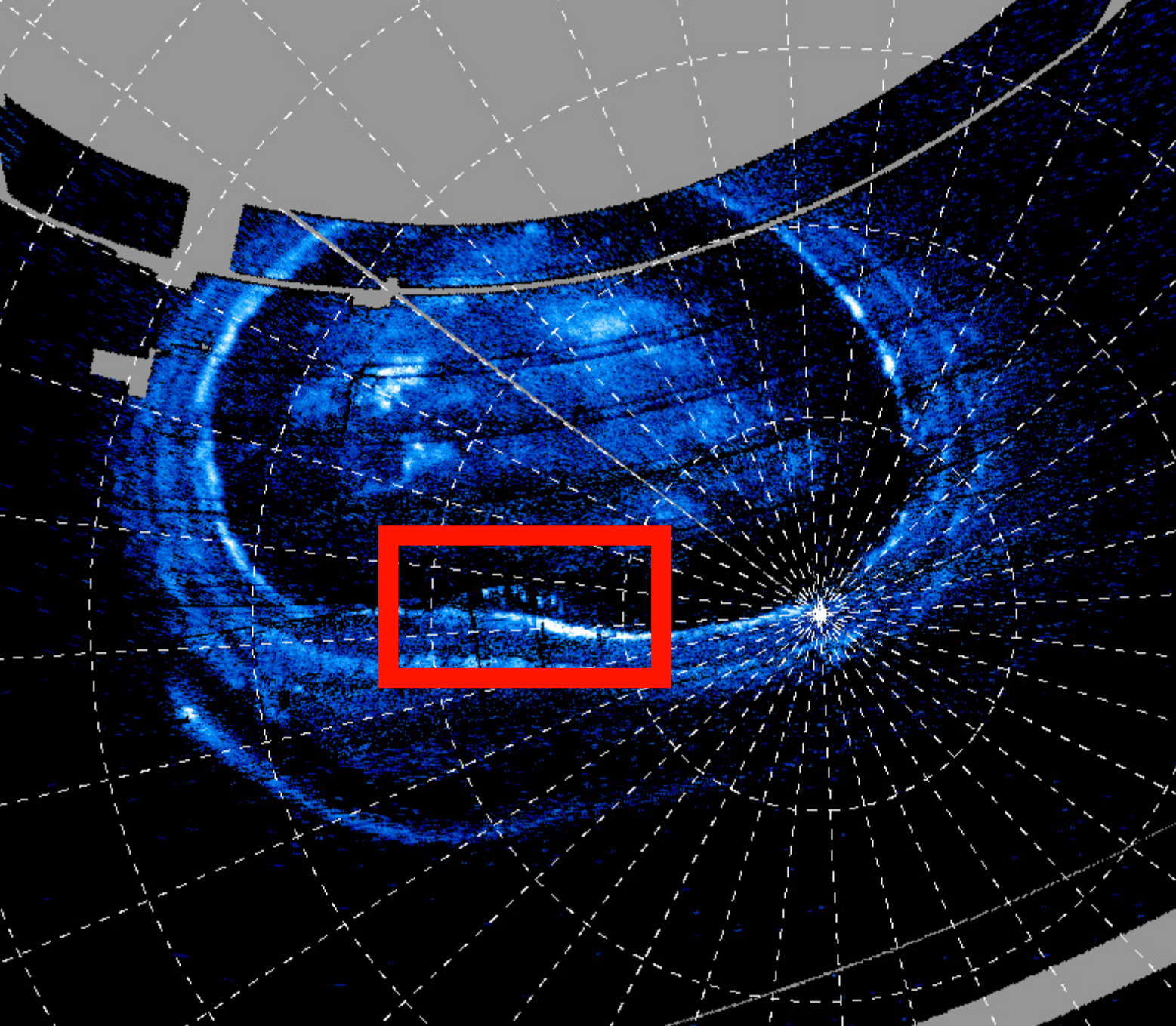
First bright spot



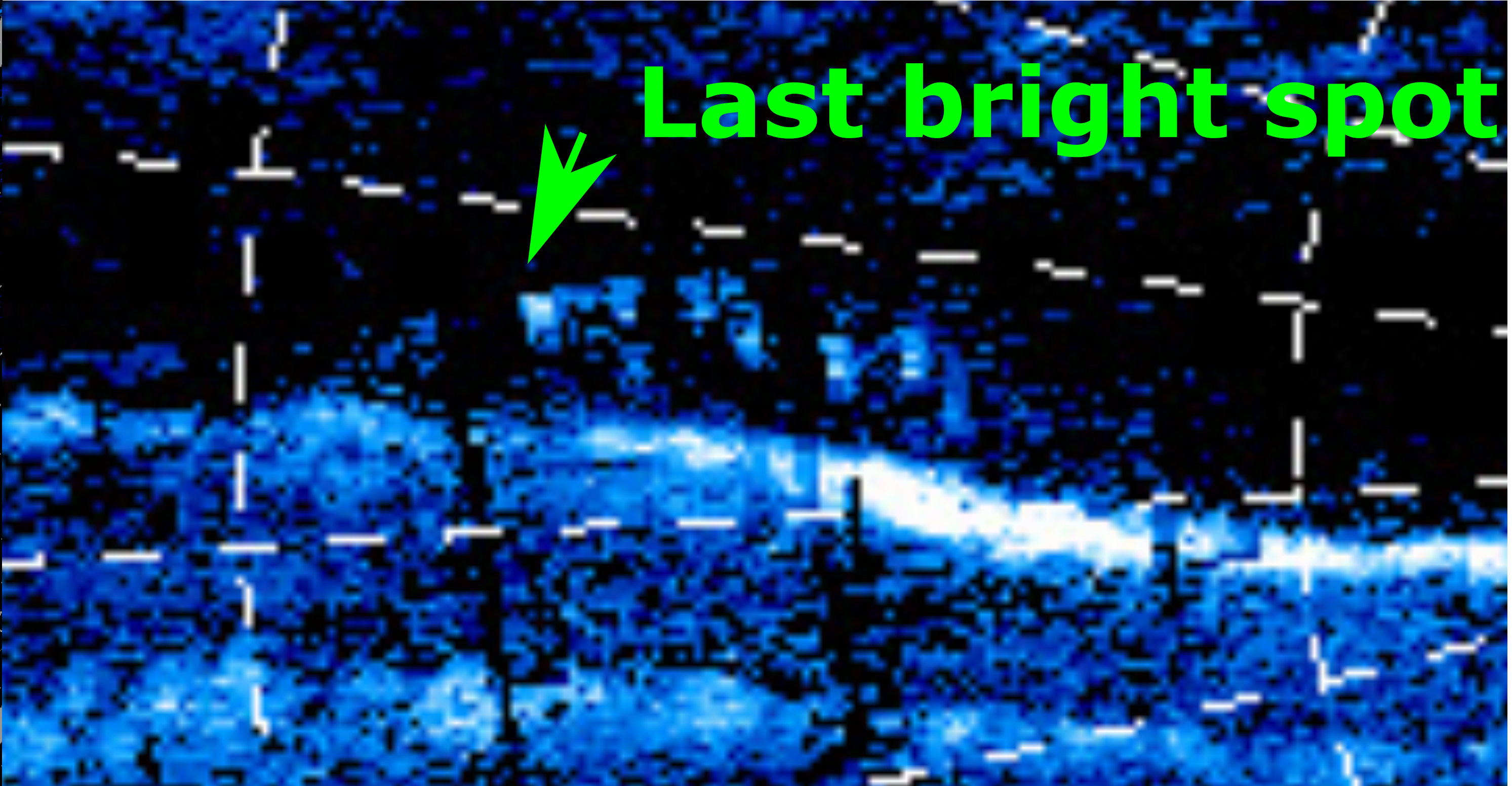
2018-02-07 13:15:10



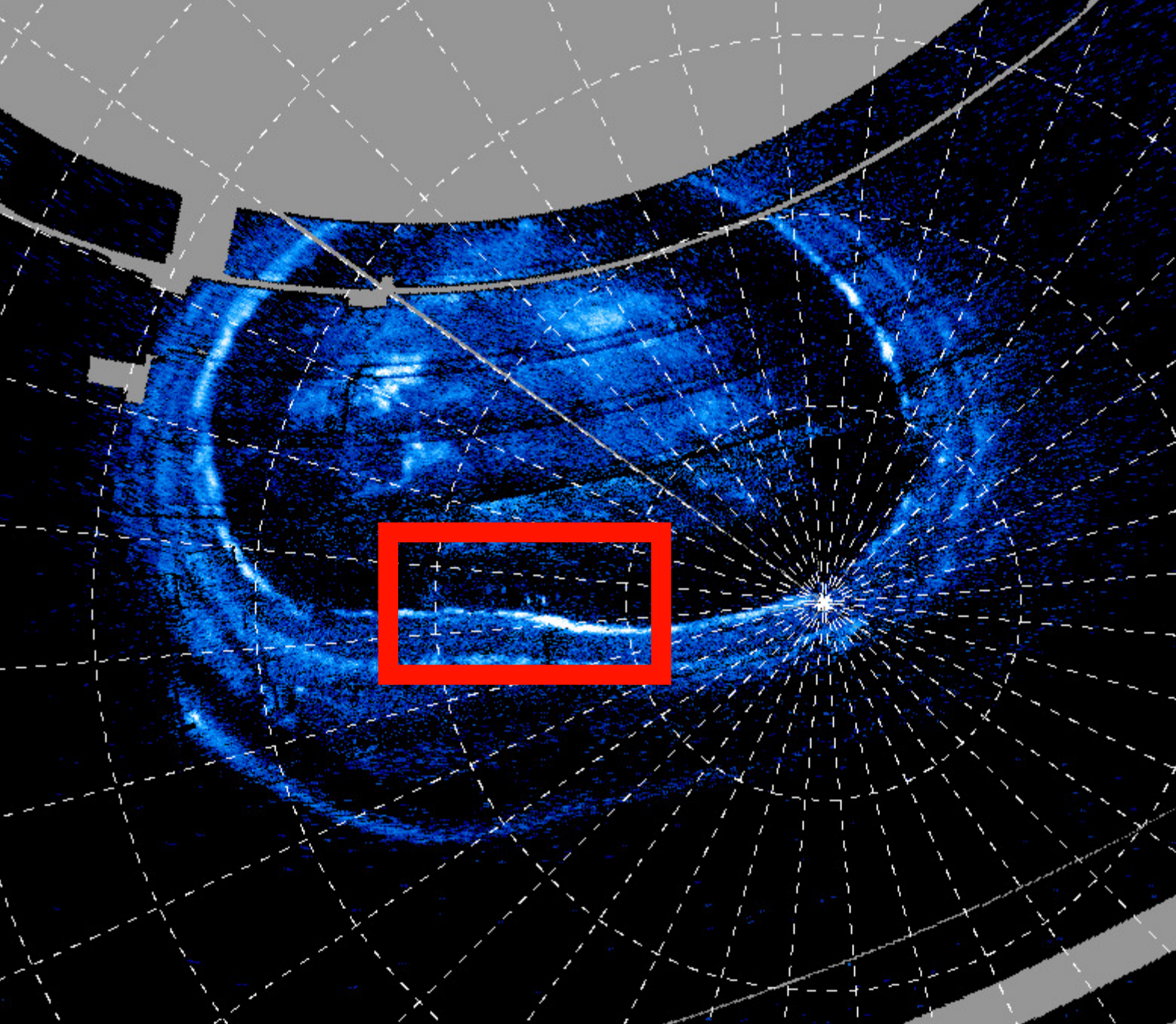
2018-02-07 13:16:41



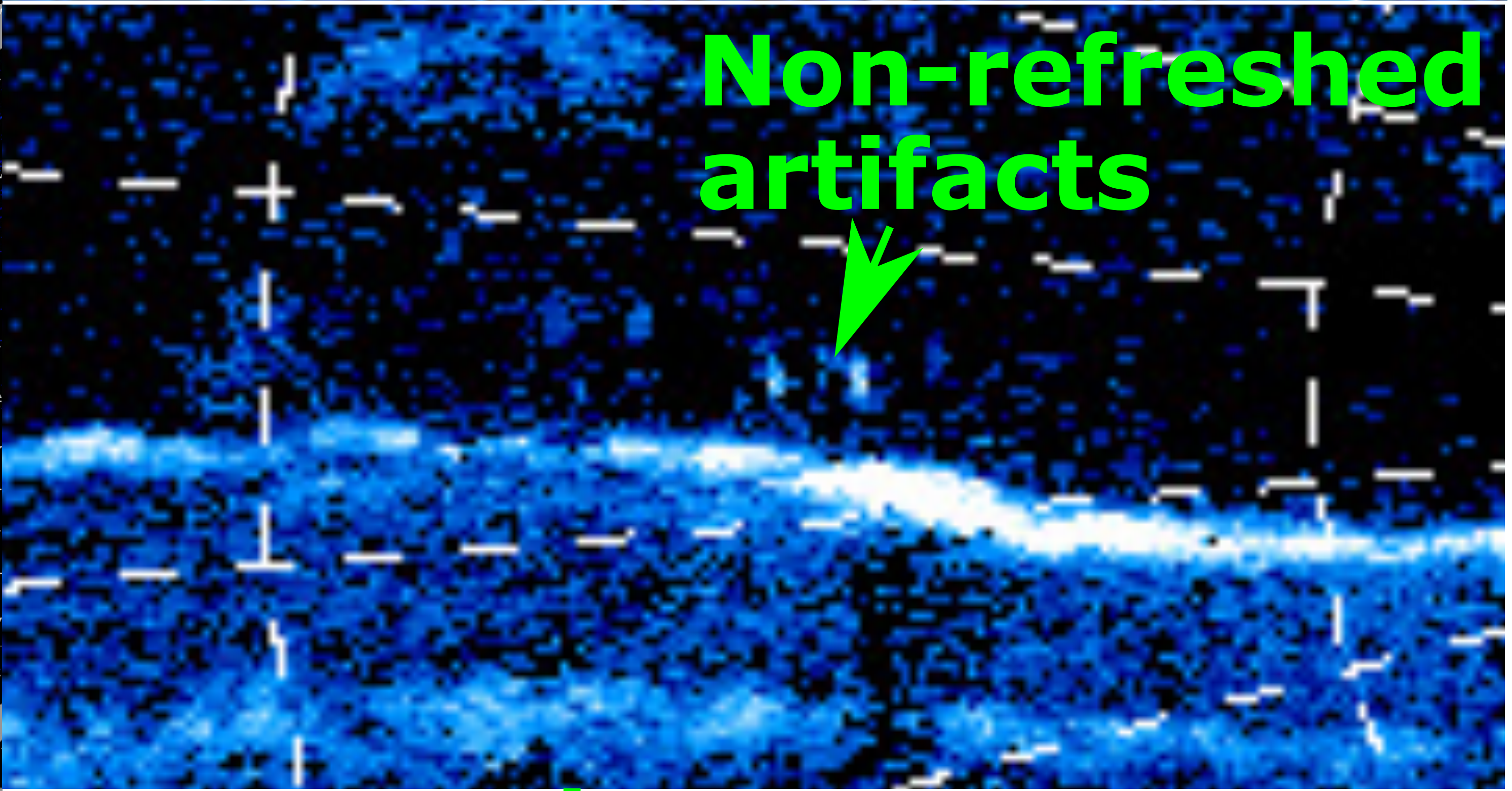
Last bright spot



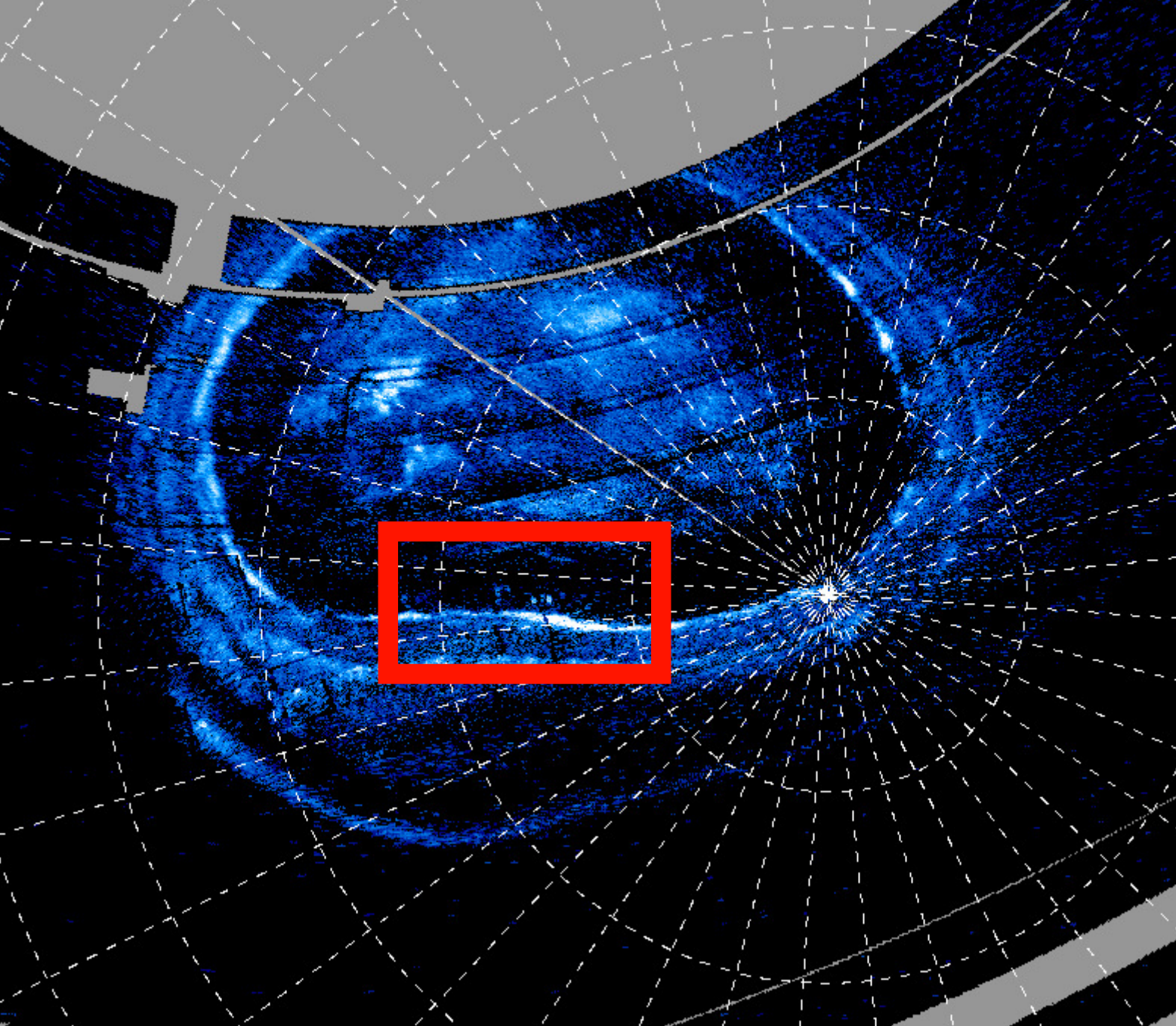
2018-02-07 13:19:11



Non-refreshed artifacts

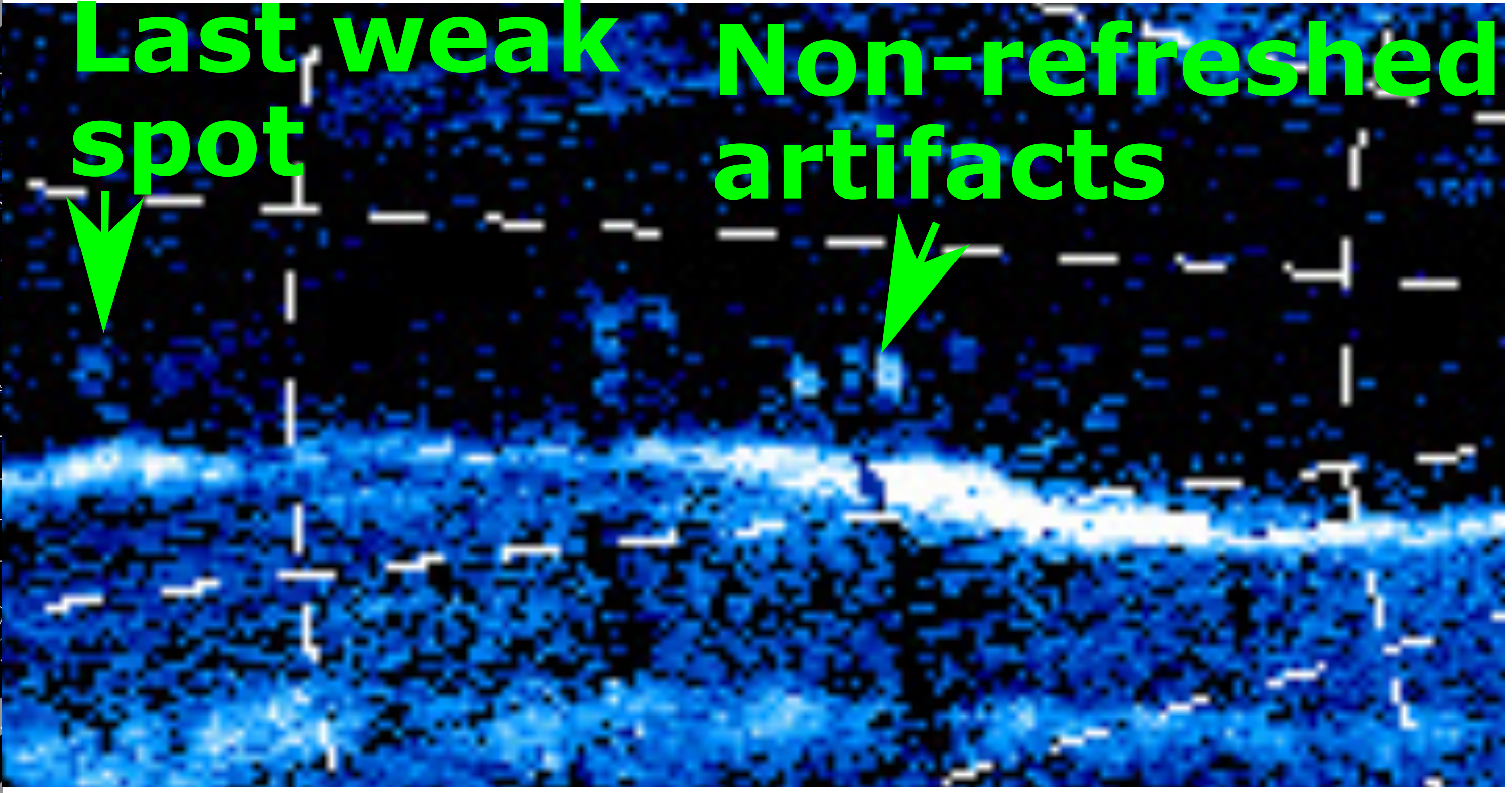


2018-02-07 13:21:42

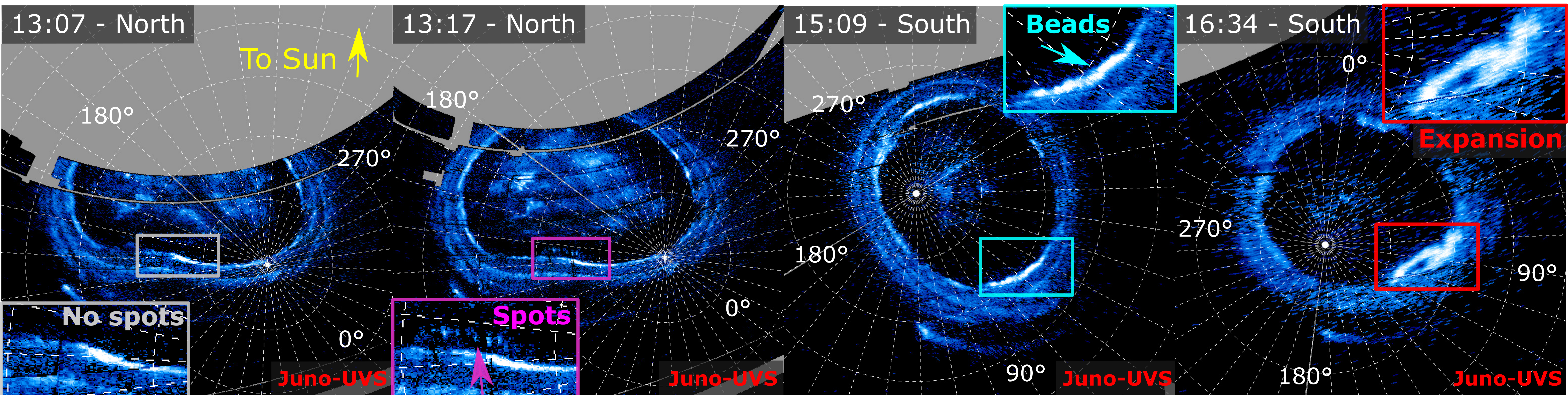


Last weak spot

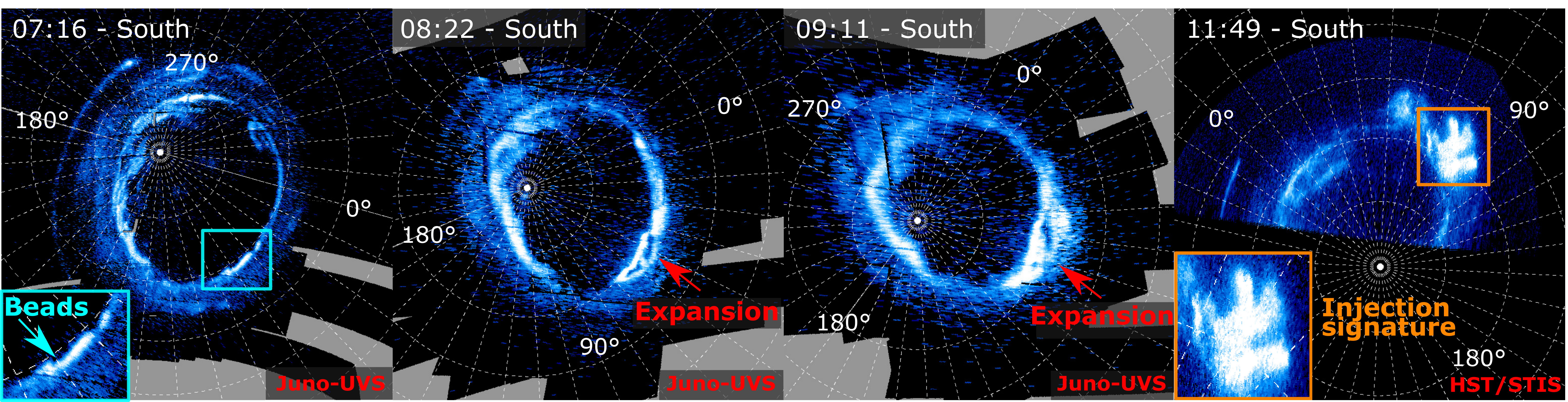
Non-refreshed artifacts



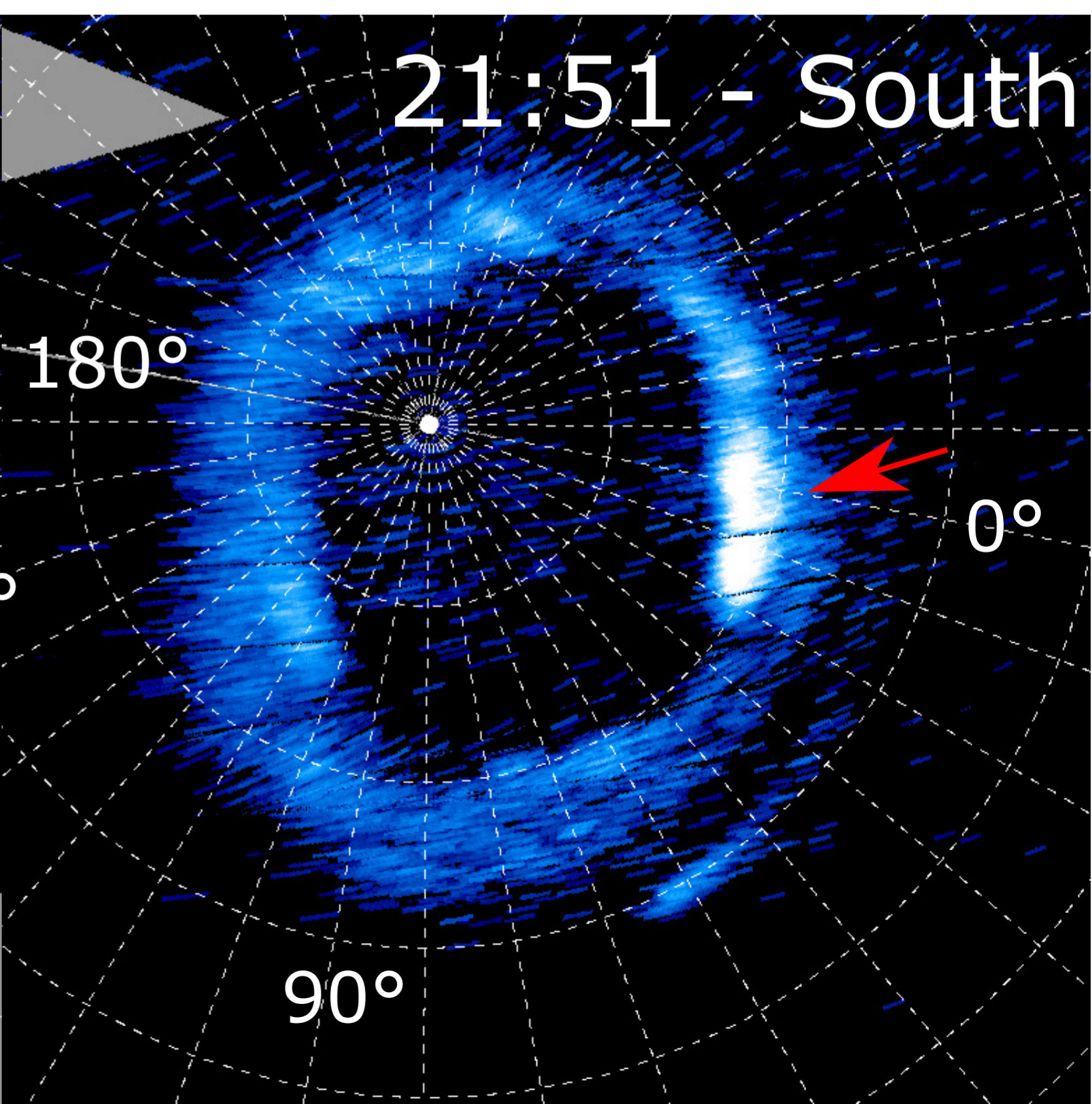
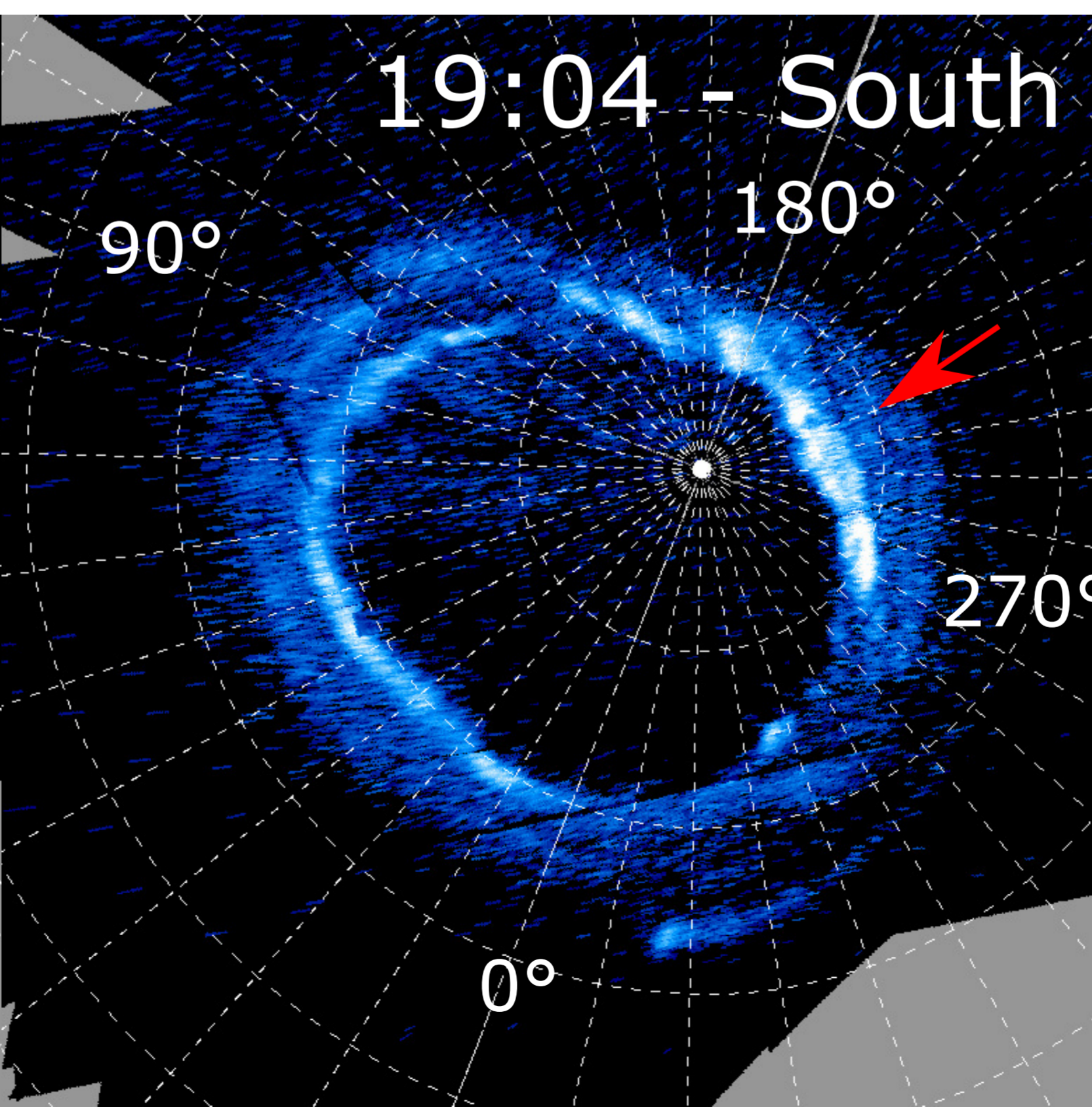
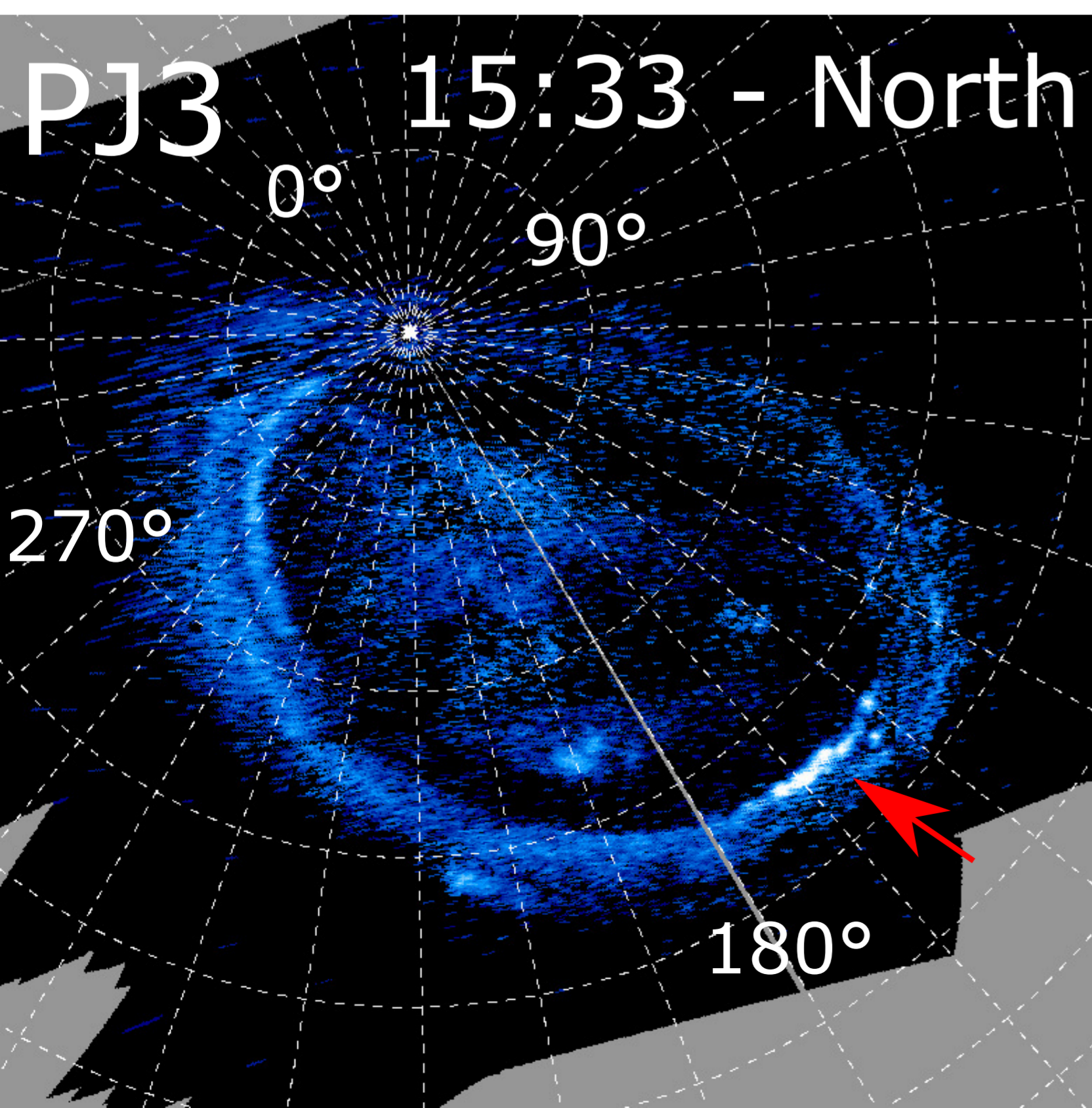
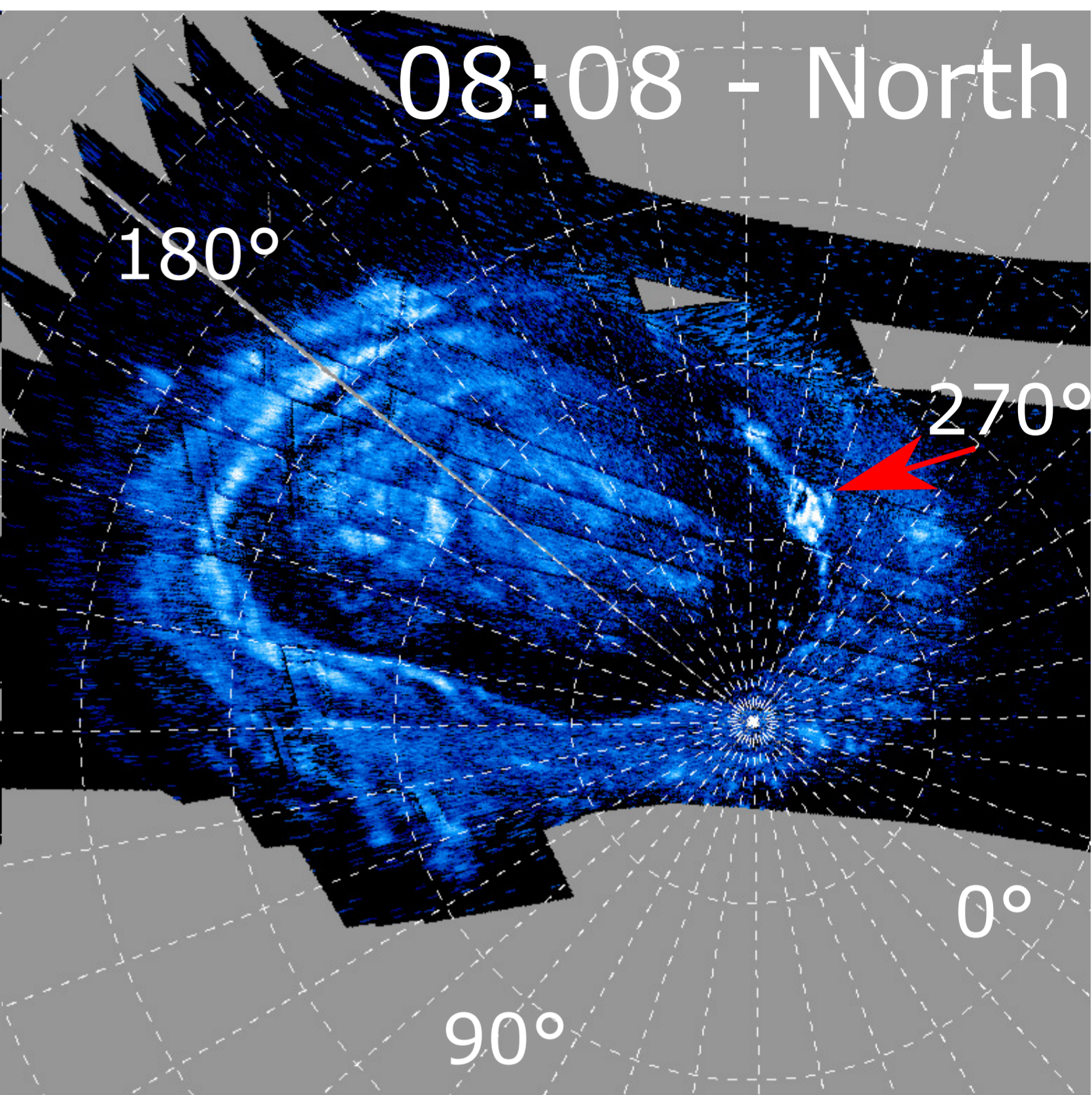
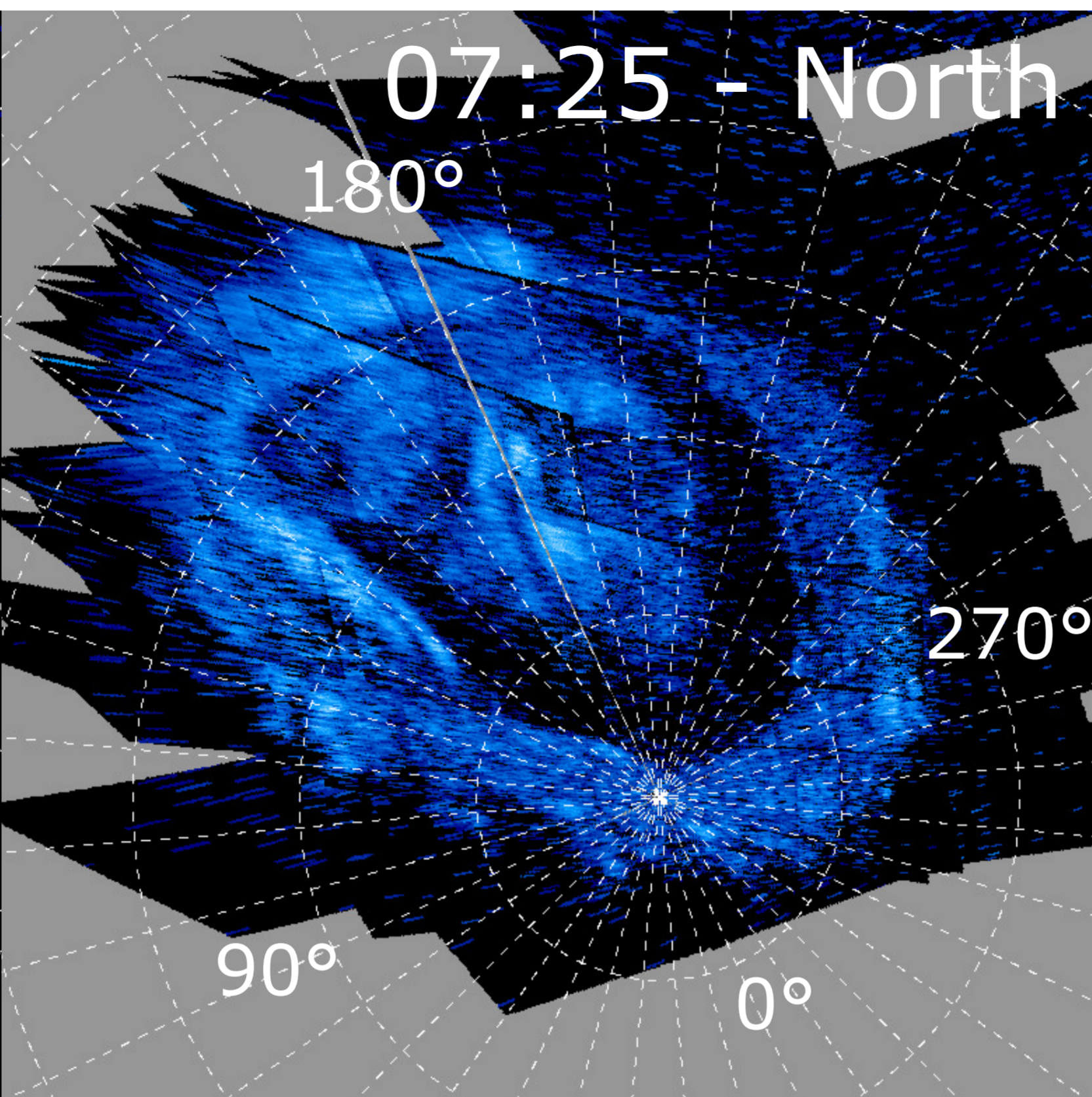
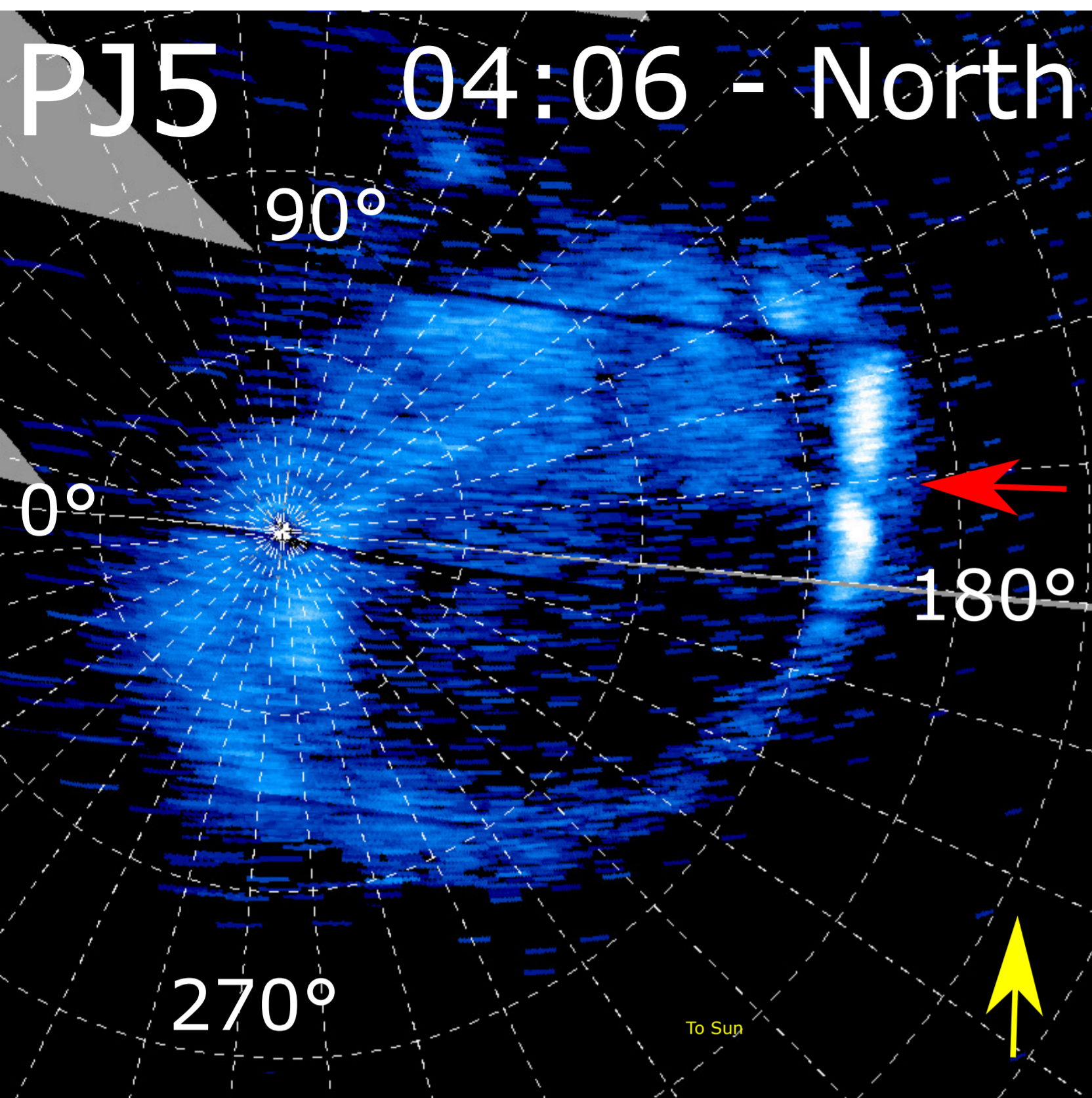
PJ11



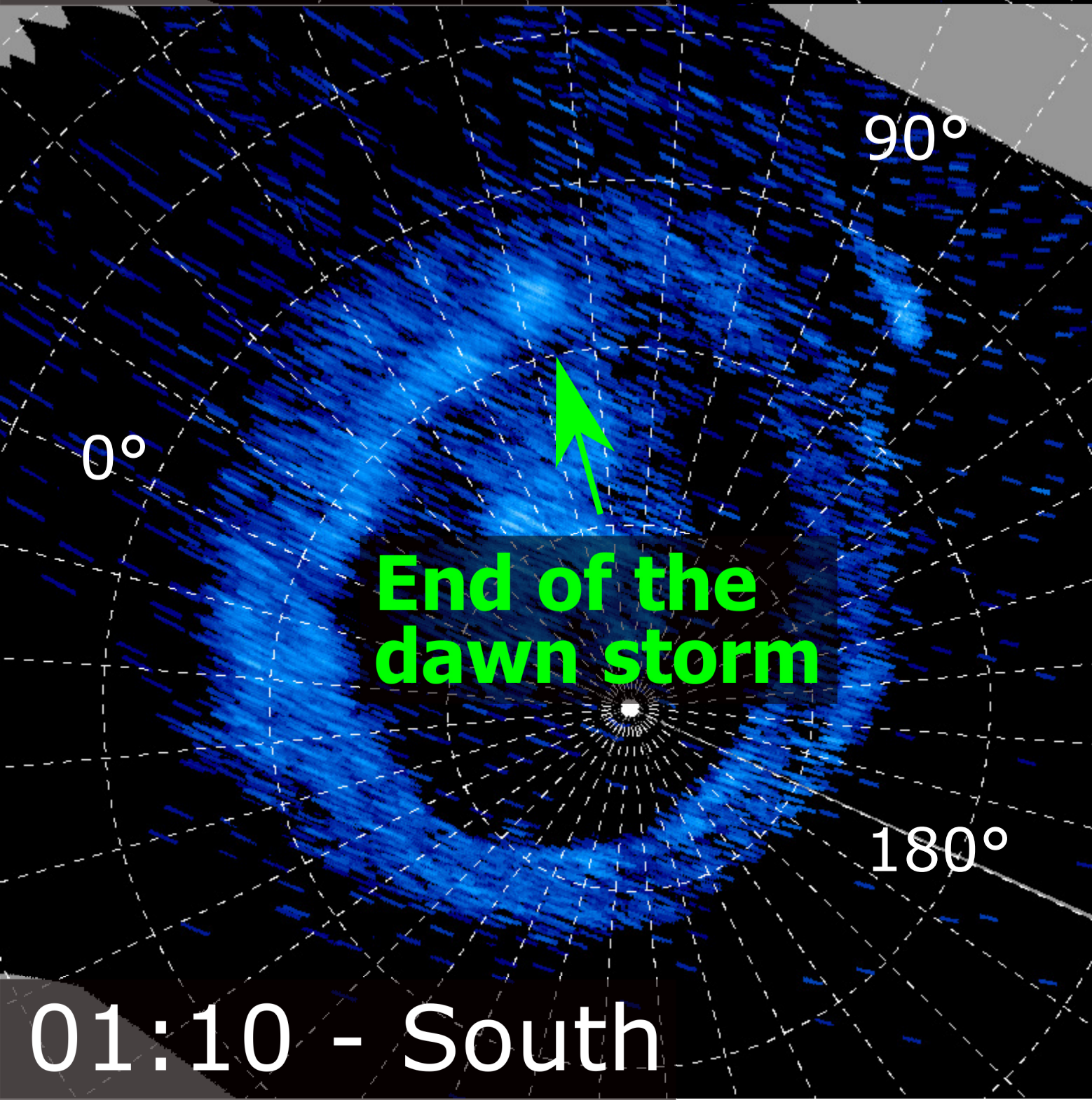
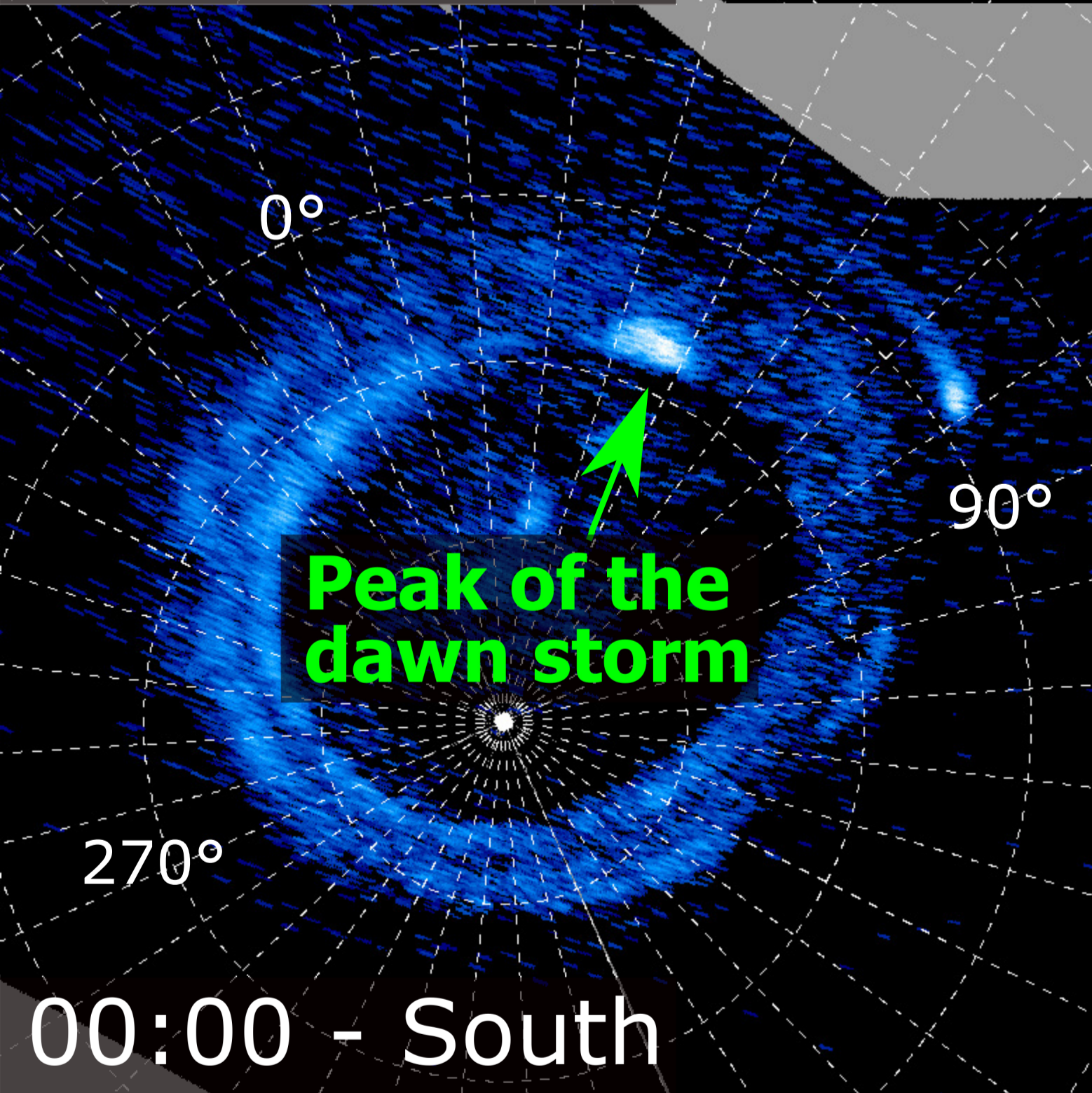
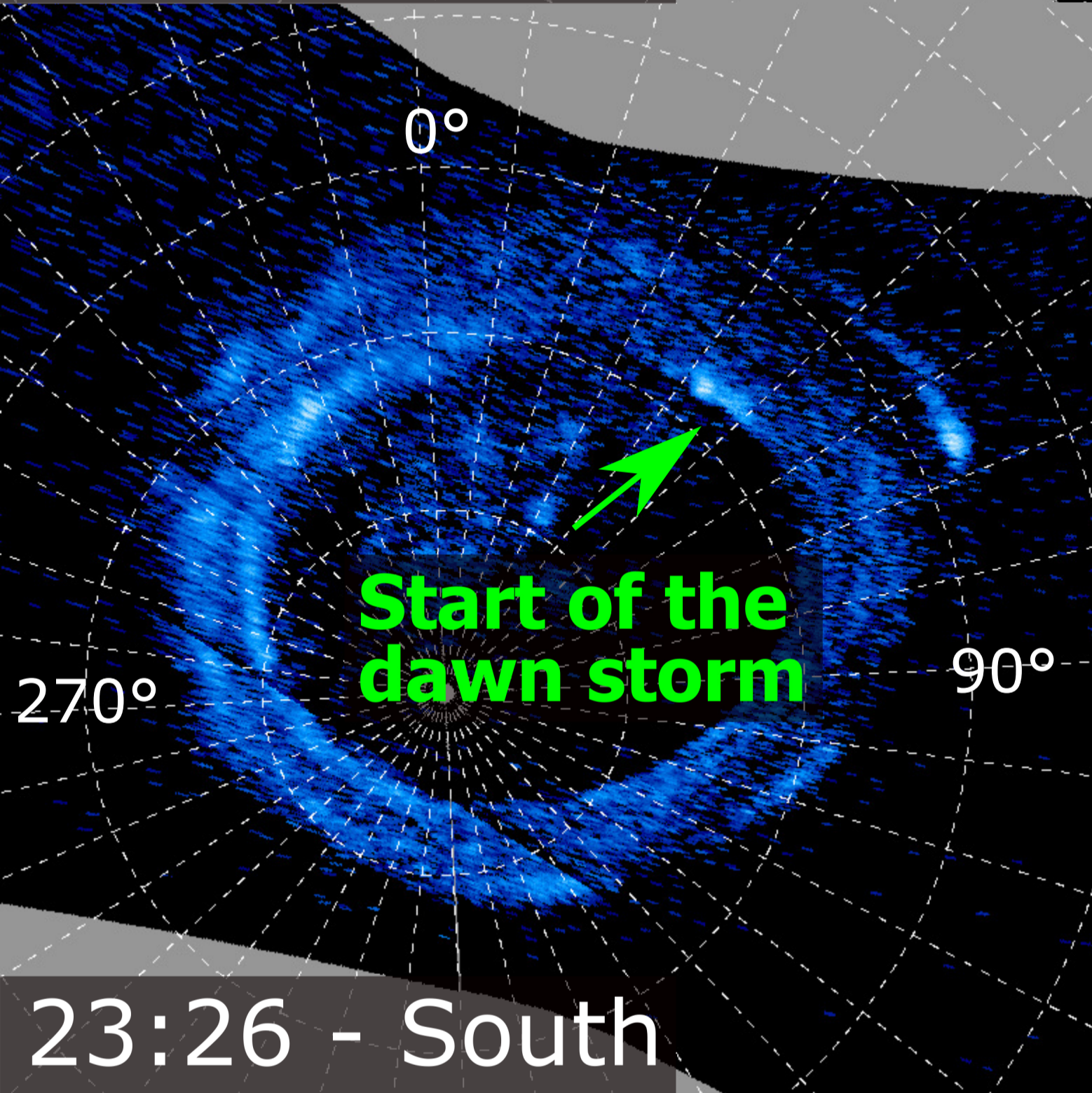
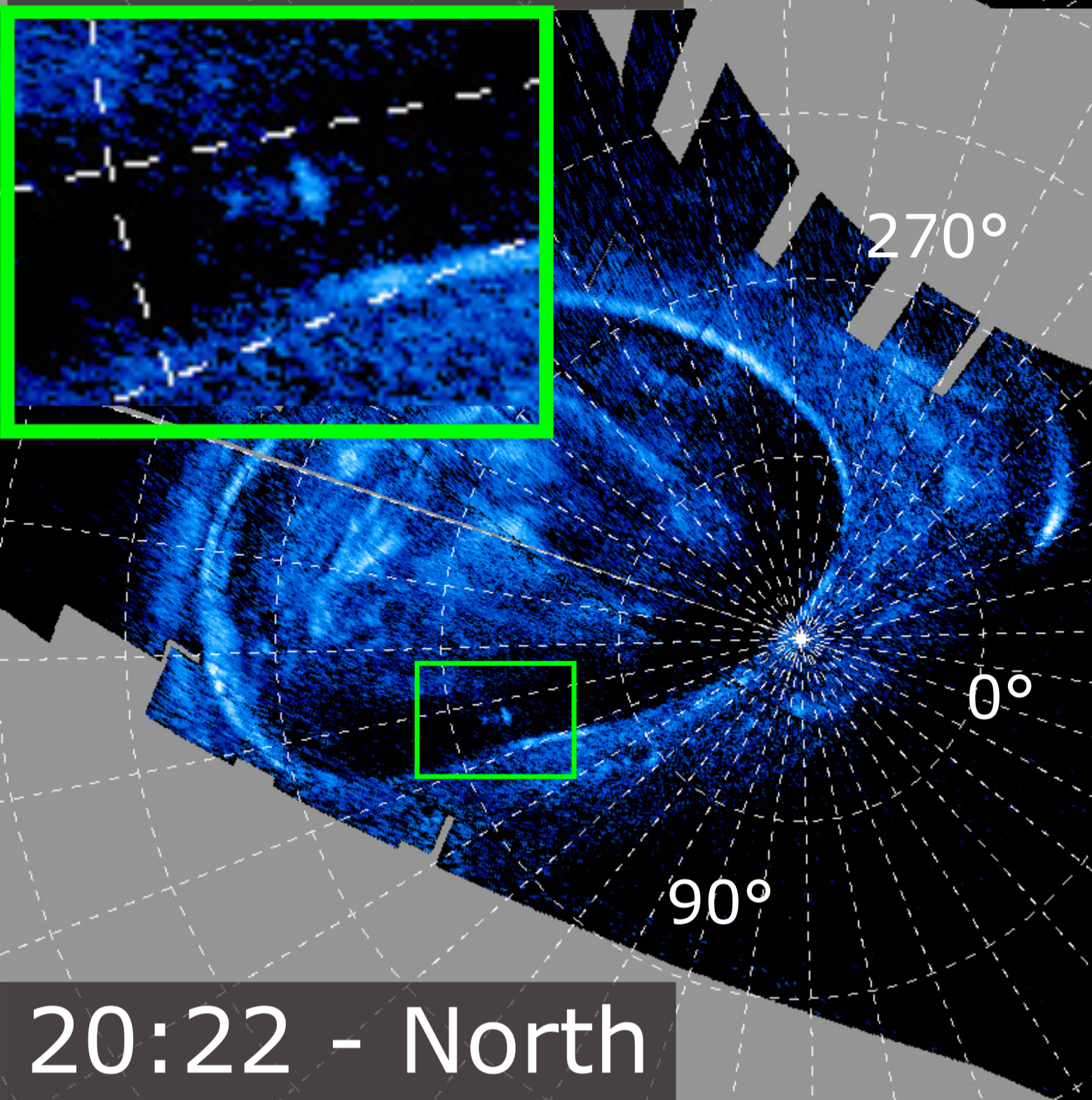
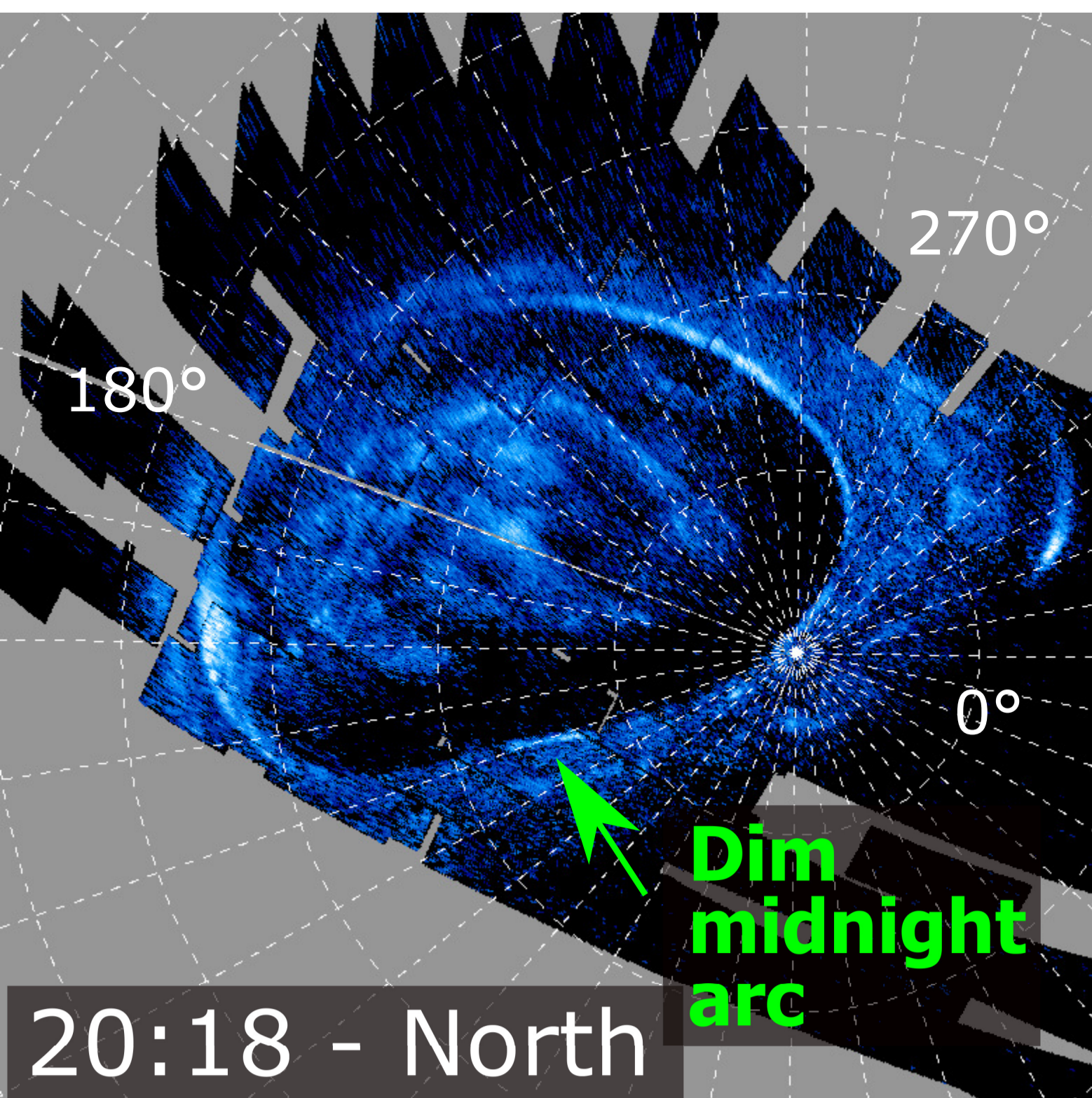
PJ6



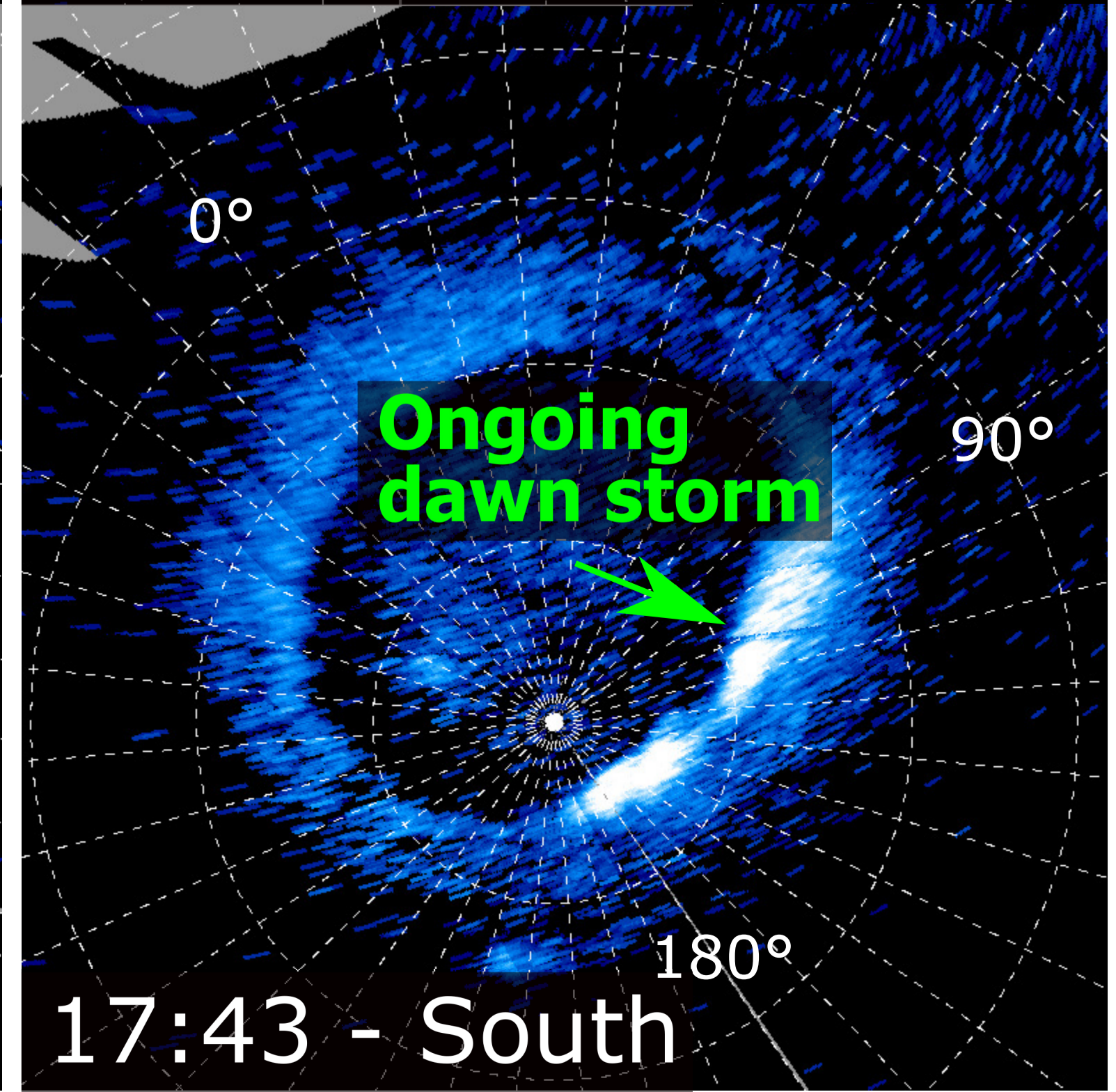
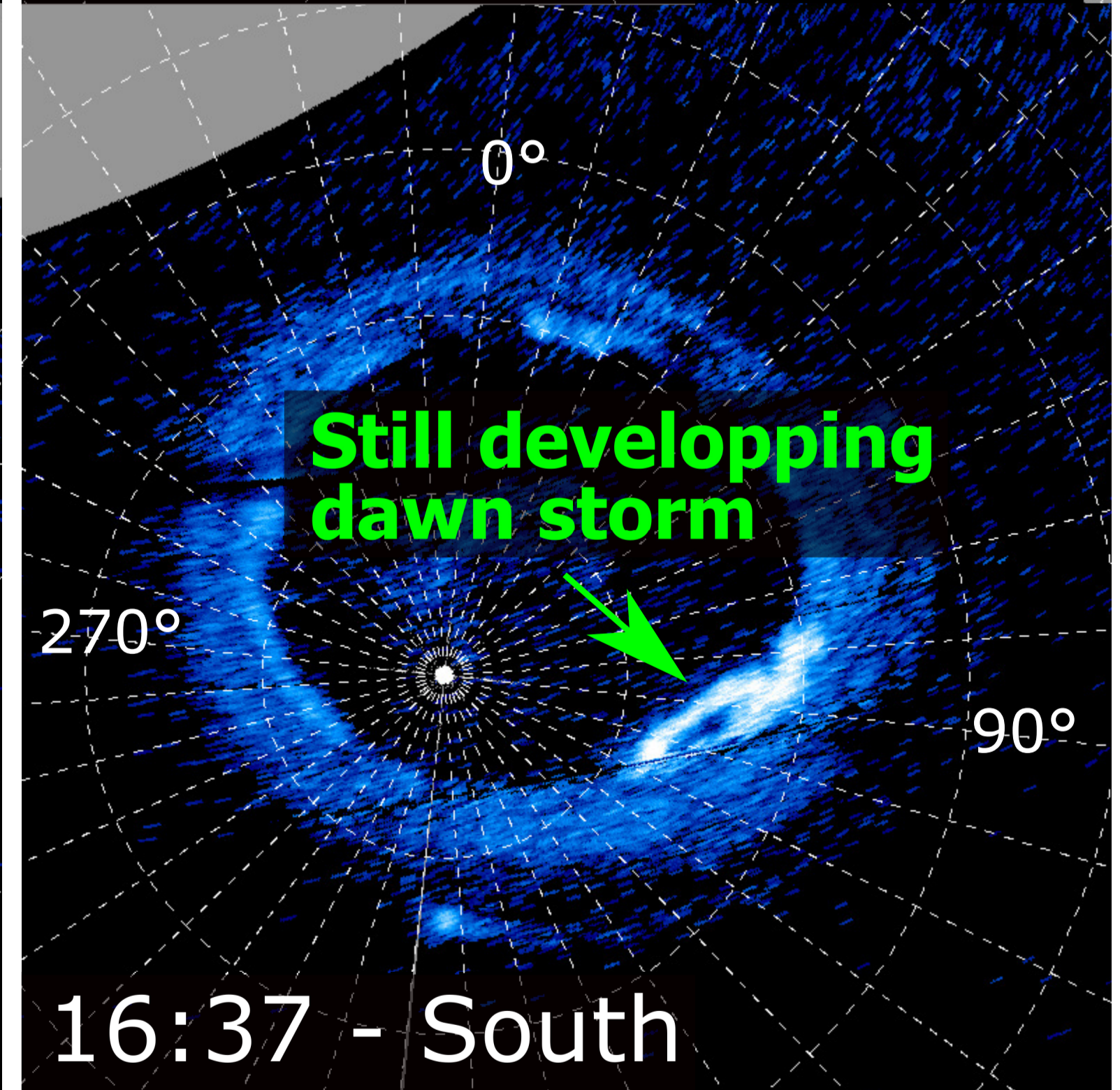
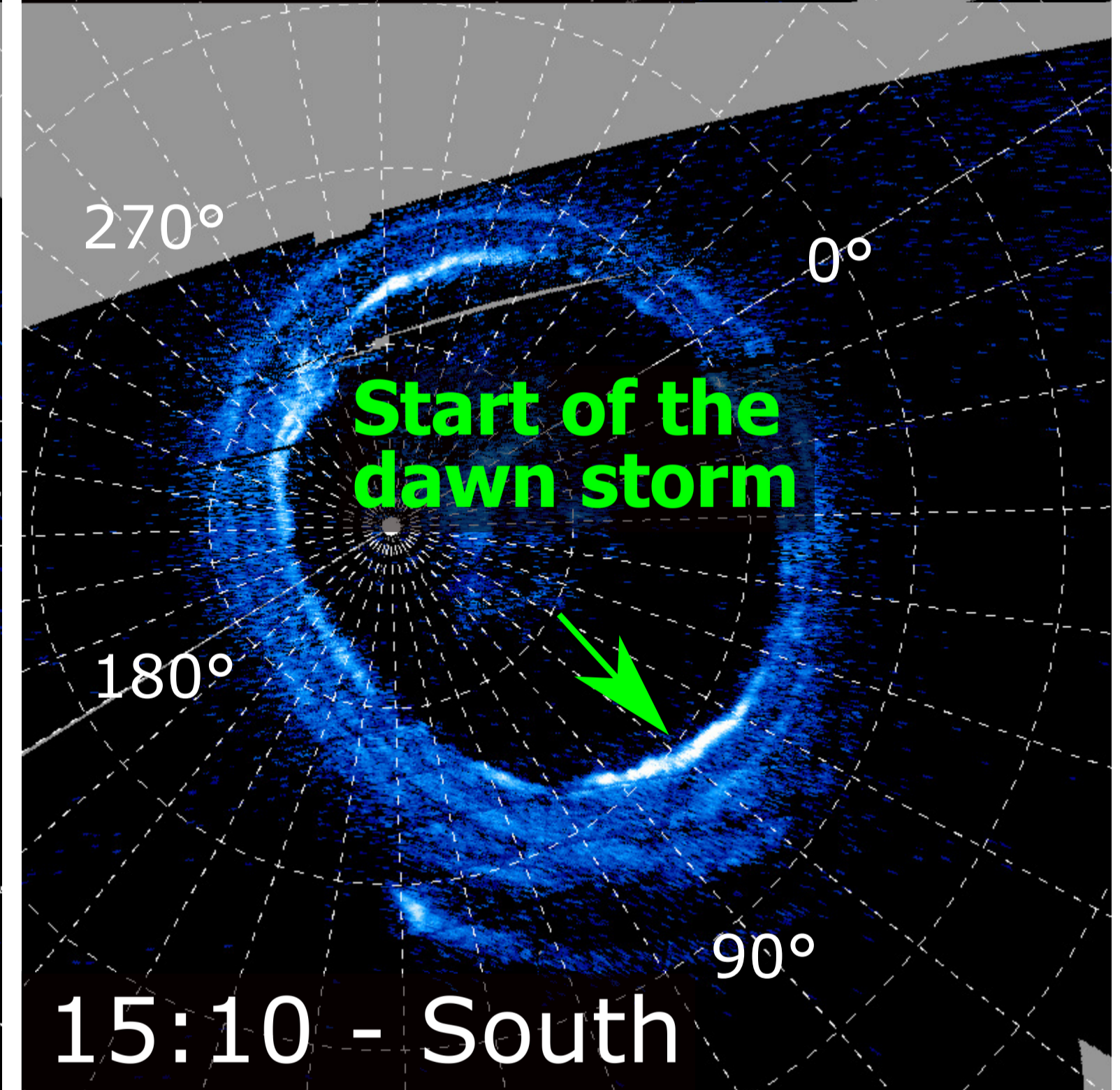
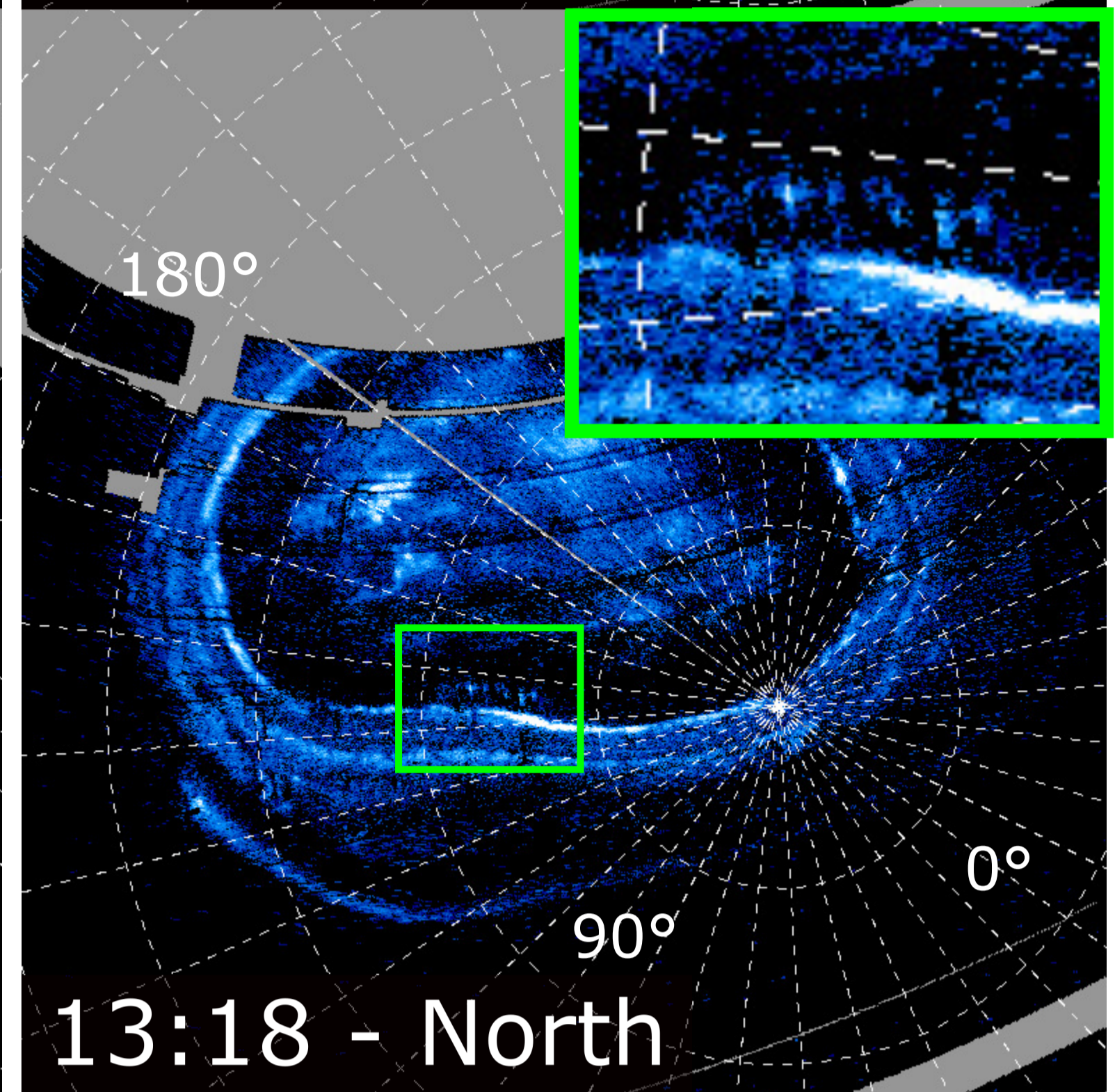
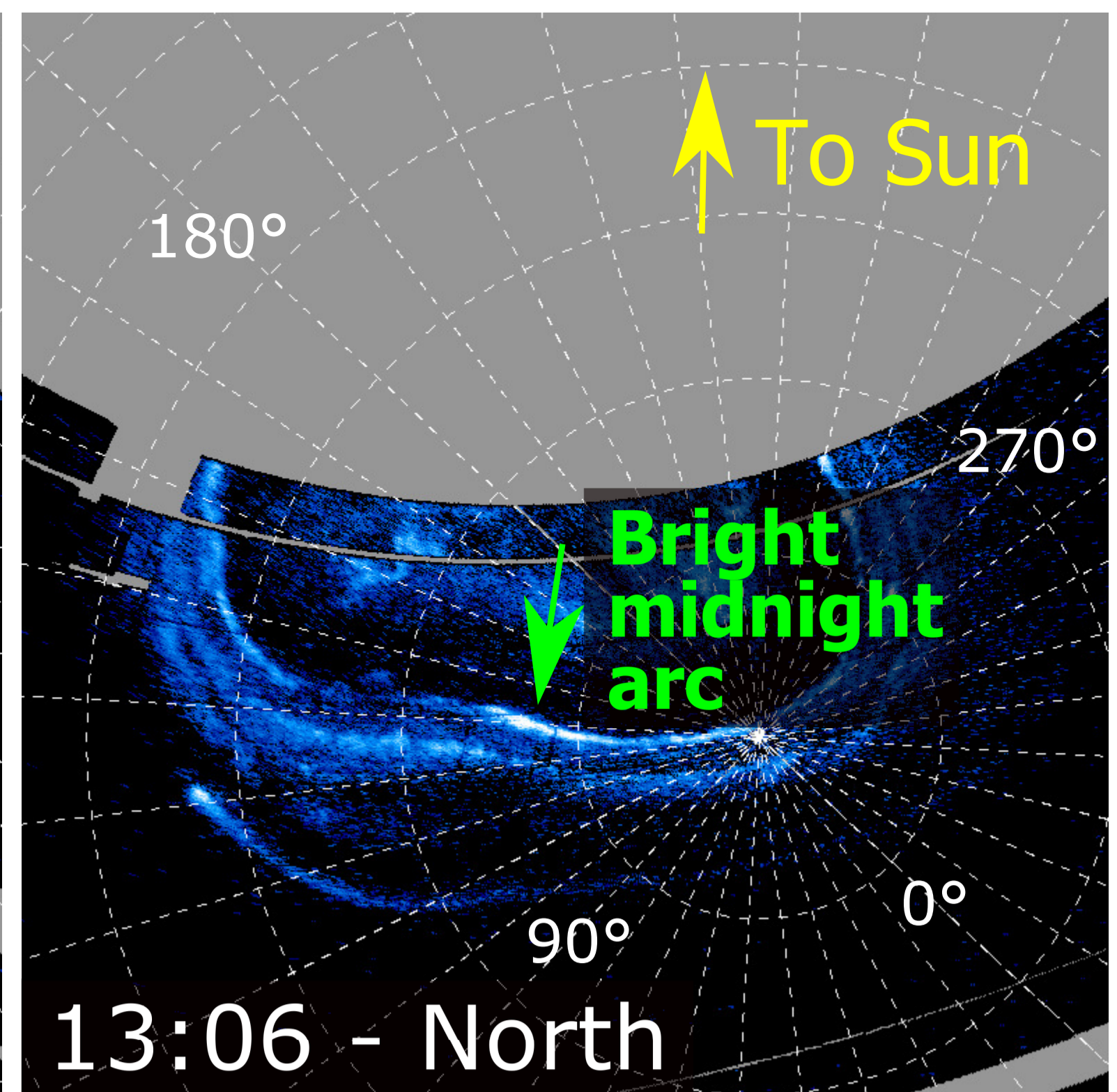
Non-Isolated Dawn Storms



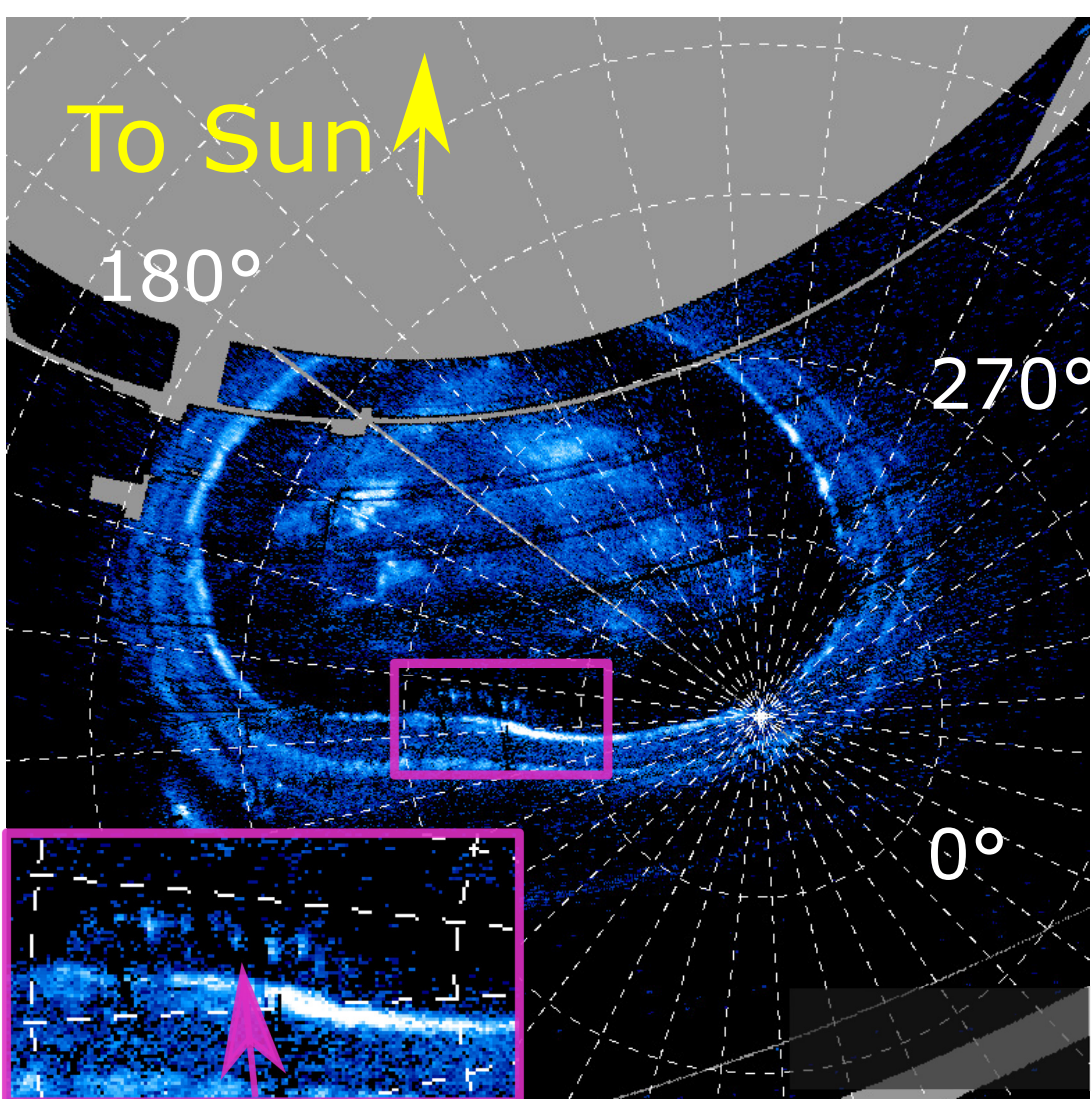
PJ16



PJ11

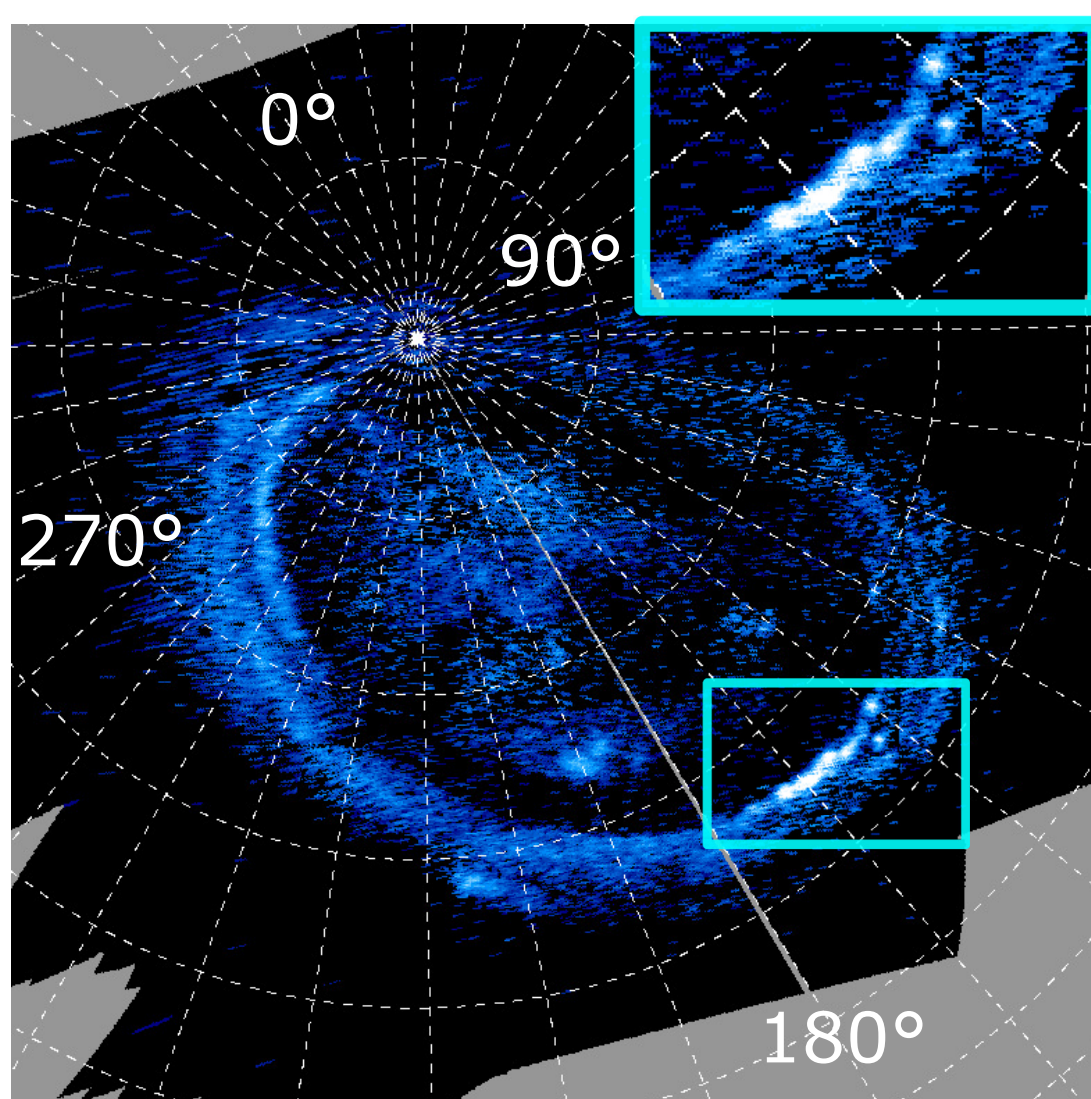


Midnight spots



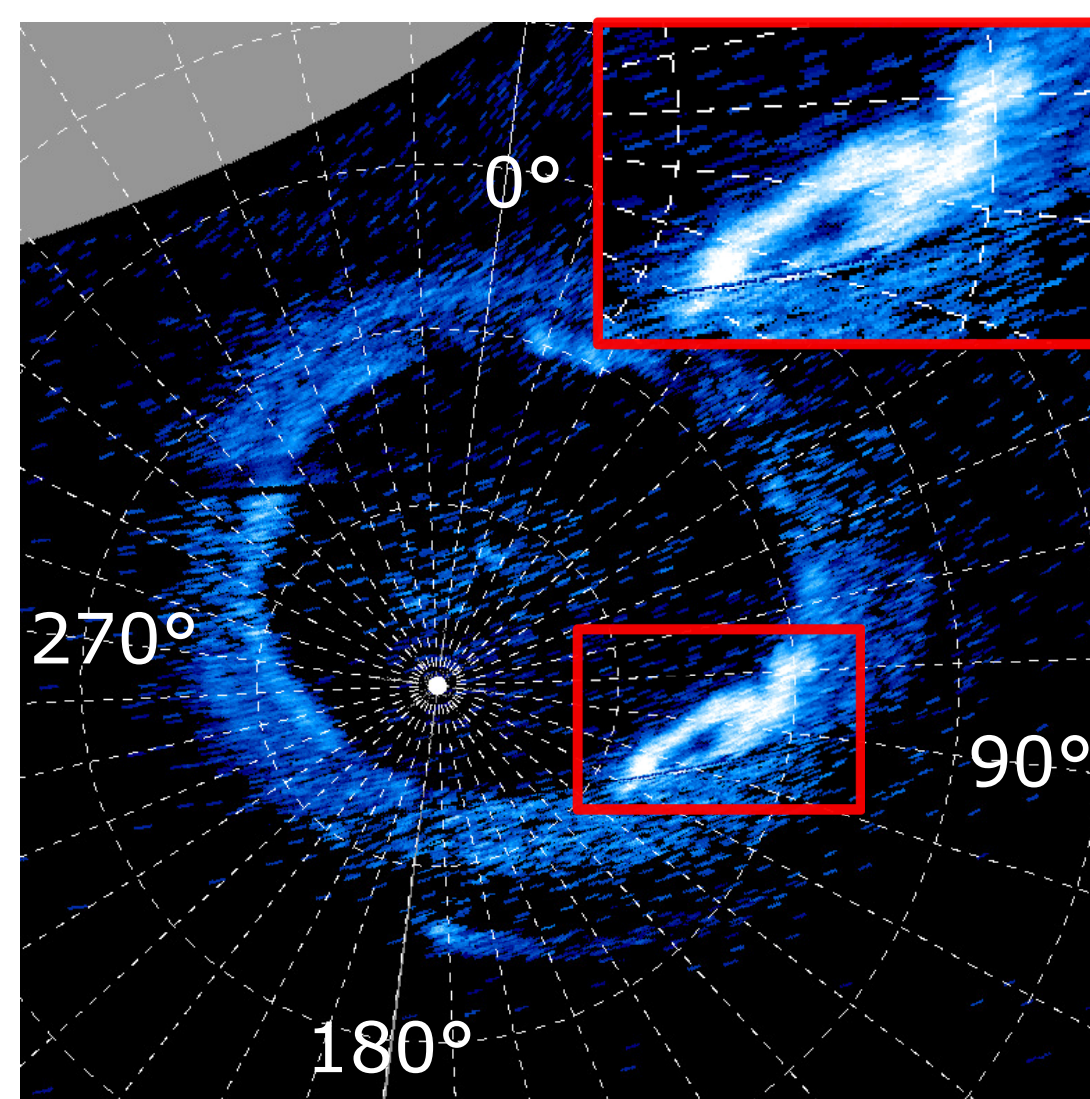
Juno-UVS 2018-02-07 13:17UT

Beads



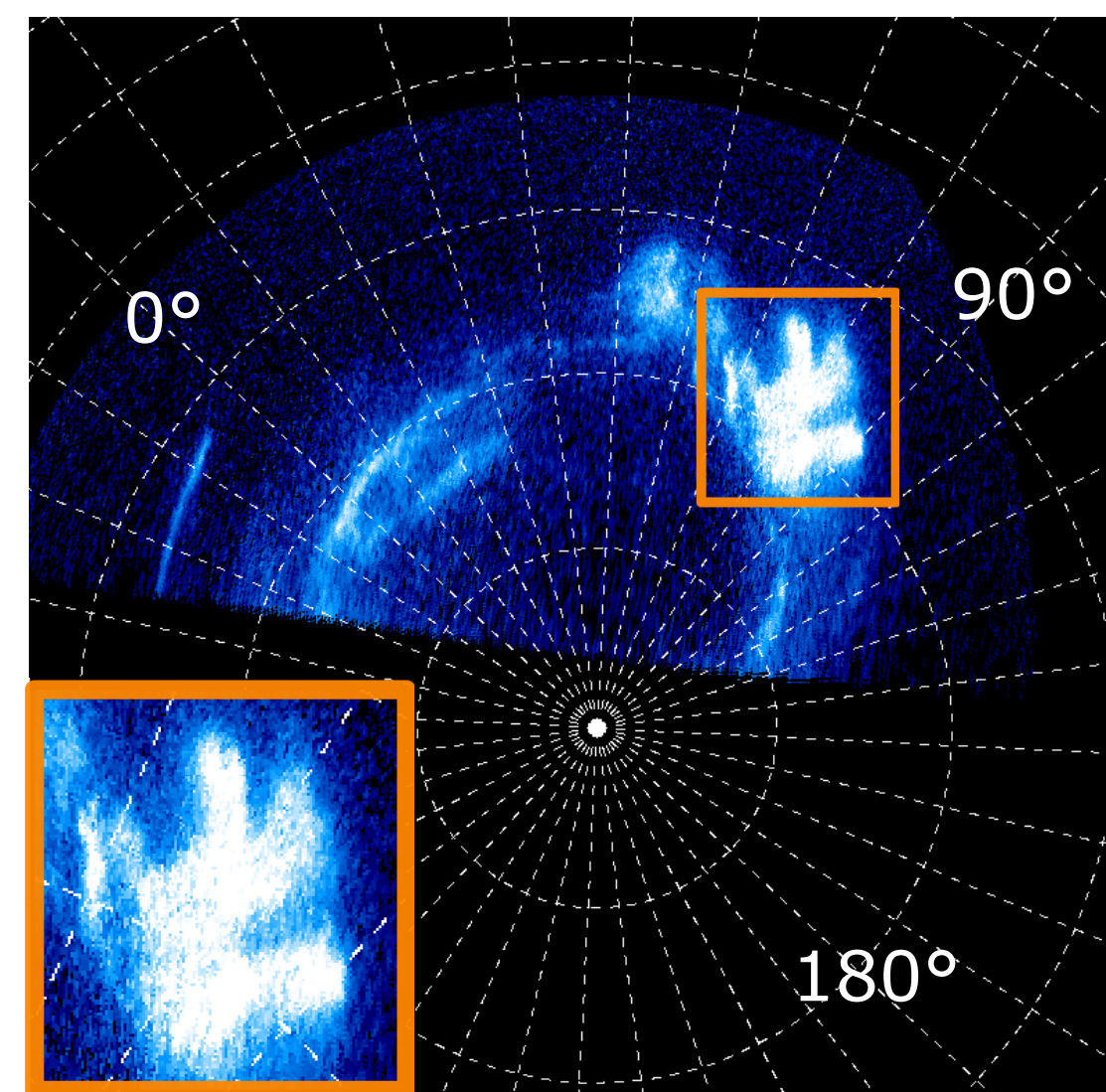
Juno-UVS 2016-11-12 15:33UT

Expansion phase

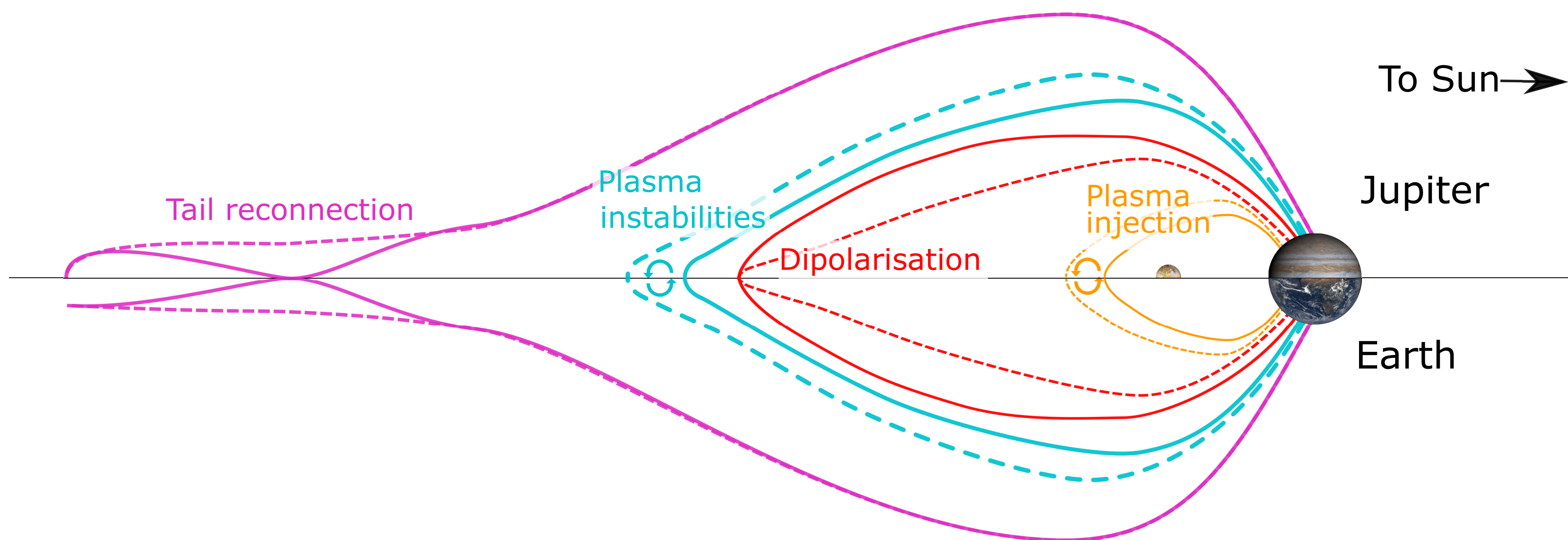


Juno-UVS 2018-02-07 16:34UT

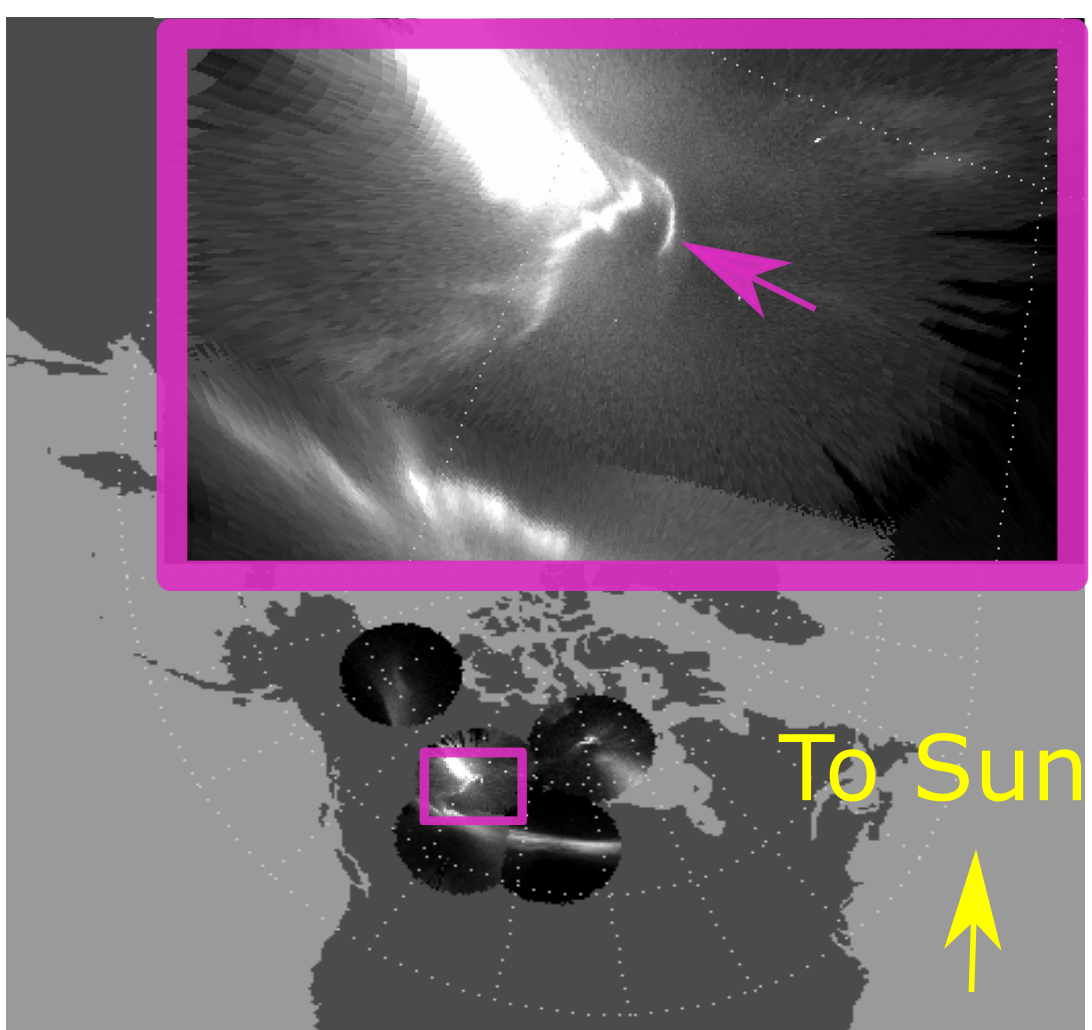
Injection signature



HST/STIS 2017-05-19 11:49UT

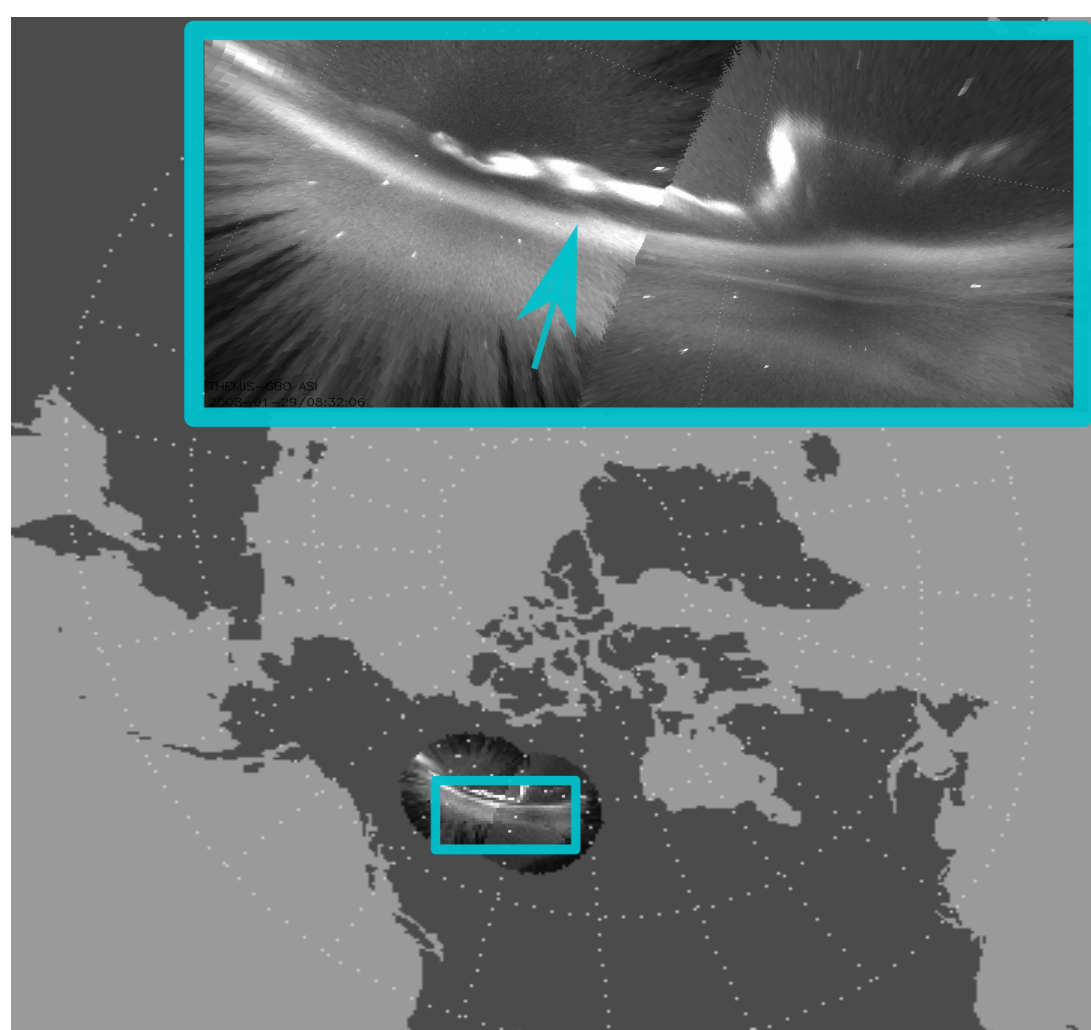


PBIs or Streamers



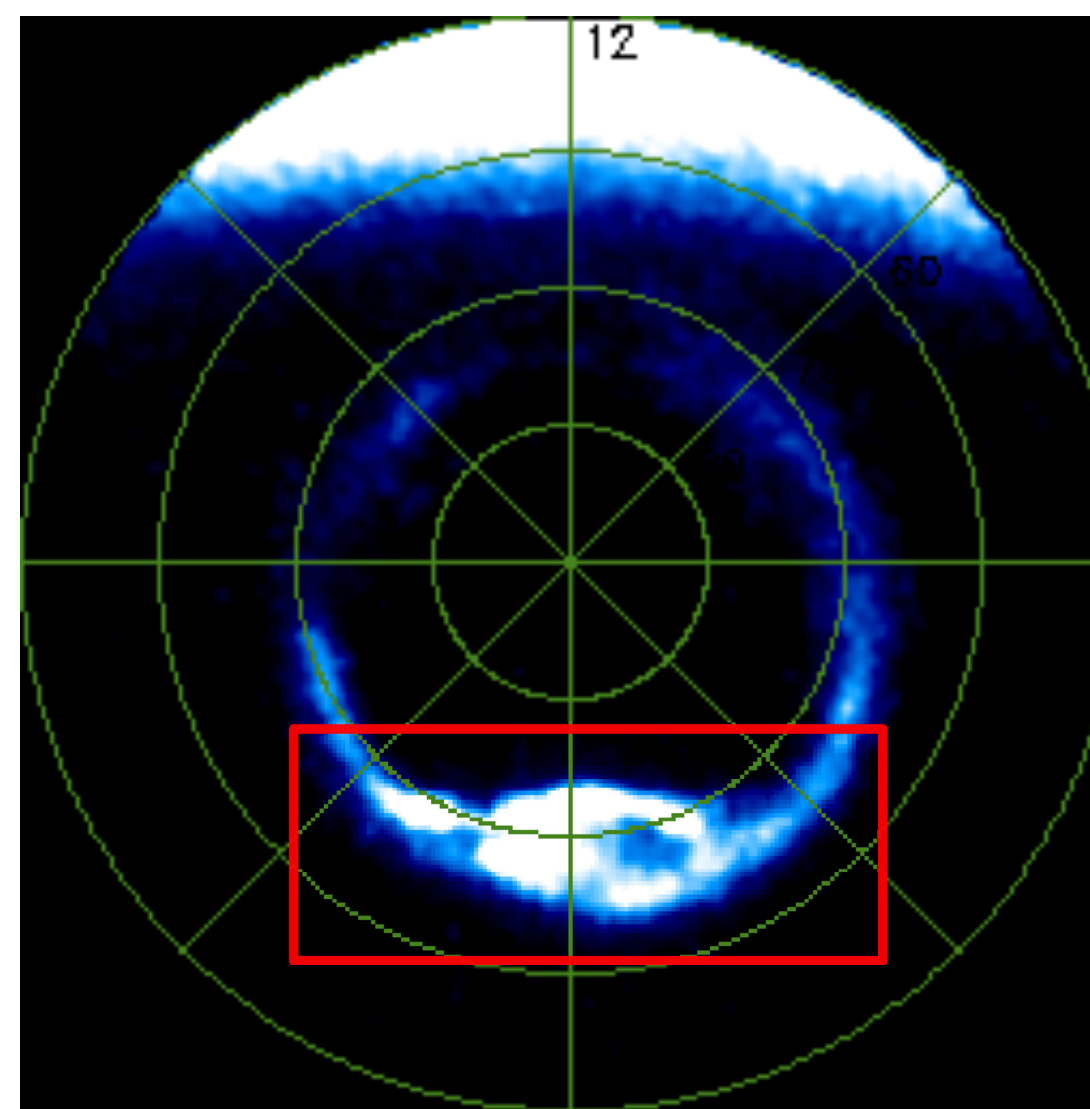
Themis all-sky cam. 2008-02-29 08:20UT

Beads



Themis all-sky cam. 2008-01-29 08:33UT

Expansion phase



Image/WIC 2001-01-14 03:59UT